NATIONAL CENTER FOR EARTHQUAKE ENGINEERING RESEARCH

ISSN 1088-3800

Ductility of Rectangular Reinforced Concrete Bridge Columns with Moderate Confinement

by

N. Wehbe, M. Saiidi, D. Sanders and B. Douglas

Technical Report NCEER-96-0003

November 7, 1996

This research was conducted at the University of Nevada at Reno and was supported by the Federal Highway Administration under contract number DTFH61-92-C-00112.

NOTICE

This report was prepared by the University of Nevada, Reno as a result of research sponsored by the National Center for Earthquake Engineering Research (NCEER) through a contract from the Federal Highway Administration. Neither NCEER, associates of NCEER, its sponsors, the University of Nevada, Reno, nor any person acting on their behalf:

a. makes any warranty, express or implied, with respect to the use of any information, apparatus, method, or process disclosed in this report or that such use may not infringe upon privately owned rights; or

b. assumes any liabilities of whatsoever kind with respect to the use of, or the damage resulting from the use of, any information, apparatus, method, or process disclosed in this report.

Any opinions, findings, and conclusions or recommendations expressed in this publication are those of the author(s) and do not necessarily reflect the views of NCEER or the Federal Highway Administration.

NATIONAL CENTER FOR EARTHQUAKE ENGINEERING RESEARCH
Headquartered at the State University of New York at Buffalo

Ductility of Rectangular Reinforced Concrete Bridge Columns with Moderate Confinement

by

N. Wehbe[1], M. Saiidi[2], D. Sanders[3] and B. Douglas[2]

Publication Date: November 7, 1996
Submittal Date: July 27, 1995

Technical Report NCEER-96-0003

NCEER Task Number 112-D-5.1(d)

FHWA Contract Number DTFH61-92-C-00112

1 Graduate Research Assistant, Department of Civil Engineering, University of Nevada, Reno
2 Professor, Department of Civil Engineering, University of Nevada, Reno
3 Associate Professor, Department of Civil Engineering, University of Nevada, Reno

NATIONAL CENTER FOR EARTHQUAKE ENGINEERING RESEARCH
State University of New York at Buffalo
Red Jacket Quadrangle, Buffalo, NY 14261

PREFACE

The National Center for Earthquake Engineering Research (NCEER) was established in 1986 to develop and disseminate new knowledge about earthquakes, earthquake-resistant design and seismic hazard mitigation procedures to minimize loss of life and property. The emphasis of the Center is on eastern and central United States *structures*, and *lifelines* throughout the country that may be exposed to any level of earthquake hazard.

NCEER's research is conducted under one of four Projects: the Building Project, the Nonstructural Components Project, and the Lifelines Project, all three of which are principally supported by the National Science Foundation, and the Highway Project which is primarily sponsored by the Federal Highway Administration.

The research and implementation plan in years six through ten (1991-1996) for the Building, Nonstructural Components, and Lifelines Projects comprises four interdependent elements, as shown in the figure below. Element I, Basic Research, is carried out to support projects in the Applied Research area. Element II, Applied Research, is the major focus of work for years six through ten for these three projects. Demonstration Projects under Element III have been planned to support the Applied Research projects and include individual case studies and regional studies. Element IV, Implementation, will result from activity in the Applied Research projects, and from Demonstration Projects.

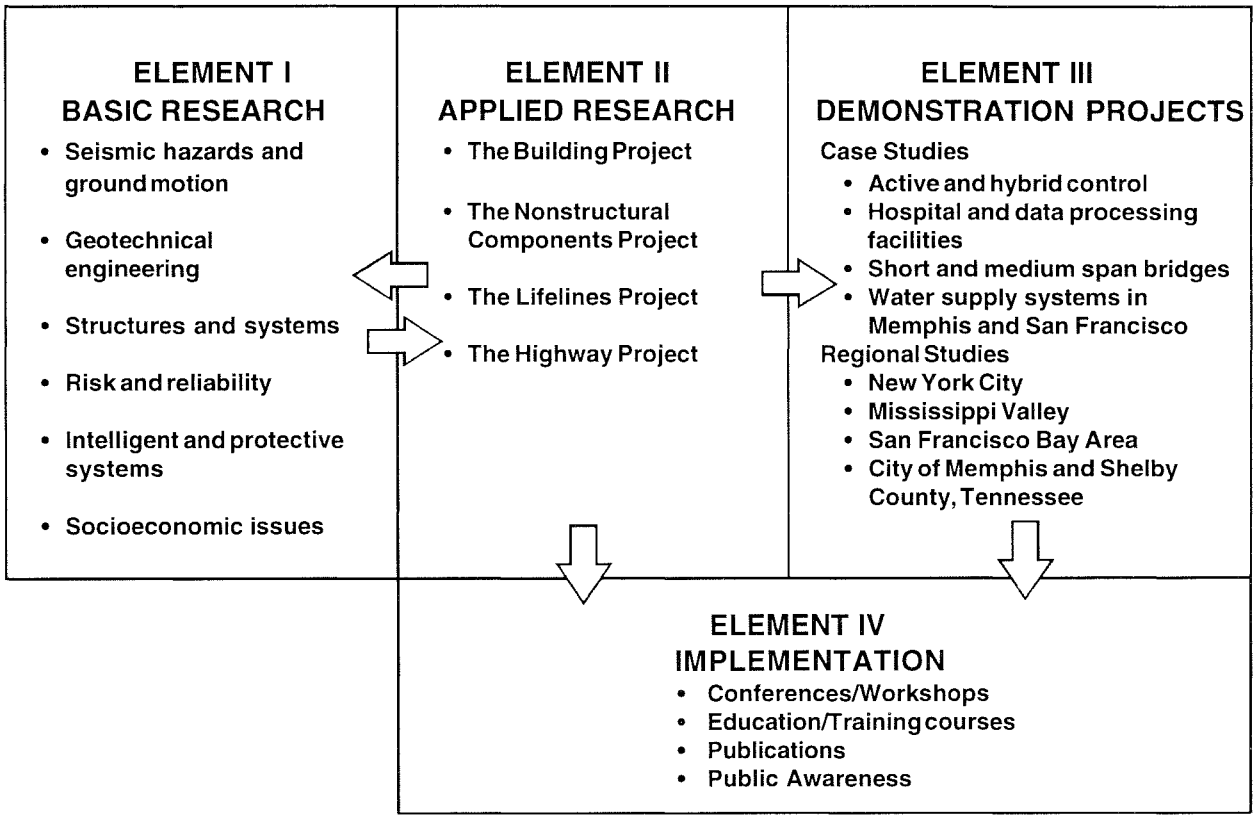

Research under the **Highway Project** develops retrofit and evaluation methodologies for existing bridges and other highway structures (including tunnels, retaining structures, slopes, culverts, and pavements), and develops improved seismic design criteria and procedures for bridges and other highway structures. Specifically, tasks are being conducted to: (1) assess the vulnerability of highway systems and structures; (2) develop concepts for retrofitting vulnerable highway structures and components; (3) develop improved design and analysis methodologies for bridges, tunnels, and retaining structures, with particular emphasis on soil-structure interaction mechanisms and their influence on structural response; and (4) review and improve seismic design and performance criteria for new highway systems and structures.

Highway Project research focuses on one of two distinct areas: the development of improved design criteria and philosophies for new or future highway construction, and the development of improved analysis and retrofitting methodologies for existing highway systems and structures. The research discussed in this report is a result of work conducted under the new highway construction project, and was performed within Task 112-D-5.1(D), "Capacity Detailing of Columns, Walls and Piers for Ductility and Shear" of the project as shown in the flowchart.

The overall objective of this task is to develop improved seismic detailing requirements for the design of bridge columns, walls and piers in areas of moderate seismicity. This report presents the results of a research project to examine the ductility and behavior of rectangular reinforced concrete bridge columns with moderate confinement. Both experimental and analytical investigations of the response of these columns subjected to lateral loading were conducted. The research shows that rectangular reinforced concrete columns with a moderate amount of transverse reinforcement can be expected to perform adequately in areas of moderate seismicity.

SEISMIC VULNERABILITY OF NEW HIGHWAY CONSTRUCTION
FHWA Contract DTFH61-92-C-00112

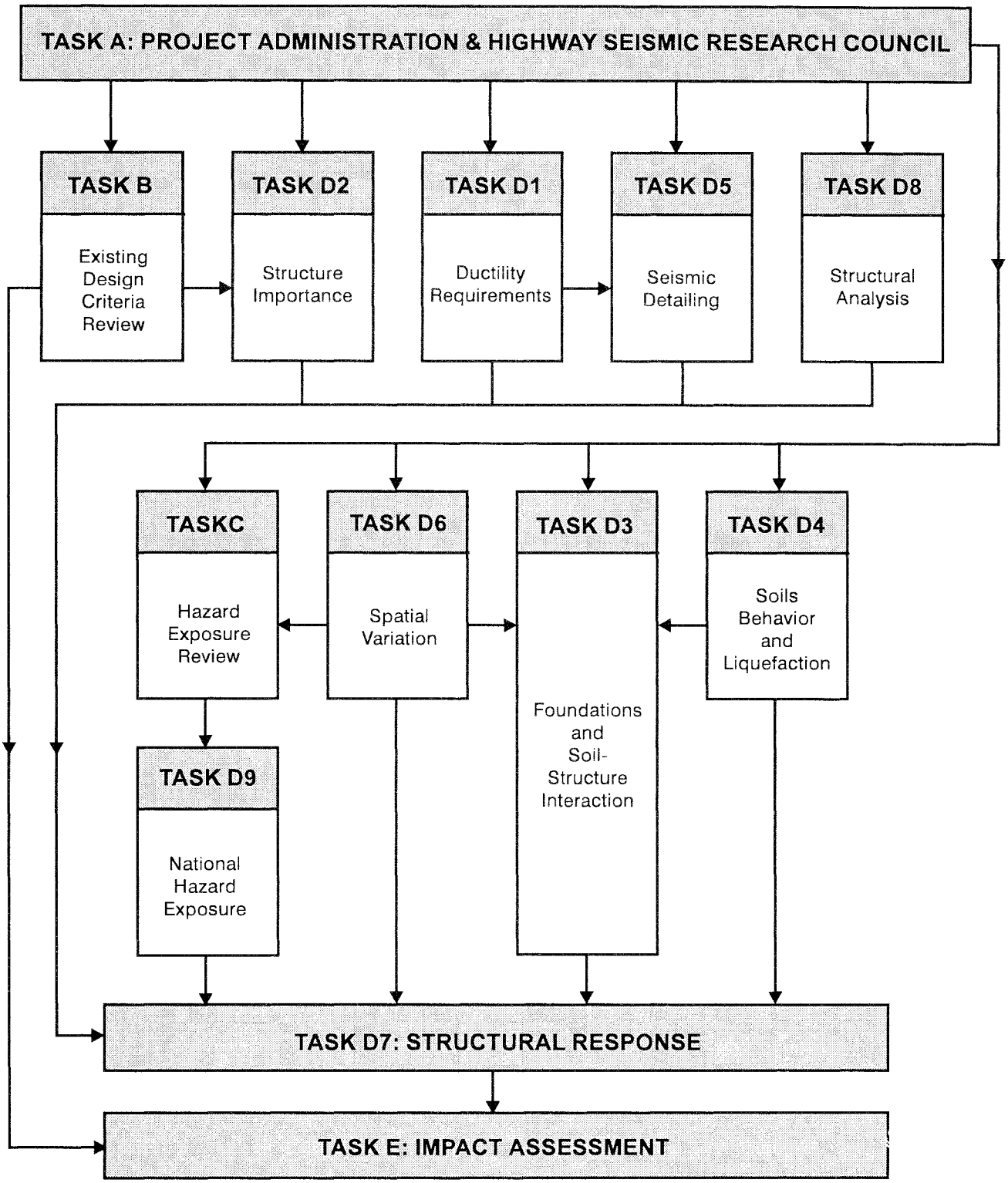

ABSTRACT

This study is part of a project to develop detailing guidelines for reinforced concrete bridge columns and walls in areas of moderate seismicity. The research examined the ductility and behavior of rectangular reinforced concrete bridge columns with moderate confinement. The research comprised experimental and analytical investigation of the response of such columns when subjected to lateral loading.

Four half-scaled rectangular bridge columns were built and tested. The geometrical dimensions and the amount of longitudinal reinforcement were kept the same for all specimens. Each specimen was tested under constant axial load while subjected to lateral load reversals with increasing drift levels. The lateral loading was quasi-static and uniaxial in the column strong direction.

Two parameters were varied: the transverse steel reinforcement amount and the axial load level. Based on the amount of lateral steel, the specimens were divided into two groups. The transverse reinforcement ratios, $A_s/(s \cdot h)$, in the long direction for the two groups corresponded to 42 percent and 54 percent of the minimum lateral reinforcement required by AASHTO for seismic detailing. The applied axial loads were approximately $0.1\, f_c' A_g$ and $0.25\, f_c' A_g$. The specimens exhibited moderate displacement ductilities ranging between 4 and 7.

In the analytical study, several existing models pertaining to the concrete stress-strain relationship and the plastic hinge length were utilized and compared. For unconfined concrete, the Kent and Park model was used. On the other hand, the modified Kent and Park model and the model by Mander et al. (as modified by Paulay and Priestley) were utilized to represent the constitutive relationship of confined concrete. The equivalent plastic hinge length was calculated using two different models, the Baker's model and the model by Paulay and Priestley. The analytical study revealed that for rectangular bridge columns with relatively low axial loads and moderate confinement, it is possible to predict with reasonable accuracy the response of the columns to lateral cyclic loading.

TABLE OF CONTENTS

SECTION	TITLE	PAGE
1	**INTRODUCTION**	1
1.1	Bridge Design Philosophy in Areas of High Seismic Risk	1
1.2	Current Seismic Provisions	1
1.2.1	American Concrete Institute (ACI)	1
1.2.2	American Association of State Highway and Transportation Officials (AASHTO)	2
1.2.3	California Department of Transportation (Caltrans)	2
1.2.4	Paulay and Priestley	3
1.2.5	New Zealand Code	3
1.2.6	Commission of the European Communities	4
1.2.7	Example Bridge Column	5
1.3	Review of Previous Works	6
1.4	Objective and Scope	7
2	**DUCTILITY OF REINFORCED CONCRETE COLUMNS**	9
2.1	Introductory Remarks	9
2.2	Concrete Stress-Strain Models	9
2.2.1	Modified Kent and Park	9
2.2.2	Mander, et al. as Modified by Paulay and Priestley	10
2.3	Verification and Comparison of Concrete Models	12
3	**EXPERIMENTAL STUDIES**	15
3.1	Introduction	15
3.2	Design of Test Specimens	15
3.2.1	Column Cross Section	15
3.2.2	Column Height	15
3.2.3	Transverse Reinforcement	17
3.2.4	Footing Design	20
3.3	Construction of Test Specimens	22
3.4	Material Properties	23
3.5	Instrumentation	27
3.6	Test Setup	29
3.7	Experimental Procedure and Results	31
3.7.1	General Remarks	31
3.7.2	Specimen A1	33
3.7.3	Specimen A2	37
3.7.4	Specimen B1	43
3.7.5	Specimen B2	51
3.8	Summary and Observations	57

TABLE OF CONTENTS (Cont'd)

SECTION	TITLE	PAGE
4	**ANALYTICAL STUDY**	59
4.1	Introduction	59
4.2	Theoretical Analysis	59
4.2.1	Lateral Deflection	59
4.2.2	Moment-Curvature Analysis	63
4.2.3	Plastic Hinge Length	66
4.2.4	Calculated Deflections	67
4.3	Remarks and Observations	70
5	**SUMMARY AND CONCLUSIONS**	73
5.1	Summary	73
5.1.1	Experimental Study	73
5.1.2	Analytical Study	74
5.2	Conclusions	75
5.3	Recommendations	75
6	**REFERENCES**	77
Appendix A	**BOND SLIP ROTATION**	81

LIST OF FIGURES

FIGURE	TITLE	PAGE
1-1	Cross Section of the Example Column	5
1-2	Confinement Steel Requirements for Different Design Methods	6
1-3	Available Test Data for Cyclic Response of Square Columns	7
3-1	Column Details for Specimens in Group I	16
3-2	Column Details for Specimens in Group II	16
3-3	Footing Details of the Test Specimens	21
3-4	Reinforcement Cage of a Test Specimen	23
3-5	Measured Stress-Strain Relationship of ϕ 6 mm (#2) Steel Bars	25
3-6	Measured Stress-Strain Relationship of ϕ 10 mm (#3) Steel Bars	25
3-7	Measured Stress-Strain Relationship of ϕ 19 mm (#6) Steel Bars	26
3-8	Averaged Measured Properties of Steel Bars	26
3-9	Strain Gaging of Longitudinal Bars	27
3-10	Strain Gaging of Transverse Steel	28
3-11	LVDT Setup for the Test Specimens	29
3-12	Test Setup	30
3-13	Idealized Moment-Curvature Relationship	32
3-14	Experimental Determination of Effective Yield Displacement	32
3-15	Lateral Load History for Specimen A1	34
3-16	Measured Lateral Load-Deflection Hysteresis Loops for Specimen A1	34
3-17	Specimen A1 at μ_Δ = +1 (1st Excursion)	35
3-18	Specimen A1 at μ_Δ = +4 (1st Excursion)	36
3-19	Specimen A1 at μ_Δ = +6 (1st Excursion)	36
3-20	Plastic Hinge in Specimen A1 at the End of the Test	37
3-21	Measured Lateral Load-Strain Hysteresis in Specimen A1 Longitudinal Bar	38
3-22	Measured Lateral Load-Strain in Specimen A1 Lateral Steel at SG 19	38
3-23	Measured Lateral Load-Strain in Specimen A1 Lateral Steel at SG 22	39
3-24	Measured Curvature Envelop along the Plastic Hinge of Specimen A1	39
3-25	Lateral Load History for Specimen A2	40
3-26	Measured Lateral Load-Deflection Hysteresis Loops for Specimen A2	41
3-27	Specimen A2 at μ_Δ = +1 (2nd Excursion)	41
3-28	Specimen A2 at μ_Δ = -2 (2nd Excursion)	42
3-29	Specimen A2 at μ_Δ = -4 (1st Excursion)	42
3-30	Plastic Hinge in Specimen A2 at the End of the Test	43
3-31	Measured Lateral Load-Strain Hysteresis in Specimen A2 Longitudinal Bar	44
3-32	Measured Lateral Load-Strain in Specimen A2 Lateral Steel at SG 18	44
3-33	Measured Lateral Load-Strain in Specimen A2 Lateral Steel at SG 19	45
3-34	Measured Curvature Envelop along the Plastic Hinge of Specimen A2	45
3-35	Lateral Load History for Specimen B1	46

LIST OF FIGURES (Cont'd)

FIGURE	TITLE	PAGE
3-36	Measured Lateral Load-Deflection Hysteresis Loops for Specimen B1	47
3-37	Specimen B1 at μ_Δ = -4 (1st Excursion)	47
3-38	Specimen B1 at μ_Δ = -6 (1st Excursion)	48
3-39	Specimen B1 at μ_Δ = +8	48
3-40	Plastic Hinge in Specimen B1 at the End of the Test	49
3-41	Measured Lateral Load-Strain Hysteresis in Specimen B1 Longitudinal Bar	49
3-42	Measured Lateral Load-Strain in Specimen B1 Lateral Steel at SG 20	50
3-43	Measured Lateral Load-Strain in Specimen B1 Lateral Steel at SG 22	50
3-44	Measured Curvature Envelop along the Plastic Hinge of Specimen B1	51
3-45	Lateral Load History for Specimen B2	52
3-46	Measured Lateral Load-Deflection Hysteresis Loops for Specimen B2	53
3-47	Specimen B2 at μ_Δ = -1 (1st Excursion)	53
3-48	Specimen B2 at μ_Δ = +3 (1st Excursion)	54
3-49	Specimen B2 at μ_Δ = +4 (1st Excursion)	54
3-50	Plastic Hinge in Specimen B2 at the End of the Test	55
3-51	Measured Lateral Load-Strain Hysteresis in Specimen B2 Longitudinal Bar	55
3-52	Measured Lateral Load-Strain in Specimen B2 Lateral Steel at SG 19	56
3-53	Measured Lateral Load-Strain in Specimen B2 Lateral Steel at SG 22	56
3-54	Measured Curvature Envelop along the Plastic Hinge of Specimen B2	57
4-1	Flexural Deflection of a Cantilever Column	60
4-2	Bending Moment and Curvature at Yield of Fixed End	61
4-3	Idealized Curvature at the Equivalent Plastic Hinge	61
4-4	Idealized Stress-Strain Curve of Main Steel	64
4-5	Unconfined Concrete Models	64
4-6	Confined Concrete Models for Specimens A1 and A2	65
4-7	Confined Concrete Models for Specimens B1 and B2	65

LIST OF TABLES

TABLE	TITLE	PAGE
1-1	Specimen Data of Previous Research	8
2-1	Calculated and Measured Ductilities of Square Columns	13
3-1	Lateral Steel Ratios inside Potential Plastic Hinge Regions of Test Specimens	18
3-2	Estimated Shear Demand and Shear Capacity of the Test Specimens	20
3-3	Measured Concrete Properties	24
3-4	Measured Steel Properties	24
3-5	Measured Displacements and Ductilities	33
3-6	Measured Lateral Loads, Yield Curvatures, and Plastic Hinge Lengths	57
4-1	Calculated Curvature	66
4-2	Calculated Equivalent Plastic Hinge Lengths	68
4-3	Calculated Ultimate Plastic Displacement, Δ_p	68
4-4	Calculated Beam Shear Deflections	69
4-5	Calculated Displacements and Ductilities-Modified Kent and Park Model	69
4-6	Calculated Displacements and Ductilities-Mander et al. Model	70
4-7	Measured and Calculated Displacements at Yield	71
4-7	Comparison of Measured and Calculated Displacements at Ultimate	71

SECTION 1
INTRODUCTION

1.1 Bridge Design Philosophy in Areas of High Seismic Risk

Structures in earthquake-prone areas should be designed to withstand strong earthquakes without collapse. For the majority of structures, it is often more economical to dissipate the large seismic energy through inelastic deformations. This can be accomplished by plastic hinging at predetermined locations of a structure.

Concrete bridge structures should remain functional after large earthquakes. This requires that bridge superstructures do not undergo plastic deformations and that bridges maintain their gravity load carrying capacities. Thus, inelastic deformations in concrete bridges should be accommodated through the formation of plastic hinges in the columns.

In the case of reinforced concrete bridge columns, it is necessary to allow for relatively large ductilities without sudden shear failure or significant strength degradation. It is well established that high ductilities could be achieved in reinforced concrete members by furnishing adequate lateral confinement steel. When properly detailed, lateral steel would provide higher ductilities, prevent premature buckling of main reinforcement, and avert shear failure.

1.2 Current Seismic Provisions

Different methods are available for the design of confinement reinforcement. A summary of the methods for the plastic hinge region of rectangular columns is presented in this section. Note that the required steel areas need to be satisfied for each orthogonal principal direction of the column section.

1.2.1 American Concrete Institute (ACI)

The American Concrete Institute (1992) provisions consider a structural member to be a column if the axial load index, $P_u/(f_c' A_g)$, exceeds 0.1 . Parameters P_u , f_c', and A_g are the factored axial load, concrete compressive strength, and the gross cross sectional area of the member, respectively. Bridge columns typically meet this requirement. The minimum total cross sectional area of rectangular hoops and cross ties is the greater of

$$A_{sh} = 0.3\, s\, h_c \frac{f_c'}{f_y}\left[\left(\frac{A_g}{A_{ch}}\right) - 1\right] \qquad (1\text{-}1)$$

and

$$A_{sh} = 0.09\, s\, h_c \frac{f_c'}{f_{yh}} \qquad (1\text{-}2)$$

where

s = spacing of transverse reinforcement along the axis of the member.
h_c = cross-sectional dimension of column core measured center-to-center of confining reinforcement.
A_g = gross area of section.
A_{ch} = cross-section area of a structural member measured out-to-out of transverse reinforcement.
f_{yh} = specified yield strength of transverse reinforcement.

The general purpose of the requirements is to improve ductility of concrete. The above equations intend to provide the same degree of confinement as that in spiral columns. In the ACI equation for spiral reinforcement, the lateral confining pressure provided by the spiral on the core concrete is based on axially loaded columns. The spiral is proportioned so that the compressive strength lost by the spalling of the cover concrete is equal to the additional compressive strength provided by the core concrete due to the lateral pressure exerted by the spiral when it is stressed to yield. Considering that ACI provisions are generally for building design, the applicability of the requirements to bridge columns is not addressed in the code. The spacing of lateral reinforcement is limited to the smaller of 100 millimeters (4 inches) or one-quarter of the minimum member dimension.

1.2.2 American Association of State Highway and Transportation Officials (AASHTO)

The current provisions of AASHTO (1992) are adopted from those of ACI. The lateral steel area is based on Equation 1-1, but Equation 1-2 has a coefficient of 0.12 instead of 0.09. The maximum spacing limits in AASHTO are the same as those in ACI.

1.2.3 California Department of Transportation (Caltrans)

The Caltrans (1983) provisions specify Equation 1-1 as one of two expressions for the minimum area of transverse reinforcement. The other equation is:

$$A_{sh} = 0.12\, s_t\, h_c \frac{f_c'}{f_y}\left(0.5 + 1.25 \frac{P_e}{f_c' A_g}\right) \qquad (1\text{-}3)$$

where

s_t = spacing of transverse reinforcement along the axis of the member.
P_e = axial load

Equation 1-3 acknowledges that tests have shown that confinement requirement should be a function of the magnitude of axial force. This equation is adopted from the New Zealand Code. A minimum spacing of 50 mm (2 in.) is specified for the transverse steel. The maximum spacing limit is the smallest of one-fifth of the column section dimension, 200 mm (8 in.), and six times the longitudinal bar diameter. The last limit is to prevent buckling of the column bars. These limits apply regardless of whether the lateral reinforcement is controlled by shear or confinement.

1.2.4 Paulay and Priestley

Based on research on bridge columns conducted at the University of Canterbury, New Zealand, Zahn et al. (1986) and Watson et al. (1994) derived an equation relating the amount of confinement steel in columns to the applied axial load and the required curvature ductility. Paulay and Priestley (1992) simplified the equation as follows

$$A_{sh} = k\, s\, h_c \frac{f_c'}{f_y} \frac{A_g}{A_c} \left(\frac{P}{f_c' A_g} - 0.08 \right) \tag{1-4}$$

where $k = 0.25$ for a required curvature ductility $\mu_\phi = 10$ and $k = 0.35$ when $\mu_\phi = 20$. Other values may be found by linear interpolation or extrapolation.

In addition to the axial load, this equation depends on the expected curvature ductility demand. The flexibility provided by including the ductility demand makes the expression useful for not only bridge columns which experience large drifts but also those which are in areas of moderate seismicity where the ductility demand may be lower. For low values of the axial load index, $P_u / (f_c' A_g)$, the confinement requirements become relatively small and shear will control the design. The maximum spacing of the confinement bars is limited to the smallest of one-third of the minimum column dimension, six times the longitudinal bar diameter, and 180 mm (7 in.).

1.2.5 New Zealand Code

The New Zealand code (1982) specifies the larger of steel area from two expressions both of which are functions of the axial load. The total area of transverse bars in each direction is the larger of

$$A_{sh} = 0.3\, s\, h_c \left(\frac{A_g}{A_c} - 1 \right) \frac{f_c'}{f_{yh}} \left(0.5 + \frac{1.25\, P_e}{\varphi f_c' A_g} \right) \tag{1-5}$$

and the steel area from Equation 1-3. These equations are similar to the AASHTO requirement except that they are modified by the factor which reflects the effect of axial load. The vertical spacing of the transverse steel is limited to the smallest of six longitudinal bar diameter, one-fifth of the minimum dimension of the column section, and 200 mm (8 in.).

1.2.6 Commission of the European Communities

A draft document for the seismic design of bridges was prepared in March 1994 by the Commission of the European Communities (1994). In this document, bridge piers with an axial load index of 0.08 are required to be detailed to provide concrete confinement in the plastic hinge region. A mechanical reinforcement ratio is defined for each direction of the column as follows:

$$\omega_{wd} = \rho_w \frac{f_{yd}}{f_{cd}} \tag{1-6}$$

where

ρ_w = transverse reinforcement ratio
= $A_{sw}/s.b$
A_{sw} = total area of hoops or ties in the one direction of confinement
b = dimension of the concrete core perpendicular to the direction of confinement under consideration, measured to the outside of the perimeter hoop
f_{yd} = design strength of longitudinal reinforcement
f_{cd} = concrete compressive design strength related to the specified compressive strength, f_c'

The reinforcement ratio is determined from

$$\omega_{wd} = 1.30\left(0.15 + 0.01\,\mu_c\right)\frac{A_c}{A_{cc}}\left(\eta_K - 0.08\right) \geq 0.08 \tag{1-7}$$

where

μ_c = required curvature ductility
A_c = gross concrete area of the section
A_{cc} = confined (core) concrete area of the section
η_k = normalized axial load
= $N_c/(A_c f_{ck})$
N_c = axial load
f_{ck} = characteristic concrete strength

The minimum amount of transverse ties is specified as

$$\frac{A_t}{s} = \frac{\Sigma A_s f_{ys}}{1.6 f_{yt}} \quad (mm^2/m) \tag{1-8}$$

where

A_t = area of one leg tie, mm^2
s = distance between tie legs, mm^2

ΣA_s = sum of the areas of the longitudinal bars restrained by the tie, mm^2
f_{yt} = yield strength of tie
f_{ys} = yield strength of the longitudinal reinforcement

The vertical spacing of the transverse steel is limited to the smaller of six longitudinal bar diameter and one-fifth of the minimum dimension of the column core section.

.2.7 Example Bridge Column

To compare the confinement steel designed based on different guidelines, a representative rectangular bridge columns was designed. The cross section of the column excluding the transverse reinforcement is shown in Figure 1-1. The longitudinal steel ratio in this column is approximately 2.2 percent. The concrete compressive strength was assumed at 27.6 MPa (4,000 psi) and the steel yield stress was assumed at 414 MPa (60,000 psi). The confinement steel ratio was determined as a function of the axial load ratio using different guidelines. The ACI and AASHTO minimum transverse steel requirements for gravity loads only were also included in the analysis.

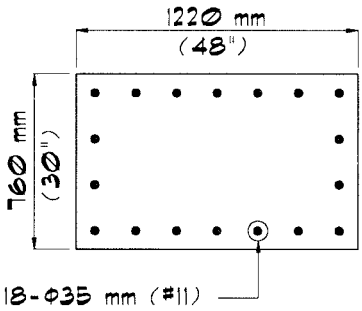

Figure 1-1 Cross Section of the Example Column

Figure 1-2 shows the results. The confinement steel ratios based on Paulay and Priestley's method are for an assumed column height of 6.1 m (20') and for displacement ductilities, μ_Δ, ranging from 2 to 8. Notice that the value of the multiplier k in Equation 1-4 depends on the curvature ductility. To present the plot of Equation 1-4 in terms of displacement ductility, a plastic hinge length of 610 mm (24") was assumed for the example column. The plastic hinge length is equivalent to one half the section depth as recommended by Paulay and Priestley (1992). For low values of axial load, shear and not confinement would control the amount of lateral reinforcement. Future provisions for some bridge columns which are located in areas of moderate seismicity could perhaps require reinforcement ratios which may be in between the gravity load design and the seismic design requirements. Note that the ACI and AASHTO requirements are independent of the level of axial load, whereas Caltrans results depend on the axial load level although to a lesser degree than the results based on Paulay and Priestley.

For the example column, it can be seen in Figure 1-2 that the lateral reinforcement ratio required by AASHTO for seismic design is 33 percent more than that required by ACI. Moreover, for an axial load index of less than 0.4 which is typical in bridge columns, AASHTO seismic specifications require more transverse steel than that required by Caltrans. The difference between AASHTO and Caltrans requirements decreases as the axial load index approaches 0.4. At relatively low axial loads, the equation given by Paulay and Priestley results in a reinforcement ratio that is considerably less than those required by the codes. For instance, at an axial load index of 0.2 and a displacement ductility of 8, the calculated lateral steel ratio for the example column according to the equation by Paulay and Priestley is 33 percent less than the minimum ratio required by either ACI or Caltrans and 50 percent less than the minimum ratio required by AASHTO.

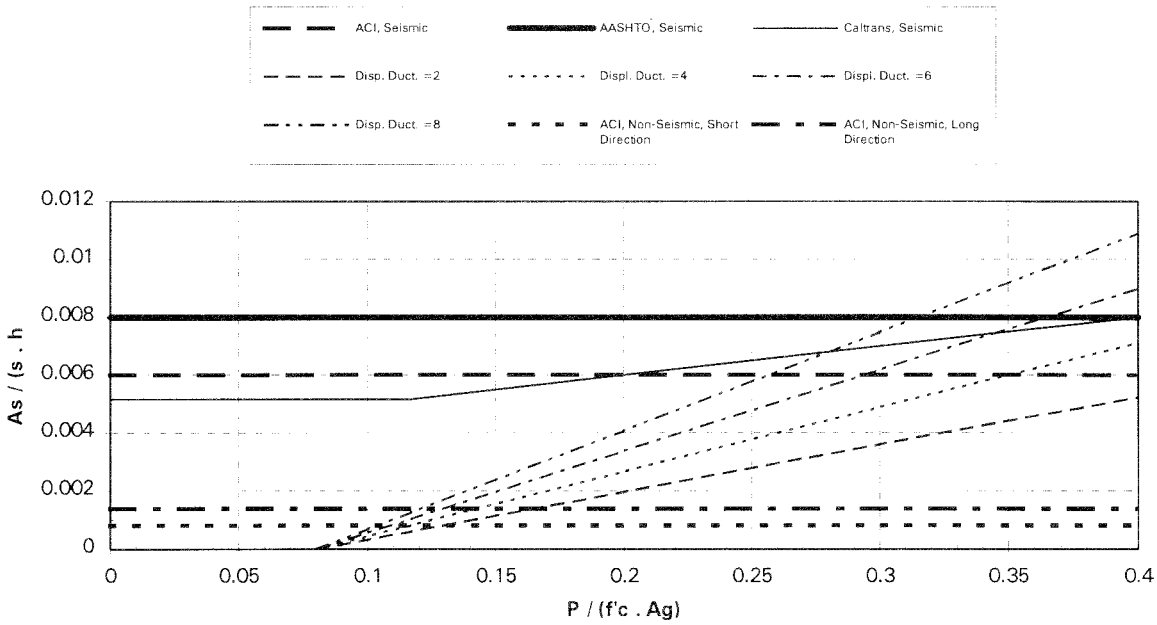

Figure 1-2 Confinement Steel Requirements for Different Design Methods

1.3 Review of Previous Works

Because of the apparent similarity of the confinement provided by square ties to that of the rectangular ties and due to a lack of experimental data on the earthquake response of rectangular columns, a review of previous cyclic load tests of square columns with rectilinear ties and cross ties was conducted (Azizinamini et al, 1992, Ozcebe et al., 1987, Park et al., 1982, Priestley et al., 1987, Sheikh et al., 1993 and Soesianawati et al, 1987). Figure 1-3 shows a summary of the peak displacement ductilities in terms of the axial load index, $P_u / (f_c' A_g)$, where P_u, f_c', and A_g are the applied axial load, concrete compressive strength, and the gross cross sectional area of the member. The numbers in the figure refer to the names of the first authors of the publications from which the data were obtained. The ductilities are the maximum values attained by specimen failure or by terminating the test. Table 1-1 presents the main data from each reference. It can be seen that the

material properties are generally in the range of the values used in bridge columns, and the dimensions may be thought of as being one-fourth to one-half scaled representation of prototype bridge columns. The longitudinal steel ratios in the specimens tested by Ozcebe and Sheikh are somewhat larger than what is usually used in bridge columns.

The axial load ratio for bridge columns is typically less than 0.3. It can be noted in Figure 1-3 that for moderate ductility demand of the order of 2 to 4, and for columns with a relatively small axial load ratio, very little data are available on specimens with rectilinear transverse steel. This is particularly true in light of the fact that the data points marked by "4" are for columns with a longitudinal steel ratio which is higher than that of bridge columns.

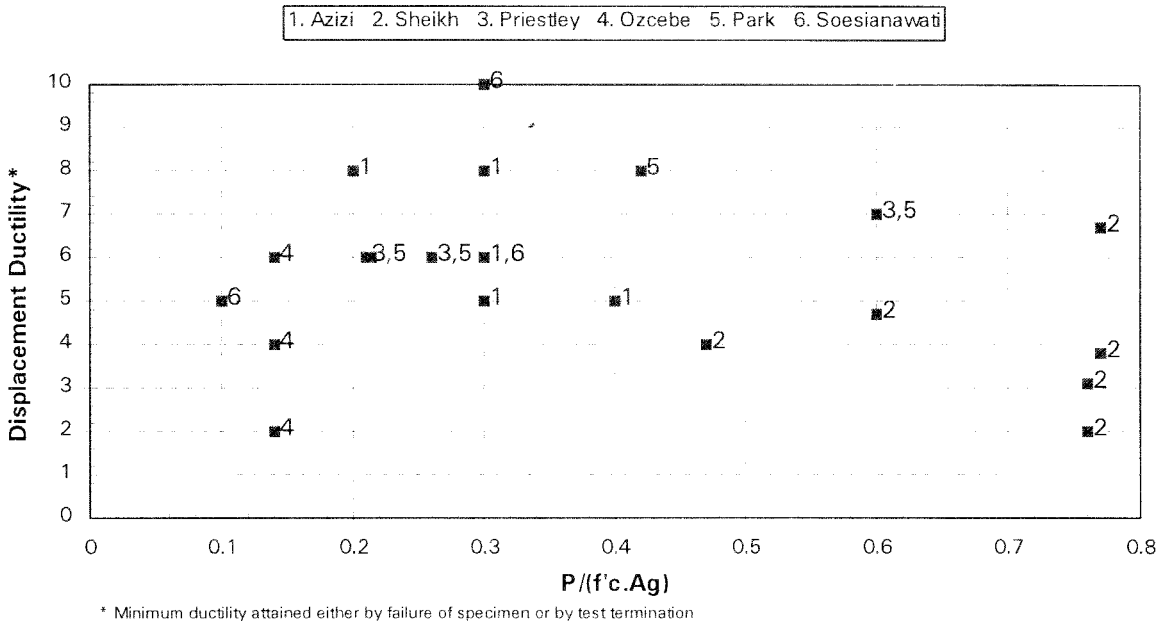

Figure 1-3 Available Test Data for Cyclic Response of Square Columns

1.4 Objective and Scope

The objective of this study was to investigate the ductility of reinforced concrete bridge columns and develop detailing guidelines for areas of moderate seismicity. Because it was observed that the amount of test data on circular and square columns may be sufficient, the focus of the research was on rectangular columns. To investigate moderate ductilities of rectangular bridge columns, the effect of limited lateral reinforcement below the minimum required by current codes for seismic design was studied experimentally and analytically.

Four half-scaled rectangular bridge columns were built and tested. The geometrical dimensions and the amount of longitudinal reinforcement were kept the same for all specimens. Based on the amount of lateral confinement, the specimens were divided into two groups, Group I (Specimens A1

and A2) and Group II (Specimens B1 and B2). The lateral confinement for the specimens in Group I and Group II corresponded to approximately 40 percent and 60 percent, respectively, of the current AASHTO seismic requirement. The column specimens were tested under constant vertical axial loads representing the dead load of the superstructure. Columns A1 and B1 were each subjected to an axial load of $0.1 f'_c A_g$. For columns A2 and B2, the axial load was increased to $0.25 f'_c A_g$. The specimens were subjected to cyclic lateral loads with increasing drift levels. Bending was about the strong axis of the columns.

Table 1-1 Specimen Data of Previous Research

Specimen	Lateral Steel Ratio ρ_t, %	Lateral Steel Yield Strength f_{yh}, MPa (Ksi)	Longitudinal Steel Ratio ρ_l, %	Axial Load % of $f_c' A_g$	Displacement Ductility μ_Δ
Azizi	2.35	414 (60)	1.95	20	8
	1.29	414 (60)	1.95	30	5
Priestley	1.5	297 (43)	1.79	26	6
	3.5	297 (43)	1.79	60	7
Ozcebe	1.69	470 (63.5)	3.32	15	2
	1.95	425 (61.6)	3.32	15	>6.5
Park	2.3	316 (45.8)	1.79	21	>6
	2	297 (43.1)	1.79	42	8
Soesianawati	0.84	364 (53)	1.51	10	10
	0.9	364 (53)	1.51	30	≤6

SECTION 2
DUCTILITY OF REINFORCED CONCRETE COLUMNS

2.1 Introductory Remarks

Ductility of a structural member can be described as the ability of that member to deform beyond the elastic limit without significant strength degradation. Ductility is usually defined as the ratio of ultimate deformation to yield deformation. Thus, curvature ductility μ_φ of a section is the ratio φ_u/φ_y where φ_u and φ_y are the ultimate and yield curvatures, respectively. Similarly, displacement ductility, μ_Δ, is the ratio of the displacement at ultimate to the displacement at yield, Δ_u/Δ_y .

As mentioned earlier, ductility of bridge columns is essential in seismic design of bridges. The formation of plastic hinges in bridge columns allows for the dissipation of seismic energy through inelastic deformation and prompts the bridge system to "attract" smaller lateral loads under earthquake motion.

The ability of reinforced concrete columns to deform beyond the elastic limit and the column ultimate deformation capacity depend mainly on the level of confinement of the core concrete. The confinement provided by lateral hoops and cross ties delays the spalling of the core concrete and allows concrete to attain higher strains.

2.2 Concrete Stress-Strain Models

To calculate the failure displacement, a representative constitutive model for concrete is needed. The primary features of the stress-strain relationship for concrete are the peak stress and the failure strain. Other parameters such as the shape of the stress-strain relationship do not generally affect the outcome (Paulay and Priestley, 1992). The peak stress and the failure strain are both sensitive to the amount and distribution of the confinement steel. Many models have been developed for the constitutive relationship of confined concrete, the majority of which are based on compression loading of test specimens (Kent and Park, 1971, Mander et al, 1988, Saatcioglu and Razvi, 1992, and Sheikh and Uzumeri, 1982).

Based on a review of different models and their applicability to rectangular hoops, two confinement relationships, the modified Kent and Park (1971) and the other by Mander et al. (1988), were selected for this study. Compared to the test data on square columns described in previous sections, these models appear to provide the upper and lower bound estimates of displacement ductilities. These models are briefly described herein.

2.2.1 Modified Kent and Park (1971)

In this model, strength and ductility of core concrete are enhanced by the confinement provided by transverse hoops. The model consists of an ascending parabolic branch and a descending straight branch. The concrete strength, $K f_c'$, is reached at a strain of $0.002K$. K is defined in Equation 2-2.

The stress-strain relationship is

(i) For $\epsilon_c \leq 0.002K$:

$$f_c = Kf_c' \left[\frac{2\epsilon_c}{0.002K} - \left(\frac{\epsilon_c}{0.002K} \right)^2 \right] \tag{2-1}$$

$$K = 1 + \frac{\rho_s f_{yh}}{f_c'} \tag{2-2}$$

(ii) For $\epsilon_c > 0.002K$:

$$f_c = Kf_c' \left[1 - Z_m \left(\epsilon_c - 0.002K \right) \right] \geq 0.2Kf_c' \tag{2-3}$$

$$Z_m = \frac{0.5}{\frac{3 + 0.26f_c'}{145f_c' - 1000} + \frac{3}{4}\rho_s \sqrt{\frac{h''}{s_h}} - 0.002K} \quad \text{(MPa)} \tag{2-4}$$

where:

ϵ_c = strain of confined concrete
f_c = stress of confined concrete
f_c' = unconfined concrete compressive strength
f_{yh} = yield stress of the confining steel
ρ_s = lateral steel volumetric ratio measured to outside of hoops
h'' = width of confined core measured to outside of hoops
s_h = center to center spacing of hoop sets

2.2.2 Mander et al. (1988) as Modified by Paulay and Priestley (1992)

In this model, the strength of confined concrete, f_{cc}', is related to the confining pressure, f_l', provided by the lateral reinforcement. For circular sections, or square sections of equal confining steel in both directions, the confined concrete strength is

$$f_{cc}' = f_c' \left(-1.254 + 2.254 \sqrt{1 + \frac{7.94f_l'}{f_c'}} - \frac{2f_l'}{f_c'} \right) \tag{2-5}$$

where:

f_c' = unconfined concrete compressive strength

For a rectangular section with unequal lateral steel ratios along the depth and the width of the cross section (x and y directions), the confining pressures f_{lx}' and f_{ly}', in the x and y directions, respectively, can be found as follows

$$f_{lx}' = K_{ex}\rho_x f_{yh} \tag{2-6}$$

$$f_{ly}' = K_{ey}\rho_y f_{yh} \tag{2-7}$$

where

K_{ex} = confinement effectiveness coefficient in the x direction
K_{ey} = confinement effectiveness coefficient in the y direction
ρ_x = volumetric ratio of lateral steel in the x direction
ρ_y = volumetric ratio of lateral steel in the y direction
f_{yh} = yield stress of lateral steel

Once the confining pressures in both directions are found, the confined concrete strength can be found from a set of curves. Those curves were based on multiaxial failure criterion and were verified by comparing the solution to triaxial tests results.

The strain, ϵ_{cc}, at maximum stress is given by

$$\epsilon_{cc} = 0.002\left[1 + 5\left(\frac{f_{cc}'}{f_c'} - 1\right)\right] \tag{2-8}$$

To find the ultimate strain of concrete at failure, Mander et al. applied a strain energy approach. In this method, the longitudinal compressive concrete strain at failure corresponds to the first fracture in the hoops. In addition to the monotonic stress-strain model, Mander et al. also presented a stress-strain relationship for confined concrete under cyclic loading including the effect of strain rate on the stress-strain curves. A detailed description of the model is presented in Mander et al., 1988.

Paulay and Priestley (1992) adopted a modified version of the Mander et al. model to represent the stress-strain behavior of confined concrete under monotonic loading. In the modified model, the stress-strain curve, confined strength, and strain at confined strength are kept the same as in the original model. However, the modified model prescribes a lower (conservative) ultimate concrete compression strain as follows

$$\epsilon_{cu} = 0.004 + \frac{1.4\rho_s f_{yh}\epsilon_{sm}}{f_{cc}'} \tag{2-9}$$

where

ϵ_{sm} = steel strain at maximum tensile stress

Moreover, Paulay and Priestley suggested a confinement coefficient k_e of 0.95 for circular columns, 0.75 for rectangular columns, and 0.60 for rectangular walls.

2.3 Verification and Comparison of Concrete Models

The displacement ductility of the selected square test specimens that were presented in Section 1.3 was calculated based on the confined concrete models described in the previous sections. Those columns were selected for the analysis because of their relatively low axial load index which would be representative of axial load index in bridge columns. Measured concrete and steel properties were used when they were reported. Otherwise, the specified values were used. The "yield" displacement was calculated by including the rigid body rotation of the columns due to bond slip. The bond strength was assumed to be $20\sqrt{f_c'}/d_b$ (MPa) (Leet, 1991). The plastic hinge length was assumed to be that recommended by Paulay and Priestley (1992) as follows

$$l_p = 0.08l + 0.022 d_b f_y \text{ (MPa)} \qquad (2\text{-}10)$$

where

l_p = plastic hinge length
l = length from maximum bending moment to inflection point
d_b = diameter of longitudinal bar
f_y = yield stress of longitudinal reinforcement

Equation 2-10 is based on tests of reinforced concrete columns, and it implicitly accounts for the effect of bond slip.

Comparison of calculated and measured ductilities for the selected tests are presented in Table 2-1. A ">" in the measured column indicates that the specimen did not necessarily fail at that ductility level. The "<" for the last specimen indicates that the ductility of 6 was accomplished only for one cycle followed by a drastic strength degradation.

The first specimen shown for Ozcebe was reinforced only with perimeter tie bars which is not representative of the current practice. Concrete constitutive models implicitly assume that the lateral bars are distributed within the section. As expected, the measured ductility capacity of this specimen was very low. A comparison of the measured and calculated ductilities shows that the measured values were generally within the limits predicted by Mander et al., as modified by Paulay and Priestley, and the modified Kent and Park. The modified Kent and Park model led to upper bound estimates of ductilities. The results suggest that the Modified Mander model would provide a reasonable and a lower bound estimate of the displacement ductilities.

Table 2-1 Calculated and Measured Ductilities of Square Columns

Specimen	μ_Δ[1]	μ_Δ[2]	μ_Δ[3]
Azizi	6.6	13.7	8
	3.7	5.6	5
Priestley	5.9	10.4	6
	4.1	11.6	7
Ozcebe	8.6	12.6	2
	8.7	15.7	>6.5
Park	3.2	9.5	>6
	2.5	7.3	8
Soesianawati	5.6	9.6	10
	2.5	4.0	≤6

[1] Modified Mander et al.
[2] Modified Kent and Park
[3] Measured

SECTION 3
EXPERIMENTAL STUDIES

3.1 Introduction

Four half-scale rectangular bridge columns were designed, constructed, and tested in the course of this research. The objective of the tests was to determine the ductility capacity of newly constructed columns with moderate amount of confining steel. Two parameters were varied in this study: the transverse steel reinforcement amount and the axial load level. Each specimen was tested under constant axial load while subjected to lateral load reversals in the strong direction of the column.

The specimens were designed to attain moderate ductility capacities before significant reduction in strength. To accomplish this, reduced amounts of confining steel below that required by the codes (AASHTO 1992 and Caltrans 1983) for bridge seismic design were selected. Based on the maximum lateral loads expected to be reached during the tests, the selected amounts of transverse steel were checked to ensure that the shear capacity of each specimen exceeded the corresponding shear demand to prevent shear failure. Other details pertaining to lateral and vertical spacing of ties, minimum size of tie bars, and extension of standard hooks were maintained according to code requirements.

3.2 Design of Test Specimens

The column specimens were designed to represent half-scale models of the prototype rectangular column discussed in Section 1.2.5 of this report. The columns were supported by rectangular footings which would transfer the applied loads to the strong floor of the testing laboratory. Rocking of the footing under lateral loads was prevented by tie-downs holding the footing to the floor. Each column was assumed fixed at the bottom end where it connected to the footing and hinged at the top end where the lateral load was to be applied. The loading point represented the column inflection point. Figures 3-1 and 3-2 present the final design of the test specimens in Group I and Group II, respectively. The following sections are the steps taken in designing the test specimens.

3.2.1 Column Cross Section

All four specimens had the same cross sectional dimensions and identical longitudinal reinforcement. Each test column was 380 millimeters (15 in.) wide by 610 mm (24 in.) deep and was reinforced with 18- ϕ19 mm (#6) bars, resulting in longitudinal reinforcement ratio, ρ_l, of 2.2%. The specified concrete compressive strength and steel yield stress were 27.6 MPa (4,000 psi) and 414 MPa (60,000 psi), respectively.

3.2.2 Column Height

To determine the height of the column specimens, two main factors were considered: the prototype height and the constraints of the testing facility. A height of 2050 mm (6.7 ft) was selected for the

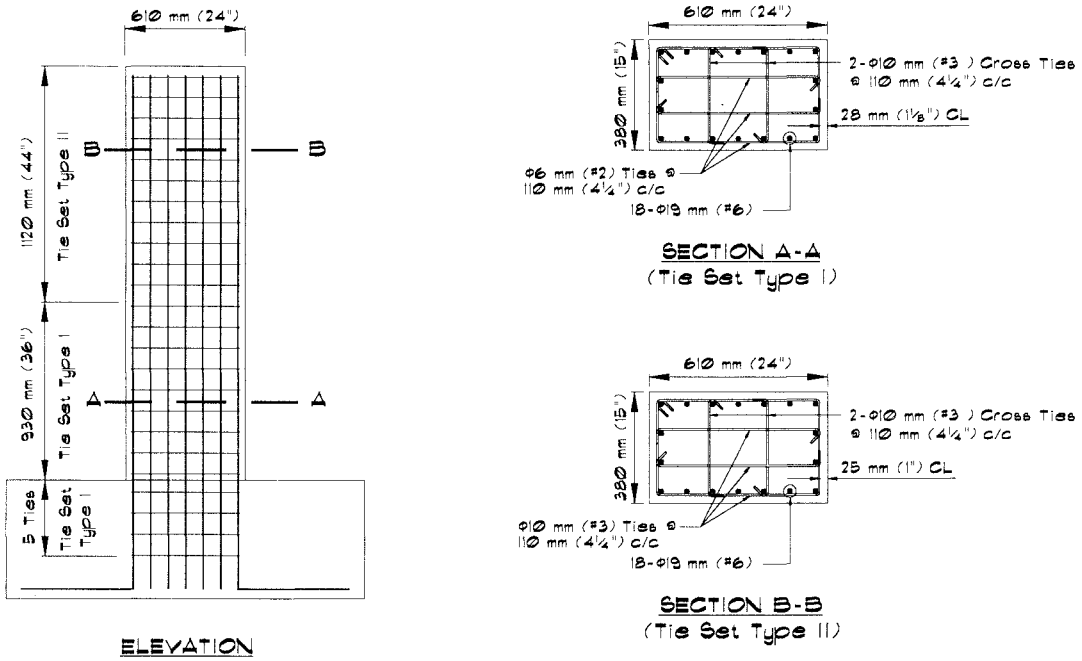

Figure 3-1 Column Details for Specimens in Group I

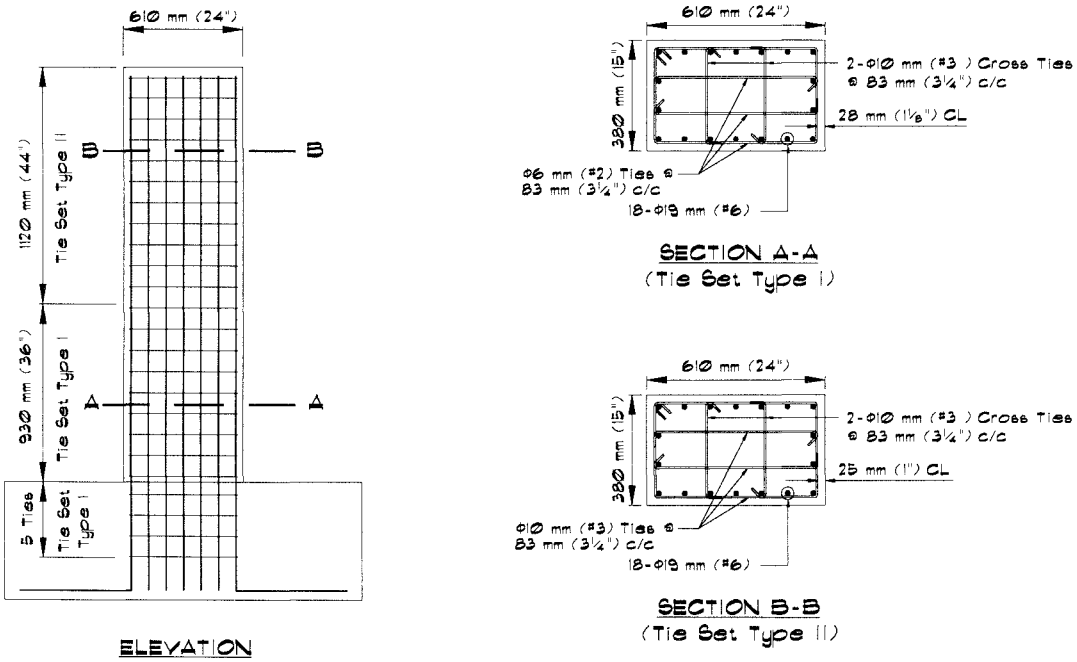

Figure 3-2 Column Details for Specimens in Group II

column specimen. The loading assembly at the top of the specimen increased the moment arm by 305 mm (12 in.), thus making the height from the horizontal loading point to the top of the footing 2355 mm (7.7 ft). For bridge columns bending in single curvature under lateral loads, this height would correspond to a prototype column height of approximately 4700 mm (15 ft). For columns which bend in double curvature, the corresponding full-scale column height would be approximately 9400 mm (30 ft).

3.2.3 Transverse Reinforcement

To design transverse reinforcement in the potential plastic hinge zone, the minimum amount required by AASHTO was first calculated according to Section 1.2.2 of this report. Based on Equations 1-1 and 1-2 with a modified coefficient of 0.12, it was found that the minimum required lateral steel ratio $A_{sh}/(s \cdot h_c)$, would be 0.008. For a transverse steel ratio of 0.004 (one-half of AASHTO requirement) and an axial load index of 0.25, Equation 1-4 given by Paulay and Priestley would predict a moderate displacement ductility of about four as can be seen in Figure 1-2. Based on this analysis, it was decided to furnish the test specimens with lateral confinement ratios in the vicinity of one-half of the minimum AASHTO requirement.

To prevent premature buckling of longitudinal bars, an upper limit on hoop set spacing, s, was set at six times the longitudinal bar diameter ($6\,d_b$) resulting in a limit of 114 mm (4.5 in.). Each tie set in the potential plastic hinge zone of the test specimens consisted of 1- ϕ 6 mm (#2) perimeter hoop, 2- ϕ 6 mm (#2) cross ties in the long direction, and 2- ϕ 10 mm (#3) cross ties in the short direction (Figures 3-1 and 3-2). Such arrangement allowed for the engagement of all longitudinal bars along the short side of the column, and every other longitudinal bar along the long side of the column. The perimeter tie free ends were 135° bends whereas the cross tie had 135° bend on one end and 90° bend on the other. In all cases the bend extension was equivalent to ten times the bar diameter. A scaled down concrete cover of 28 mm (1⅛ in.) was employed. For the specimens in Group I (Specimens A1 and A2) the tie set spacing was set at 110 mm (4.25 in.) corresponding to a transverse reinforcement ratio in the long direction of 0.0033 or 42 percent of the minimum confinement steel required by AASHTO. In Group II (Specimens B1 and B2) the spacing of the tie sets was reduced to 83 mm (3.25 in.) resulting in a transverse reinforcement ratio in the long direction of 0.0043 or 54 percent of the minimum AASHTO requirement. In the short direction, the lateral steel reinforcement ratios were 0.0034 and 0.0044 for specimens in Group I and Group II, respectively. These ratios correspond to 42 percent and 55 percent of the minimum requirement by AASHTO. The lateral steel ratios for the test specimens inside the potential plastic hinge regions are presented in Table 3-1.

Based on the described transverse steel arrangements, the shear capacities inside the plastic hinge region of the test specimens were calculated and compared with the shear demands. The nominal shear capacity, V_n, was found from the following equation (AASHTO 1992):

$$V_n = V_c + V_s \tag{3-1}$$

where

V_c = concrete nominal shear capacity

V_s = steel nominal shear capacity

V_s is given by

$$V_s = \frac{A_v f_y d}{s} \tag{3-2}$$

where

A_v = area of shear reinforcement
f_y = yield strength of shear reinforcement
d = distance from extreme compression fiber to centroid of tension reinforcement
s = spacing of shear reinforcement in direction parallel to main reinforcement

Table 3-1 Lateral Steel Ratios inside Potential Plastic Hinge Regions of Test Specimens

Specimen	Lateral Steel Ratio $A_{sh}/(s.h_c)$	
	Long Direction	Short Direction
Group I (Specimens A1 & A2)	0.0033	0.0034
Group II (Specimens B1 & B2)	0.0043	0.0044

When plastic hinging occurs, the nominal shear capacity of concrete is reduced due to the formation of flexural-shear cracks and is in inverse proportion to the ductility level. Consequently, the code equations (1) to calculate V_c for non-seismic loads are not applicable. A method used by Caltrans (Bridge Memo 20-4) relates V_c to the level of confinement, ductility ratio, and the applied axial load as follows

$$V_c = 0.083\,(F_1)(F_2)\sqrt{f_c'}\,A_e \le 0.332\sqrt{f_c'}\,A_e \quad (MPa) \tag{3-3}$$

$$V_c = (F_1)(F_2)\sqrt{f_c'}\,A_e \le 4\sqrt{f_c'}\,A_e \quad (psi) \tag{3-4}$$

where

F_1 : factor that is proportional to the level of confinement and inversely proportional to the ductility ratio. It ranges between 0.3 and 1.0

F_2 : factor that depends on the applied compressive axial stress. It ranges between 1.0 for zero axial stress and 1.5 for a compressive stress of 6.9 MPa (1000 psi)

A_e = effective concrete area which is equal to 80% of the gross cross sectional area of the column

Priestley et al. (1994) presented a different model to calculate the shear capacity. According to this model, the shear resistance is provided by three components as follows

$$V_n = V_c + V_t + V_p \tag{3-5}$$

where

V_c = shear force carried by concrete

V_t = shear force carried by truss action (lateral reinforcement)

V_p = lateral component of compression strut in the column due to the applied compressive axial load

Priestley's method is adopted in the "Seismic Retrofitting Manual for Highway Bridges" (1995) with a simplified term for V_p. In the "Seismic Retrofitting Manual for Highway Bridges," the shear capacity components for rectangular columns are obtained as follows

$$V_c = v_c A_e \tag{3-6}$$

$$V_s = \frac{A_v f_y d}{s} \cot \theta \tag{3-7}$$

$$V_p = 0.2 P \tag{3-8}$$

A_v, f_y, d, s, and A_e are the same as those defined in Equations 3-2 and 3-3. θ is the angle between the column axis and the diagonal concrete compression strut (θ is considered 45° in ACI-318). v_c depends on the attained ductility of a cross section and is obtained as follows

(i) For non-ductile regions and for plastic hinge regions where the displacement ductility of the column $\mu_\Delta \leq 2$:

$$v_c = 0.29 \sqrt{f_c'} \quad (MPa) \qquad = 3.5 \sqrt{f_c'} \quad (psi) \tag{3-9}$$

(ii) For plastic hinge regions where the displacement ductility of the column $\mu_\Delta \geq 4$:

$$v_c = 0.1\sqrt{f_c'} \quad (MPa) \qquad = 1.2\sqrt{f_c'} \quad (psi) \tag{3-10}$$

(iii) For displacement ductilities between 2 and 4, a linear interpolation is used.

To estimate the shear demand, the nominal moment capacity of each specimen was first calculated. The nominal moment capacity is defined as the moment capacity of a concrete member without taking into consideration the over strength due to confinement (14). Considering that the specimens were moderately confined, the over strength factor was assumed to be 20%. Having the over strength moment capacity and the moment arm, the shear demand was calculated and compared to the shear capacity (Table 3-2). It was found that the specimens would be safe in shear.

Table 3-2 Estimated* Shear Demand and Shear Capacity of the Test Specimens

	Shear Capacity (Caltrans) kN (Kips)			Shear Capacity (FHWA Retrofit Manual) kN (Kips)				Shear Demand kN (Kips)
Specimen	V_s	V_c	V_n	V_s**	V_c	V_p	V_n	V
A1	246 (55.3)	100 (22.5)	346 (77.8)	246 (55.3)	151 (21.9)	199 (28.8)	596 (106.0)	323 (72.6)
A2	246 (55.3)	125 (28.1)	371 (83.4)	246 (55.3)	151 (21.9)	497 (72.0)	894 (149.2)	368 (82.7)
B1	322 (72.3)	100 (22.5)	422 (94.8)	322 (72.3)	151 (21.9)	199 (28.8)	672 (123.0)	323 (72.6)
B2	322 (72.3)	125 (28.1)	447 (100.4)	322 (72.3)	151 (21.9)	497 (72.0)	970 (166.2)	368 (82.7)

* Based on specified material properties ** Based on $\theta = 45°$

3.2.4 Footing Design

The reinforced concrete footings were designed such that no flexural yielding and/or shear failure would occur under the estimated extreme loading conditions. For ease of construction and setup, a uniform footing design was adopted for all four specimens. The specified concrete compressive strength and the steel yield stress were 27.6 MPa (4,000 psi) and 414 MPa (60,000 psi), respectively. Each footing was 2.44 meters (8 feet) long by 1.83 m (6 ft) wide by 0.71 m (2.33 ft) deep. Since rocking was prevented by means of tie-downs, the footing was designed for positive and negative bending moments in both directions. Flexural reinforcement consisted of identical top and bottom steel mats. Each mat comprised 8- ϕ 25 mm (#8) bars in the long direction and 10- ϕ 25 mm (#8) bars in the short direction. The bar ends consisted of a 90° bent plus a 405 mm (16 in.) extension. The concrete cover was 75 mm (3 in.) on all sides. Shear reinforcement was not provided in the footings because it was found that the nominal shear capacity of the footing concrete exceeded the shear demand. A typical footing is shown in Figure 3-3.

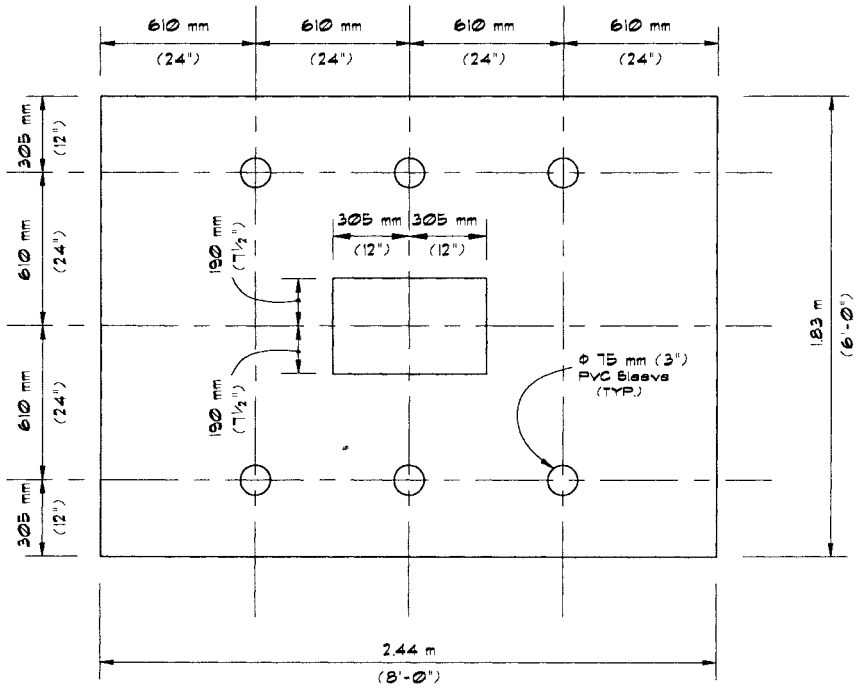

Figure 3-3 Footing Details of the Test Specimens

3.3 Construction of Test Specimens

The specimens were built in pairs at the laboratory. The footings were constructed on a flat plywood platform to provide a smooth bottom surface and to protect the concrete floor of the laboratory.

The footing form was erected then a layer of form release oil was applied to the plywood surfaces that would be in contact with concrete. The pre-assembled bottom mat of the footing reinforcing steel cage was lifted and placed inside the mould. To facilitate the placement of column ties inside the footing, the column main reinforcement was installed before placing the footing top steel mat. Although the footing depth was ample to develop the column main bars, all embedded column bar ends inside the footings were provided with 90° bends and 250 mm (10 in.) extensions for added anchorage and ease of construction. Prior to pouring concrete, six- ϕ 75 mm (3 in.) by 740 mm (28 in.) long plastic sleeves were placed vertically inside the footing mould to allow for the passage of tie-down and axial load Dywidag™ bars later during the test.

The concrete was ready mixed and was supplied by a local batch plant. Concrete slump was always measured prior to pouring. Slump measures are reported in Section 3.4 of this report. The footing concrete was poured and vibrated in 350 mm (13 in.) lifts then the surface of the footing was troweled to a smooth finish. Nine 150 mm (6 in.) diameter by 300 mm (12 in.) concrete cylinders were sampled for every footing. The footings were moisture cured for seven days.

The column steel cage was completed by tying the transverse steel around the main bars extending from the footing then the column forms were fitted in place. Figure 3-4 presents a completed steel cage prior to pouring of footing concrete. To facilitate the installation of LVDT's (linear variable differential transformers) along the potential plastic hinge length, five pairs of ϕ 6 mm (0.25 in.) by 710 mm (28 in.) long galvanized threaded rods were placed horizontally through the mould. The rods were positioned parallel to the long side of the column at predetermined height intervals and they extended about 50 mm (2 in.) outside the column face at both ends. Plastic cones were fitted at both ends of each rod to form cavities in the cover concrete around the rods. This was needed to prevent deviations in the LVDT readings during spalling of the column cover concrete. Four ϕ 35 mm ($1^3/_8$ in.) A325 anchor bolts were placed vertically at the top of the column mould to allow for the hook up of the loading mechanism. For added anchorage, the bolts were fully threaded and were fitted with 100 mm x 75 mm x 6 mm (4 in. x 3 in. x 0.5 in.) anchor plates at the embedded ends. Each bolt had a 530 mm (21 in) embedded length and 100 mm (4 in.) extension above the top of the column. The column concrete was placed and vibrated in 460 mm (18 in.) lifts, then moisture cured for seven days. Similar to the footings, nine concrete test cylinders were taken for each column.

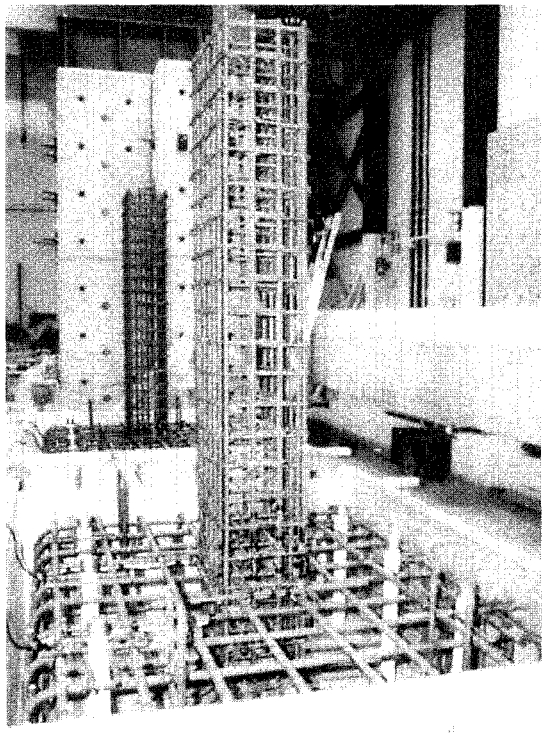

Figure 3-4 Reinforcement Cage of a Test Specimen

3.4 Material Properties

In order to evaluate the column test results, material tests were carried out to determine the actual material properties of concrete and steel.

The concrete compressive strength was obtained from compression tests of the concrete cylinders. For each batch, sets of three cylinders were tested at seven days, twenty eight days, and on the day of testing of the column specimen. Concrete slump and compressive strength results are presented in Table 3-3.

Table 3-3 Measured Concrete Properties

Specimen	Concrete Location	Concrete Slump mm (in.)	Concrete Strength*, f_c' MPa (Ksi)
A1 A2	Footing	38 (1.5)	31.7 (4.60)
	Column	50 (2)	27.2 (3.95)
B1 B2	Footing	50 (2)	29.7 (4.30)
	Column	50 (2)	28.1 (4.08)

* Average values on the day of testing

Tensile tests of the reinforcing steel were carried out for bar sizes ϕ 6 mm (#2), ϕ 10 mm (#3), and ϕ 19 mm (#6). For each bar size, three specimens were tested. Figures 3-5 to 3-7 present the measured stress-strain relationships for bar sizes ϕ 6 mm, ϕ 10 mm, and ϕ 19 mm, respectively. The average measured stress-strain values of the three bar sizes are shown on the same plot in Figure 3-8 and the average measured steel properties are also summarized in Table 3-4.

Table 3-4 Measured Steel Properties

Bar Size	@ Yield		@ Ultimate	
	ϵ_y	f_y, MPa (Ksi)	ϵ_u	f_u, MPa (Ksi)
ϕ 6 mm (#2)	0.0023	455 (66)	0.160	676 (98)
ϕ 10 mm (#3)	0.0021	428 (62)	0.121	738 (107)
ϕ 19 mm (#6)	0.0022	448 (65)	0.110	731 (106)

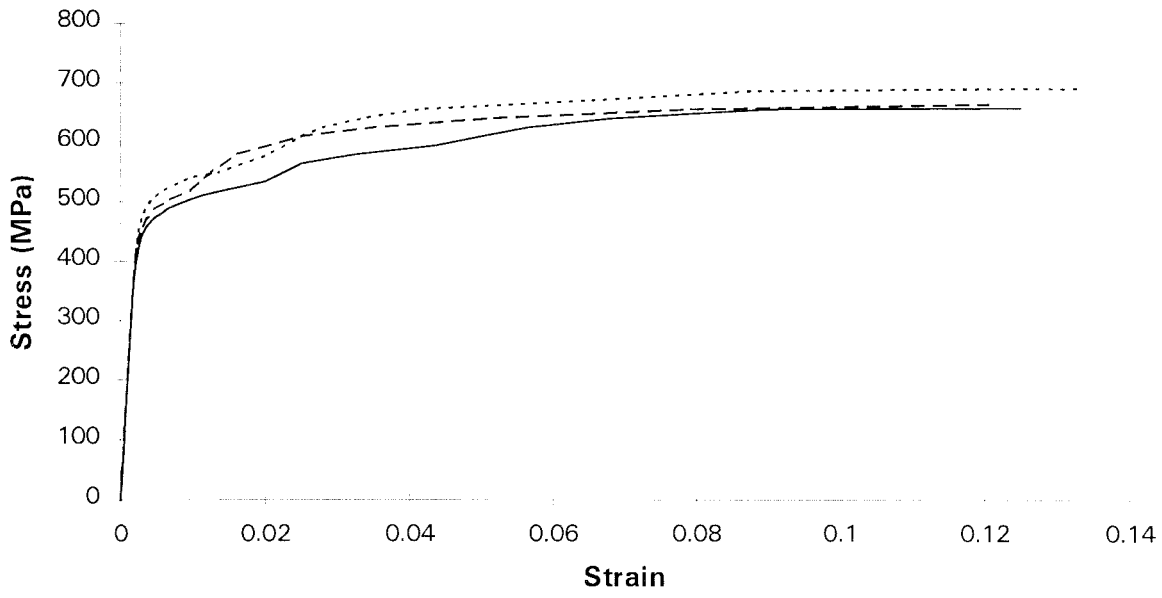

Figure 3-5 Measured Stress-Strain Relationship of ϕ 6 mm (#2) Steel Bars

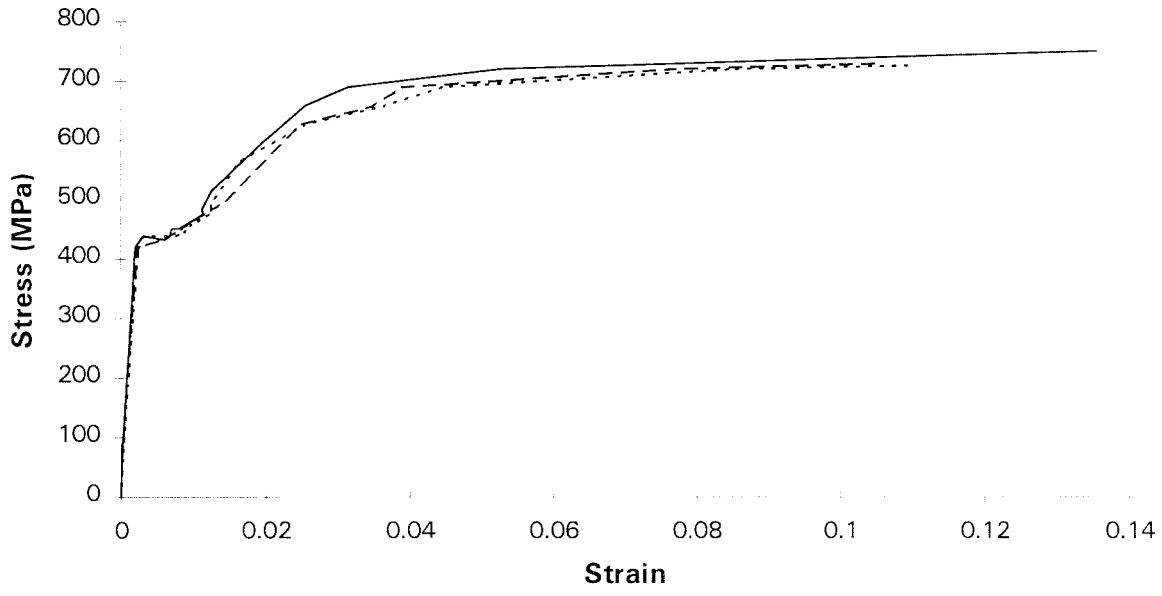

Figure 3-6 Measured Stress-Strain Relationship of ϕ 10 mm (#3) Steel Bars

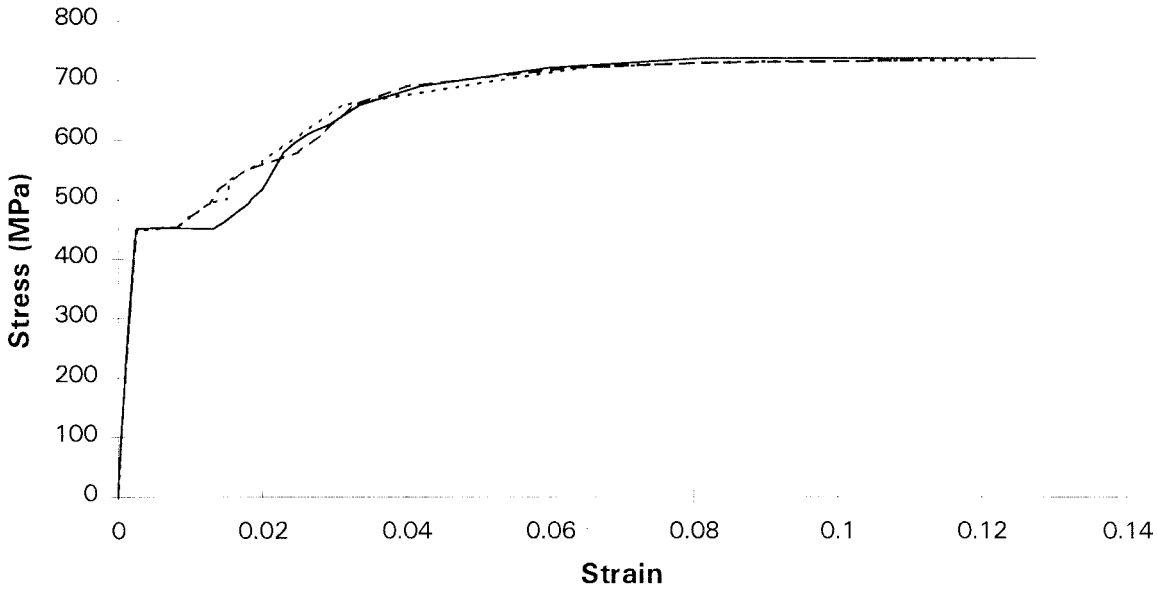

Figure 3-7 Measured Stress-Strain Relationship of ϕ 19 mm (#6) Steel Bars

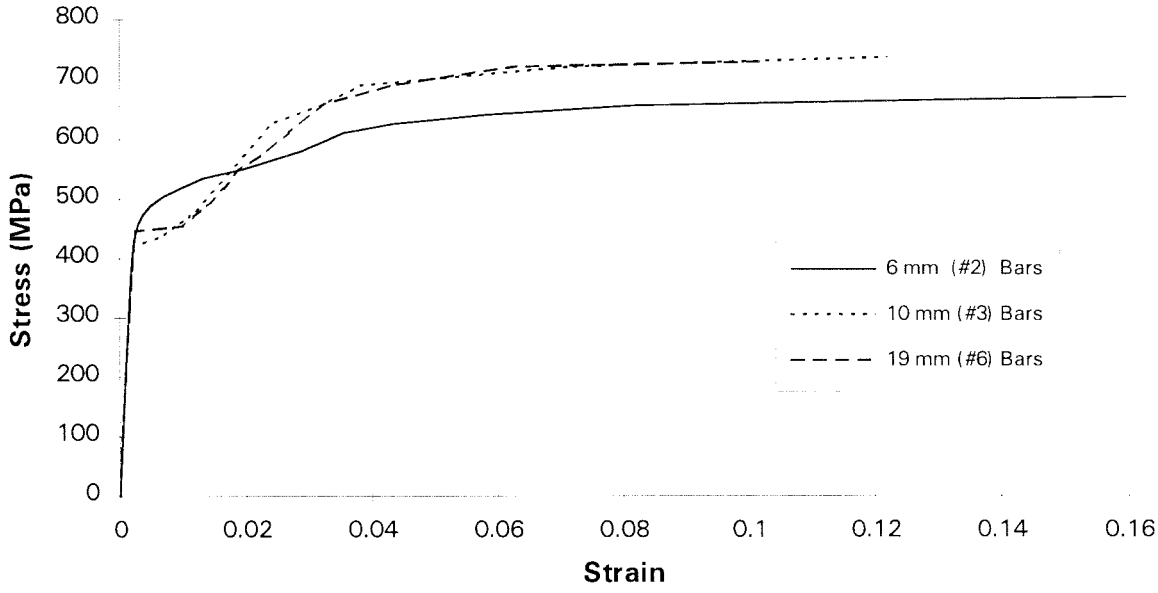

Figure 3-8 Averaged Measured Properties of Steel Bars

3.5 Instrumentation

The specimens were instrumented with an array of strain gages, LVDT's, and load cells. The instrumentation arrangement was nearly identical in the four specimens. In all, twenty eight strain gauges, eleven LVDT's, and three load cells were used to collect data from each test.

In each column specimen, eight longitudinal bars and three tie sets were instrumented with strain gages. Longitudinal bars with strain gages were placed in the first and the last two steel layers as shown in Figure 3-9. Each instrumented longitudinal bar was fitted with two strain gauges, one at the interface of the column and the footing, and the other at mid-distance between the first and the second tie sets from the bottom of the column.

To study the effectiveness of the confining steel, the first three tie sets from the bottom of the column were fitted with strain gages. For each tie set, four gauges were attached as follows: one gage at each short side of the perimeter tie, one gage at one long side of the perimeter tie, and one gage at one of the long cross ties. The strain gage arrangement in the transverse steel is shown in Figure 3-10.

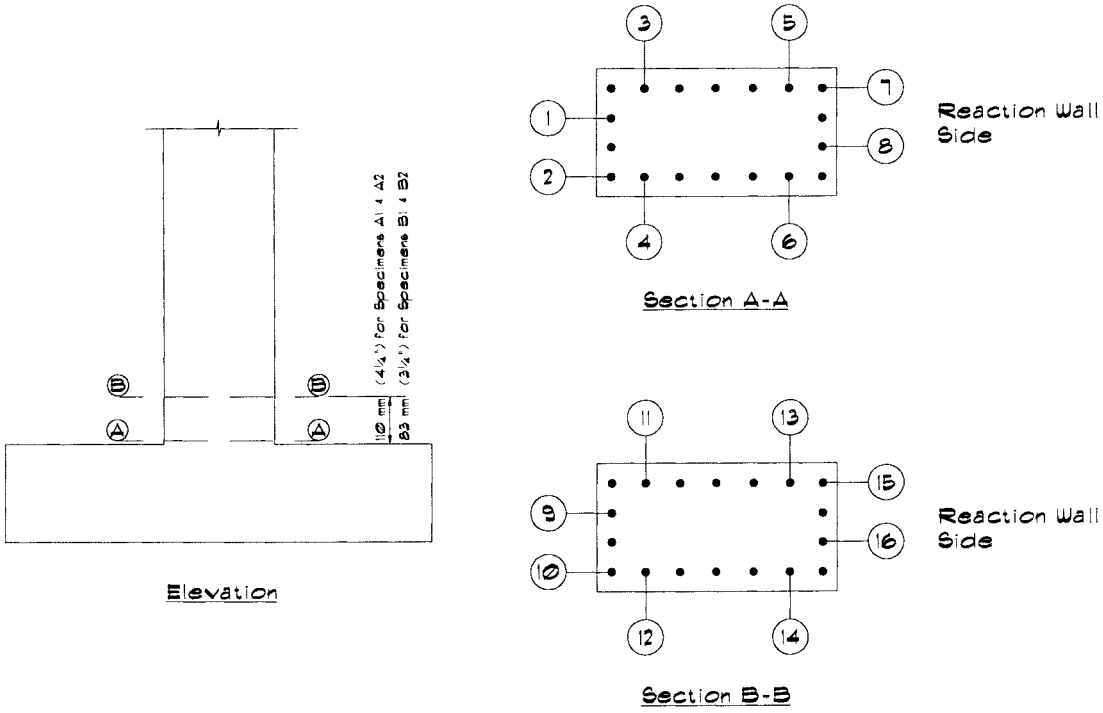

Figure 3-9 Strain Gaging of Longitudinal Bars

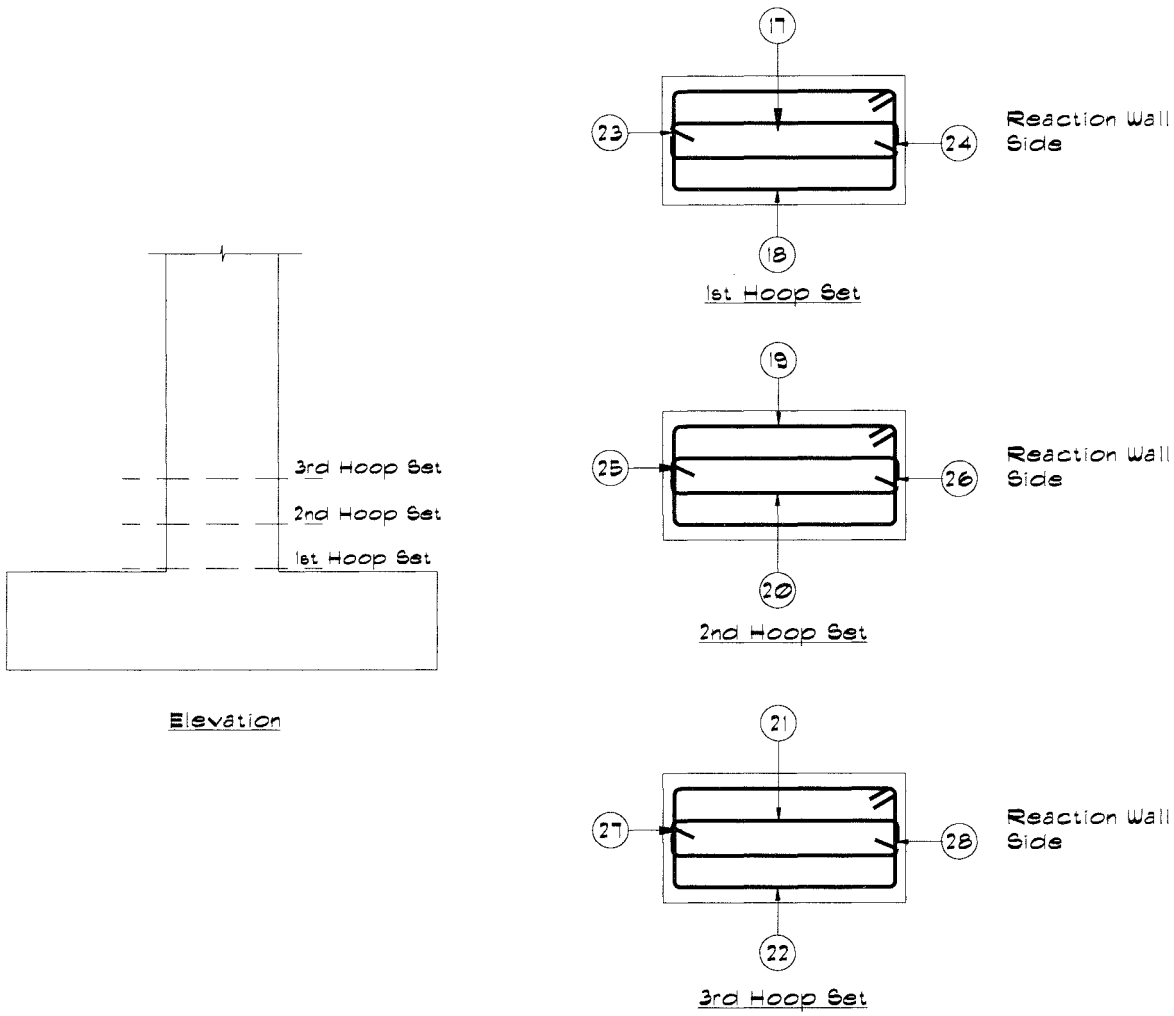

Figure 3-10 Strain Gaging of Transverse Steel

To measure strain in the concrete and section curvature along the potential plastic hinge zone, five pairs of LVDT's were fitted within a height of 685 mm (27 in.) from the bottom of the column. This height was divided into five intervals representing five gage lengths as shown in Figure 3-11. In each interval, two LVDT's were placed, one at each side of the column. Based on the gauge length, different range LVDT's were selected. The bottom 76 mm (3 in.) and 100 mm (4 in.) gage lengths were fitted with ±13 mm (±0.5 in.) and ±25 mm (±1 in.) range LVDT's, respectively. The top three gauge lengths were all fitted with ±50 mm (±2 in.) range LVDT's.

The lateral deflection of the column was measured along the centerline of the hydraulic actuator applying the lateral load. This was accomplished through the actuator LVDT.

To measure the axial load applied by the two Dywidag™ prestressing bars, a load cell was installed under the top anchor mechanism of each bar. The lateral load applied at the top of the column was measured by means of the actuator load cell.

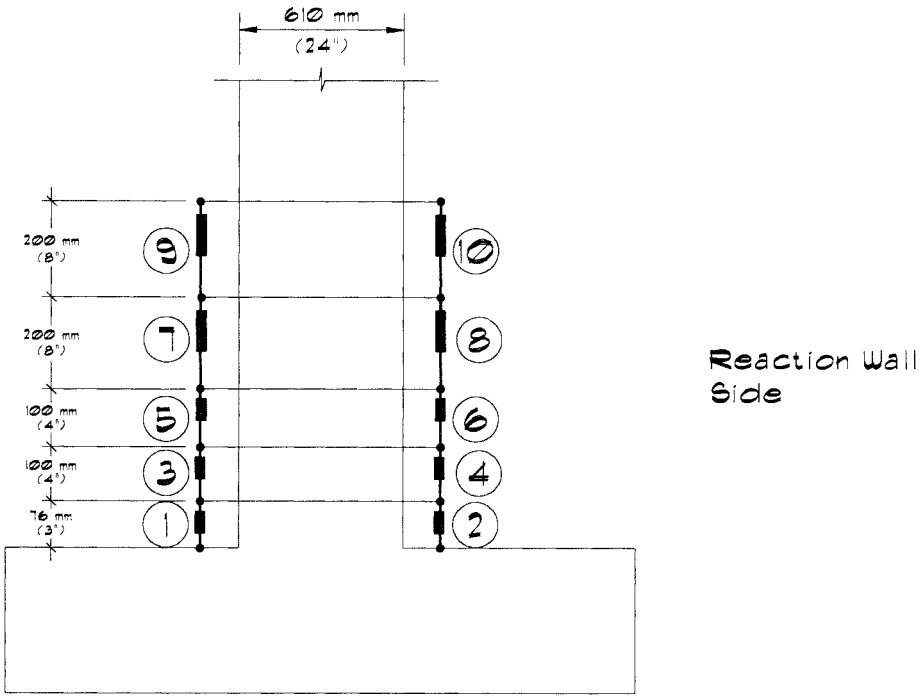

Figure 3-11 LVDT Setup for the Test Specimens

Data from strain gages, LVDT's and load cells were collected and recorded by means of a Megadac Model 5033A data acquisition system. The system was set to scan and record instrument readings at a rate of one reading per second. Data recording could be stopped and resumed at any instant during the test.

3.6 Test Setup

The test specimen was lifted and set at the test location. To level the specimen and to provide full contact between the footing and the floor of the testing laboratory, the bottom of the footing was set about 13 mm (0.5 in.) above the floor, then a mix of gypsum cement was poured to fill the gap between the bottom of the footing and the floor. The test setup is shown in Figure 3-12.

The transfer of axial and lateral loads to the specimen was accomplished through a steel I-beam that was placed across the top of the column as shown in Figure 3-12. The flange width, flange thickness and web thickness of the steel beam were 305 mm (12 in.), 50 mm (2 in.) and 25 mm (1 in.), respectively. The beam length was 1520 mm (5 ft) and the overall depth was 610 mm (24 in). Four ϕ 38 mm (1.5 in.) holes were drilled in the bottom flange of the beam to allow for the passage of the column anchor bolts. To prevent stress concentrations and cracking of the concrete at the top of the column, a 610 mm (24 in.) by 380 mm (15 in.) by 16 mm (5/8 in.) steel plate was placed between the steel beam and the top of the column. The cross beam was then placed in position and secured to the top of the column by means of four ϕ 35 mm (1 3/8 in.) nuts.

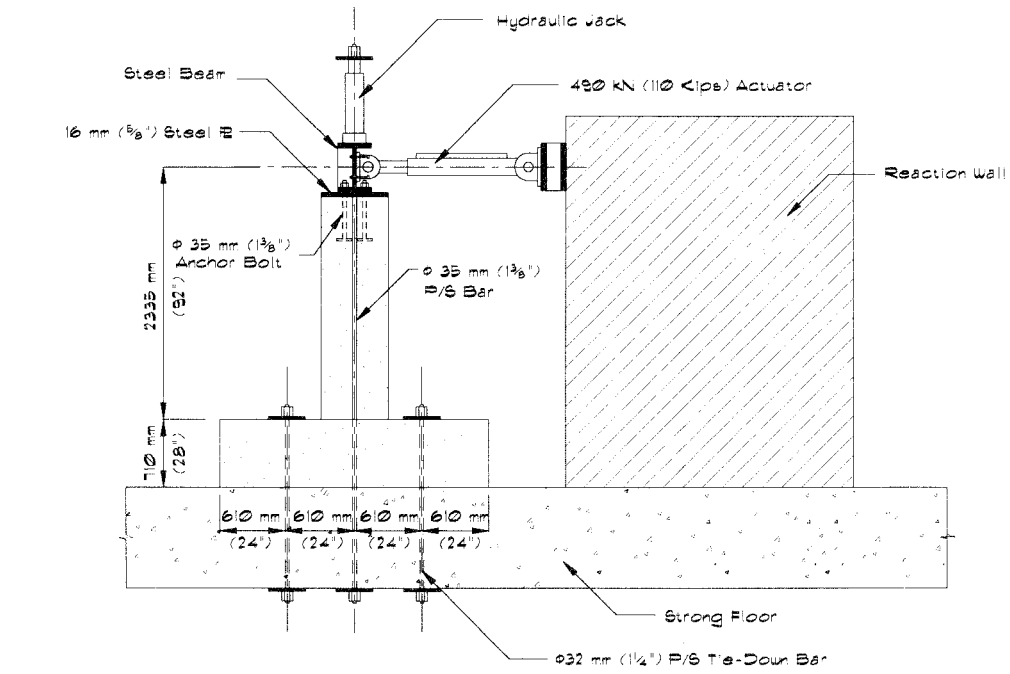

SIDE VIEW

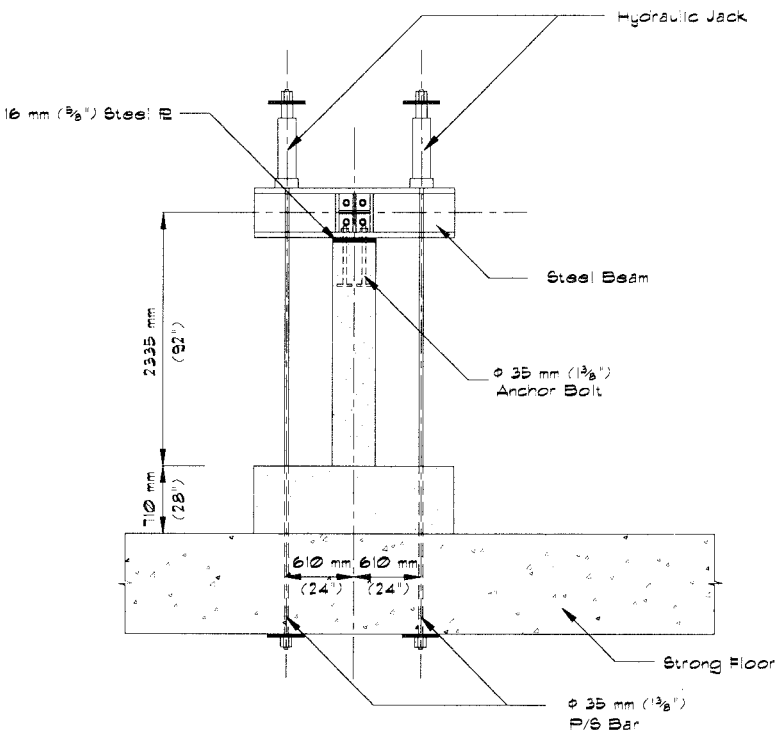

FRONT VIEW

Figure 3-12 Test Setup

To prevent rocking of the footing under the applied overturning moments during the test, four ϕ 32 mm (1.25 in.) Dywidag^{TM} bars were used to tie down the footing to the strong floor. The prestressing bars were passed through the sleeves in the footing and the strong floor. Each bar was stressed to an initial jacking force of 134 kN (30 Kips) then was anchored at the top of the footing and the bottom of the floor slab.

Lateral load was applied by means of a 490 kN (110 Kip) MTS hydraulic actuator. The actuator base was first connected to the reaction wall by means of a connector steel plate then the actuator head was extended and connected to the web of the cross beam on top of the column. In its initial position, the actuator was level and had a potential maximum stroke of ±280 mm (±11 in.).

Two ϕ 35 mm (1.375 in.) Dywidag^{TM} bars were used to apply the axial load. The initial prestressing force was applied by means of one hydraulic jack per each bar. The jacks were placed at the top of the steel cross beam, then the prestressing bars were extended vertically and anchored at the top of the jacks and the bottom of the strong floor. The jacks were identical and were connected in parallel to the same pressurizing pump. To minimize axial load fluctuation caused by variation in the prestressing bars length under different drift levels, a 70 MPa (10,000 psi) pressure accumulator was hooked to the hydraulic system between the pump and the jacks. At the beginning of each test, the desired axial load was applied prior to lateral loading.

3.7 Experimental Procedure and Results

3.7.1 General Remarks

Unlike reinforced concrete members with only two layers of steel placed at opposite ends, a concrete section with main reinforcement distributed throughout the depth of the section does not normally exhibit a well defined yield point, but rather a yield region that depends mainly on the amount and the distribution of the main reinforcement. To facilitate the analysis of such cases, it is customary to determine an effective yield point of the member as shown in Figure 3-13. For reinforced concrete columns, it is normally acceptable to assume that the calculated ultimate moment capacity of the unconfined section is the effective yield moment of the confined section (Paulay and Priestley, 1992).

Experimentally, one way to determine the effective yield displacement (Δ_y) corresponding to the effective yield load (M_y or F_y) is found as follows. First, the specimen is loaded in one direction up to 75 percent of the effective yield load then the load is reversed until it reaches 75 percent of the yield load in the other direction. The corresponding displacements are measured and the average of the maximum displacements in both direction is considered as $0.75\Delta_y$ as shown in Figure 3-14. The effective yield displacement can then be found by extrapolation. This procedure was followed in this study.

Readings of LVDT's located at the bottom of the column were employed to measure curvatures along the potential plastic hinge zone. To find the average strain at each LVDT location, the

measured displacement was divided by the corresponding gage length. This strain was considered to be the strain at the middle of the gauge length. Knowing the distance between the LVDT's placed at opposite sides, it was possible to measure curvatures at column sections along the mid-height of the gage lengths.

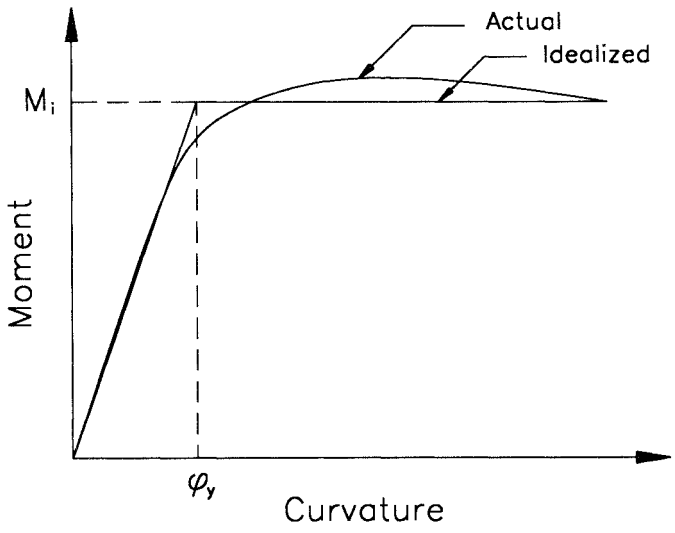

Figure 3-13 Idealized Moment-Curvature Relationship

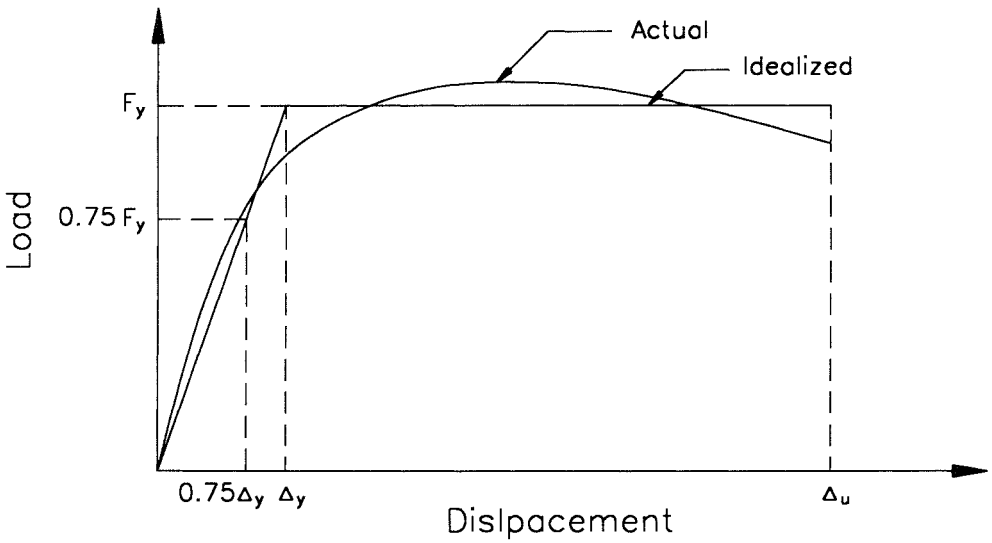

Figure 3-14 Experimental Determination of Effective Yield Displacement

On the day of testing, the desired axial load was first applied then the specimen was subjected to unidirectional lateral cyclic loading in the strong direction of the column. The lateral load was monotonic, load controlled up to ±75 percent the effective yield moment (±0.75 M_y) at the bottom of the column, and displacement controlled afterward. Each specimen was first subjected to one full cycle at post-cracking moment (M_{cr}), one full cycle at 0.75 M_y , two full cycles at a displacement ductility μ_Δ of ±1, and two full cycles at a displacement ductility μ_Δ of ±2. Afterward, in general, specimens with lower axial load (A1 and B1) were then cycled at displacement ductility increments of 2 whereas those with higher axial loads (A2 and B2) were cycled at displacement ductility increments of 1, until failure. At each ductility level, the specimen was taken through at least two full excursions. Failure of the specimen was considered to occur when the lateral load carrying capacity was reduced by at least 25% of the maximum measured section capacity. This failure criterion was set to ensure that the test specimen does not lose stability at high drift and reduced strength. Test results are summarized in Table 3-5.

Table 3-5 Measured Displacements and Ductilities

	Measured			
Specimen	Δ_y mm (in)	Δ_u mm (in.)	μ_Δ	Drift Ratio %
A1	23 (0.92)	122 (4.82)	5.2	5.2
A2	20 (0.79)	102 (4.02)	5.1	4.4
B1	23 (0.92)	161 (6.33)	6.9	6.9
B2	21 (0.82)	130 (5.10)	6.2	5.5

3.7.2 Specimen A1

Specimen A1 was first subjected to an initial axial load of 615 kN (138 Kips) corresponding to an axial load index of 0.1. Under high lateral displacements the axial load increased but was still very close to the target value of 0.1 $f_c'A_g$. In general the axial load fluctuated during the test between a minimum of 592 kN (133 Kips) and a maximum of 641 kN (144 Kips). Based on the measured material properties and an axial load of 641 kN (144 Kips), the effective yield moment of Specimen A1 was calculated as 643 kN-m (5690 Kip-in) corresponding to a lateral load of 275 kN (61.8 Kips).

The lateral cyclic load history, shown in Figure 3-15, was applied according to the procedure described in Section 3.7.1. At a lateral load of approximately 89 kN (20 Kips), two flexural cracks were visible at 125 mm (5 in.) and 230 mm (9 in.) from the bottom of the column. Prior to first bar yield, one post-crack cycle was completed to establish the effective yield displacement, Δ_y. The average measured Δ_y was 23 mm (0.92 in.). The hysteretic load-displacement response of Specimen A1 is shown in Figure 3-16. The right-hand-side Y-axis in Figure 3-16 is the applied lateral load normalized with respect to the calculated effective lateral yield load, F_y.

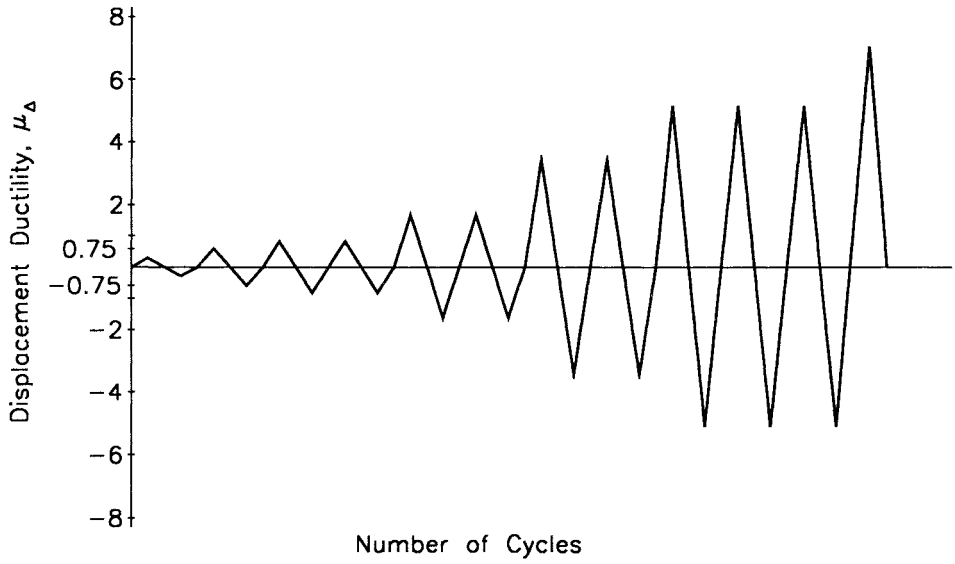

Figure 3-15 Lateral Load History for Specimen A1

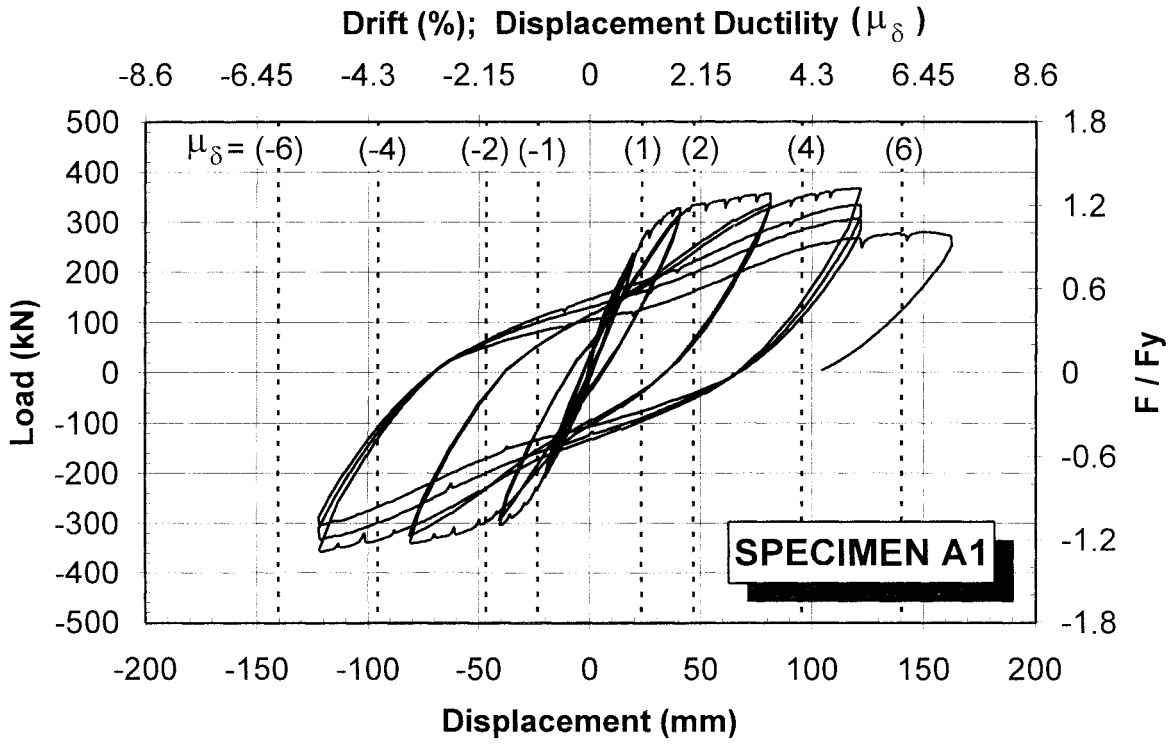

Figure 3-16 Measured Lateral Load-Deflection Hysteresis Loops for Specimen A1

At a displacement ductility μ_Δ of approximately ±1, the specimen did not show signs of strength decay or significant stiffness degradation. During the second excursion of μ_Δ = +2, slight stiffness degradation was apparent with minor decay in strength. When the specimen was taken to a second cycle of μ_Δ = -2, the cover concrete started to spall on the compression side. As the specimen was pushed to higher ductility levels, the cover concrete at the bottom of the column spalled at an increasing rate, exposing the first and second main steel layers on both sides of the column. Flexural-shear cracks were also developing along the column height. The peak measured lateral load was 361 kN (81 Kips). This peak load occurred at the end of the first excursion of μ_Δ = +5.2, corresponding to a ram displacement of 122 mm (4.82 in.). During the second excursion of μ_Δ = +5.2, the compression longitudinal bars began to buckle and the 90° hook of the second tie set from the bottom of the column started to open, accompanied by significant reduction in the column stiffness. As the specimen was cycled to a third excursion of μ_Δ =±5.2, the core concrete suffered more degradation and the 135° hooks on the second and third tie sets began to open. When the specimen was pushed to a displacement of +163 mm (6.41 in.), corresponding to μ_Δ =+7, the longitudinal bars on the compression side completely buckled and the lateral load capacity reduced to 267 kN (60 Kips). This load corresponded to 74 percent of the measured peak load and 97 percent of the effective lateral yield load. At this point the specimen was considered to have failed. Figures 3-17 through 3-20 show Specimen A1 during several stages of the test.

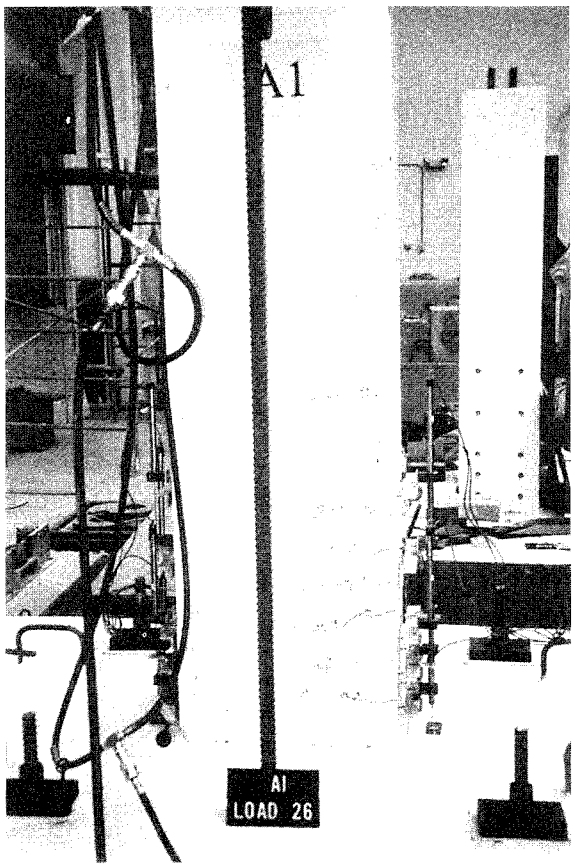

Figure 3-17 Specimen A1 at μ_Δ = +1 (1st Excursion)

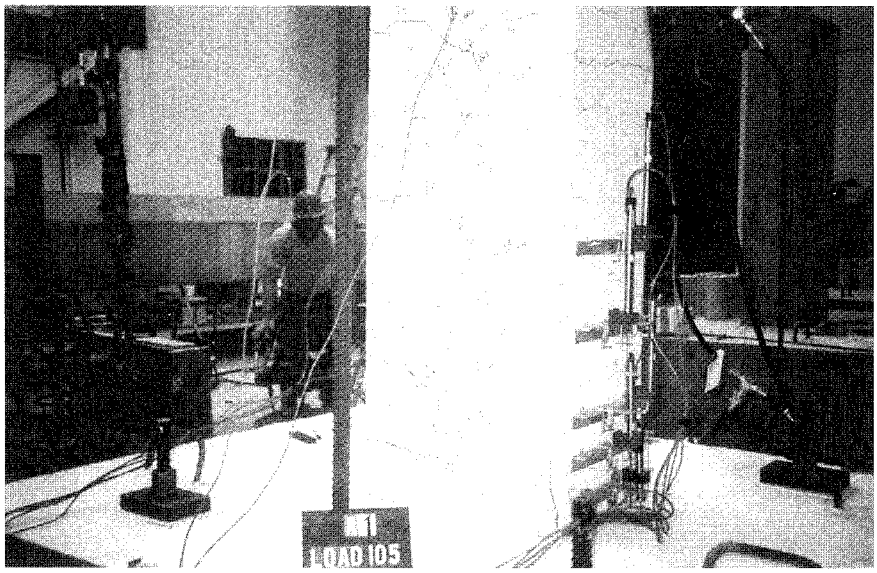

Figure 3-18 Specimen A1 at μ_Δ = +4 (1st Excursion)

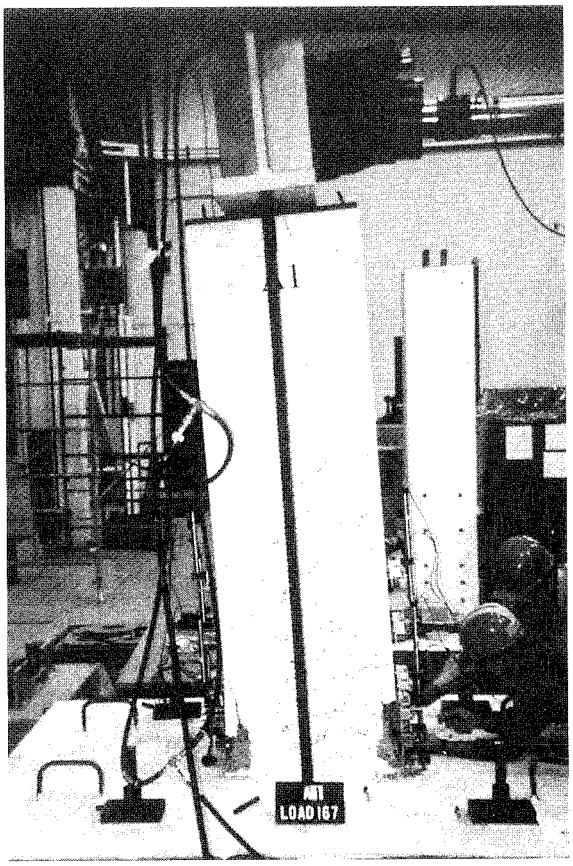

Figure 3-19 Specimen A1 at μ_Δ = +6 (1st Excursion)

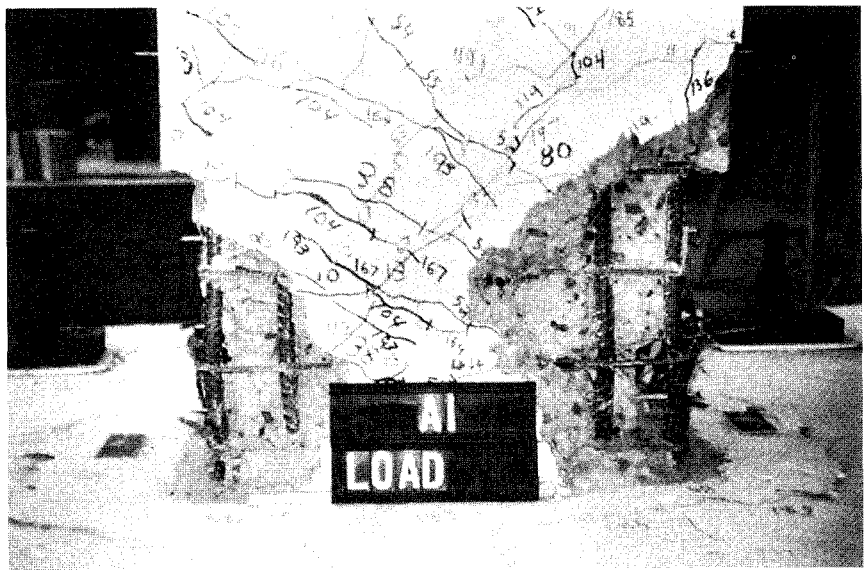

Figure 3-20 Plastic Hinge in Specimen A1 at the End of the Test

A review of the strain gage data revealed that yielding occurred in longitudinal steel at an early stage of the test before reaching the calculated effective section yield. Figure 3-21 presents the measured load-strain relationship of a first layer longitudinal bar at the column-footing interface (Gage No. 1 in Figure 3-9). On the other hand, some of the transverse steel yielded towards the end of the test and some attained high strains but did not yield. Figure 3-22 and Figure 3-23 show the measured load-strain of lateral steel at the second and third tie set levels, respectively (Gages No. 19 and 22 in Figure 3-10).

The measured curvature envelope along the potential plastic hinge was obtained from the LVDT readings and is presented in Figure 3-24. The intersection of the curvature line at yield with the curvature envelope represents the upper limit of the plastic hinge. Since the lower LVDTs' readings were not reliable at small deflections, the measured yield curvature was obtained from the measured strains in the longitudinal bars at the effective yield. The intersection point was found by linear extension of the highest branch of the envelope curve. Consequently, the measured plastic hinge length was found to be 645 mm (25.4 in.).

3.7.3 Specimen A2

For Specimen A2, the initial applied axial load was 1505 kN (338 Kips) corresponding to an actual load index of 0.24. During the test, the axial load varied between a minimum of 1479 kN (332 Kips) and a maximum of 1581 kN (355 Kips). For the purpose of determining the effective yield displacement, the effective yield moment was computed prior to the test and was found to be 732 kN-m (6480 Kip-in). This moment corresponded to a lateral load of 314 kN (70.4 Kips) at the ram level.

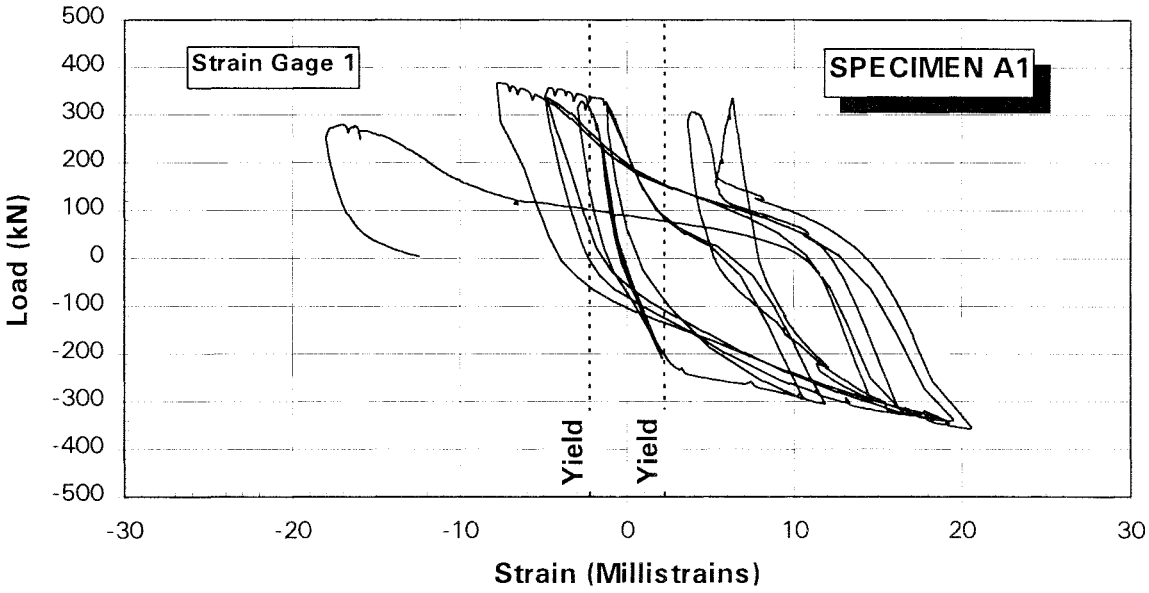

Figure 3-21 Measured Lateral Load-Strain Hysteresis in Specimen A1 Longitudinal Bar

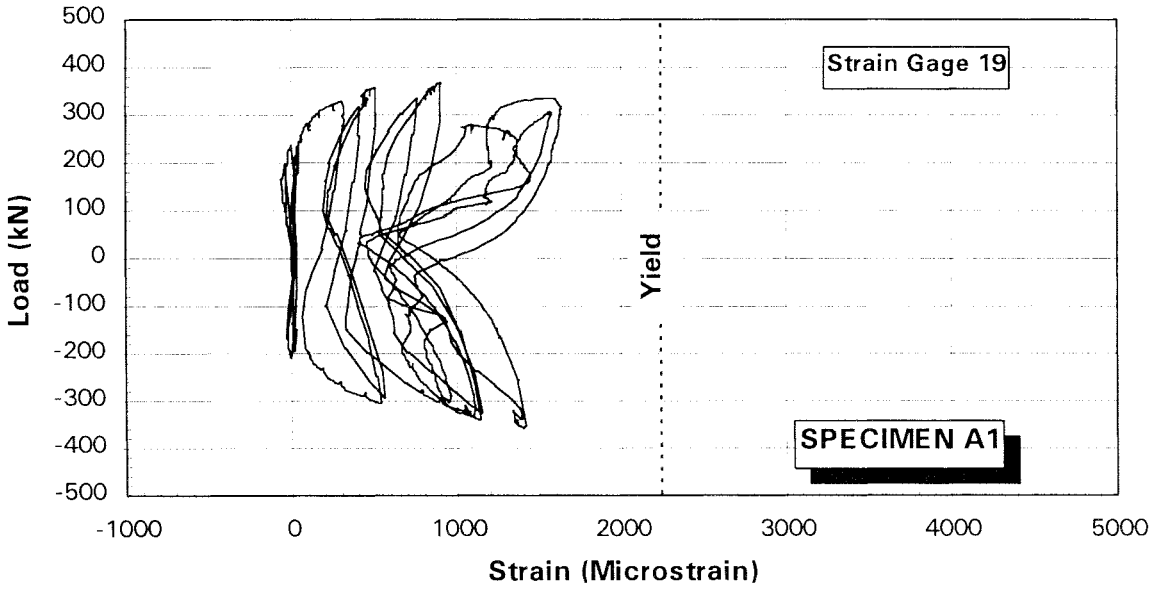

Figure 3-22 Measured Lateral Load-Strain in Specimen A1 Lateral Steel at SG 19

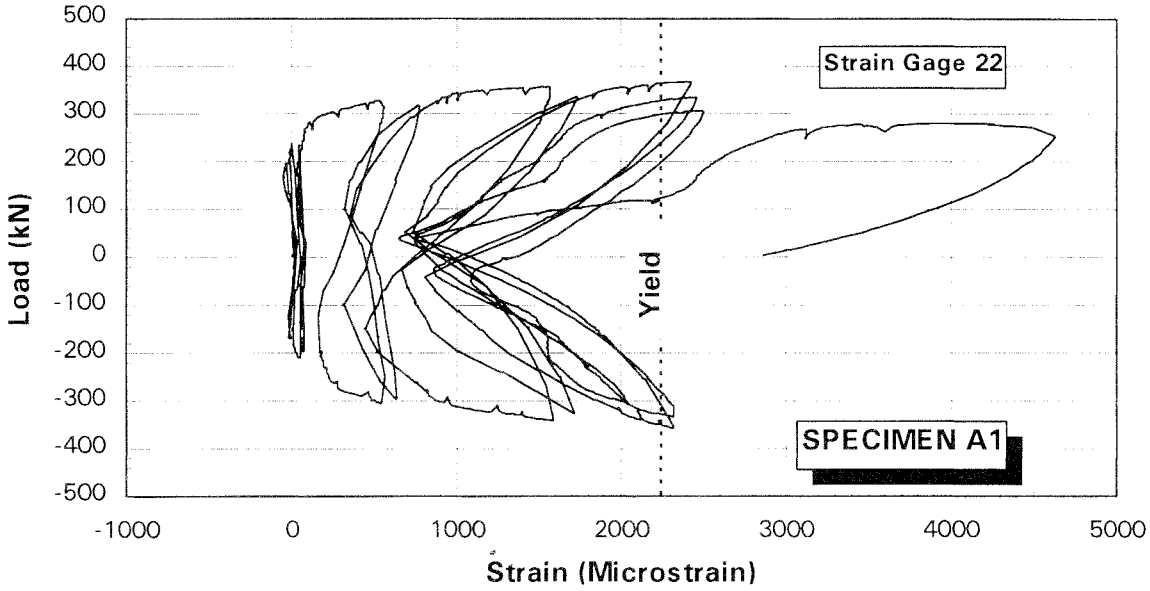

Figure 3-23 Measured Lateral Load-Strain in Specimen A1 Lateral Steel at SG 22

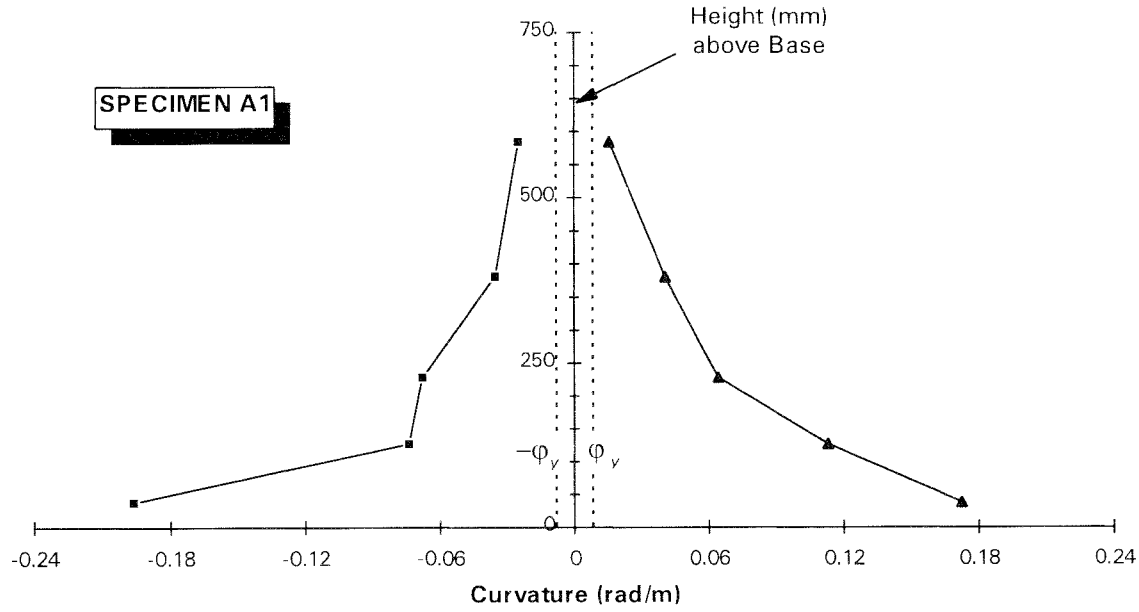

Figure 3-24 Measured Curvature Envelope along the Plastic Hinge of Specimen A1

The lateral load history for Specimen A2 is presented in Figure 3-25. The first visible flexural crack in the column occurred at approximately 280 mm (11 in.) from the column base. The corresponding lateral load was 143 kN (32 Kips). At a lateral load of 232 kN (52 Kips), several flexural cracks appeared along the bottom half of the column. The pattern of these cracks was consistent with the hoop set spacing. The effective average yield displacement was determined experimentally as 20 mm (0.79 in.). The measured lateral load-displacement response of Specimen A2 is presented in Figure 3-26.

Spalling of the cover concrete started to show at the bottom of the compression side when the column was pushed to $\mu_\Delta = +2$ for the first cycle. Despite the fact that spalling of the cover concrete was spreading on both sides of the column bottom with increasing drift, the hysteretic response was very stable and the stiffness degradation between the same ductility cycles was negligible up to $\mu_\Delta = +4$. The lateral load peaked at 396 kN (89 Kips) when the displacement ductility of +5 was attained for the first time. At $\mu_\Delta = -5$, first excursion, the longitudinal bars on the compression side started to buckle between the second and the third tie sets. During the next two cycles at displacement ductility of 5, the lateral steel end hooks were opening at the second and the third tie sets. This was accompanied by significant stiffness degradation and strength decay. At $\mu_\Delta = +6$, the longitudinal compression bars buckled completely and the lateral load dropped to 223 kN (50 Kips), signifying failure of the specimen. This load corresponded to 56 percent of the measured peak load and 71 percent of the effective lateral yield load (nominal load). Figures 3-27 through 3-30 show Specimen A2 during the development of the test.

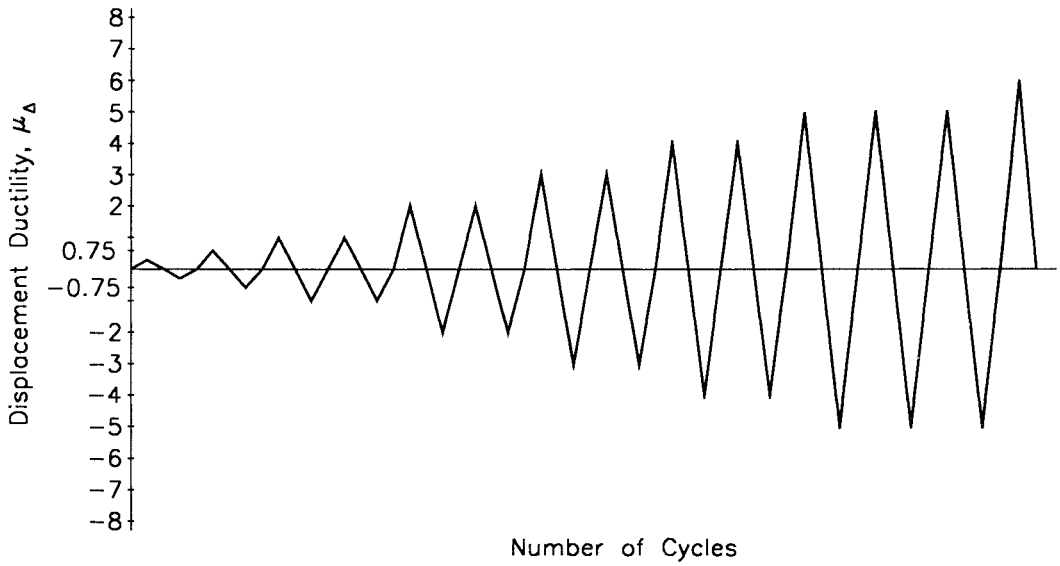

Figure 3-25 Lateral Load History for Specimen A2

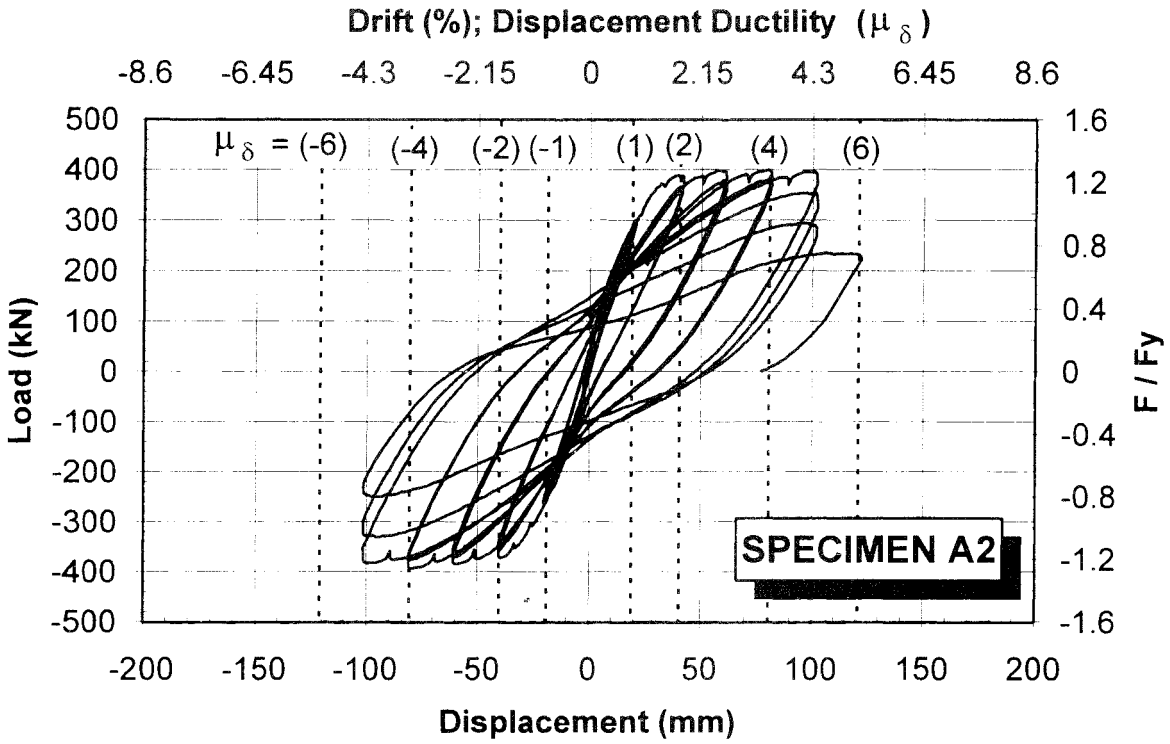

Figure 3-26 Measured Lateral Load-Deflection Hysteresis Loops for Specimen A2

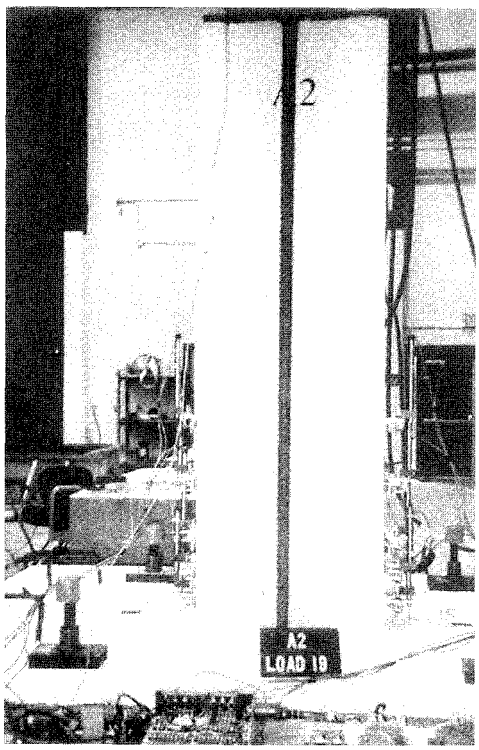

Figure 3-27 Specimen A2 at μ_Δ = +1 (2nd Excursion)

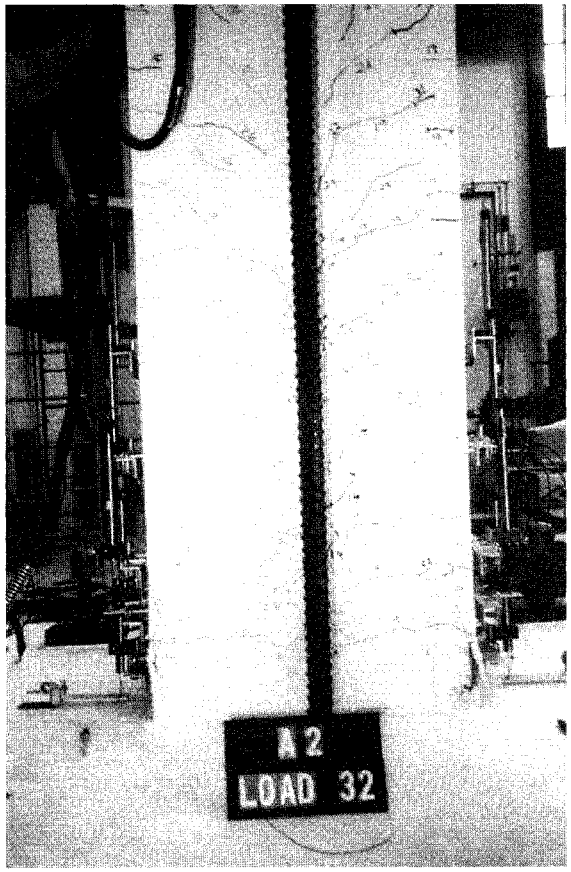

Figure 3-28 Specimen A2 at μ_Δ = -2 (2nd Excursion)

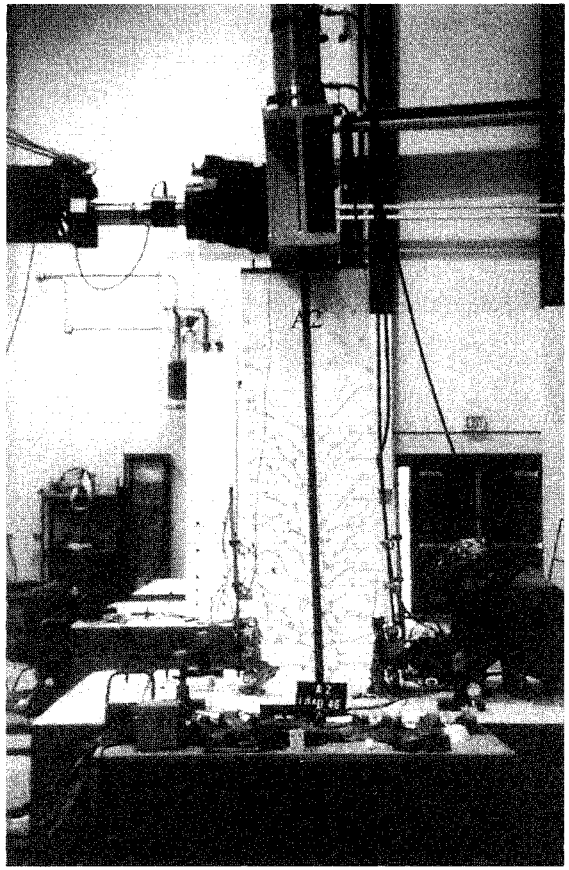

Figure 3-29 Specimen A2 at μ_Δ = -4 (1st Excursion)

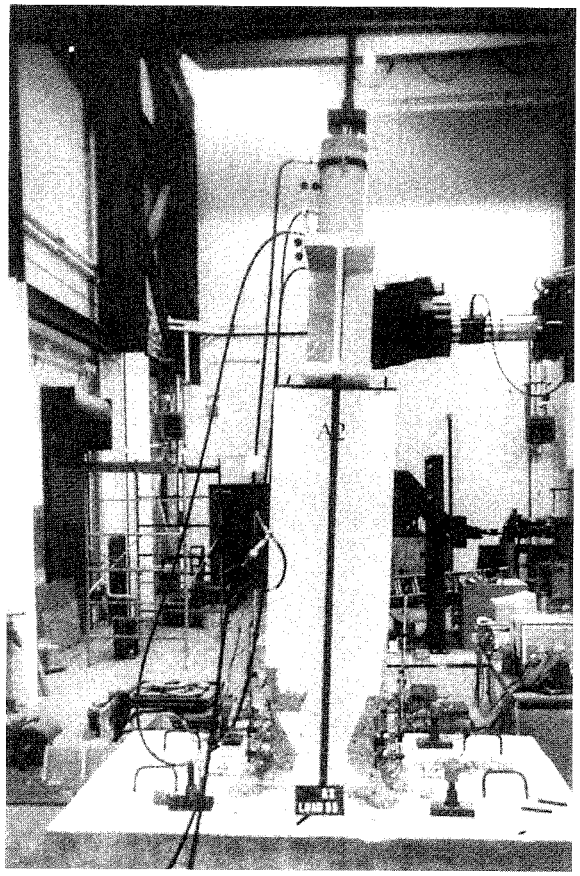

Figure 3-30 Plastic Hinge in Specimen A2 at the End of the Test

Measured strains in one longitudinal bar and two lateral bars are shown in Figure 3-31 and Figures 3-32 and 3-33, respectively (Gages No. 1, 18 and 19 in Figures 3-9 and 3-10). As with Specimen A1, yielding of the outer layer longitudinal bars in Specimen A2 was reached before the point of effective section yield. On the other hand, yielding of the lateral steel coincided with the specimen failure.

Figure 3-34 exhibits the plastic hinge measured curvature envelope for Specimen A2. The corresponding measured plastic hinge length was 747 mm (29.4 in.).

3.7.4 Specimen B1

Specimen B1 was initially subjected to an axial load of 601 kN (135 Kips) or $0.09 f_c' A_g$. At high drift levels, the axial load peaked at 637 kN (143 Kips). The calculated effective yield moment and the corresponding lateral load were 645 kN-m (5710 Kip-in) and 276 kN (62 Kips), respectively.

Figure 3-35 shows the lateral loading history of Specimen B1. No effort was made to observe the initial flexural cracks because it was believed that the column concrete was pre-cracked during specimen setup. Since the axial load of Specimen B1 was similar to that of Specimen A1, it was decided to assume that both specimens had the same effective yield displacement of 23 mm (0.92 in.). The load-displacement hysteresis for Specimen B1 is shown in Figure 3-36.

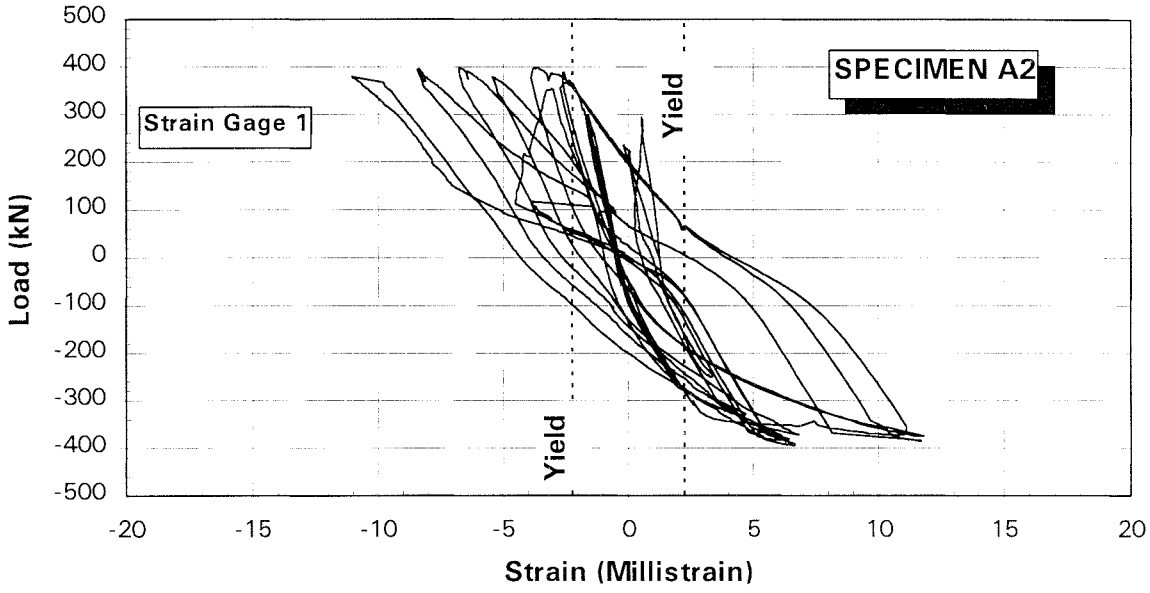

Figure 3-31 Measured Lateral Load-Strain Hysteresis in Specimen A2 Longitudinal Bar

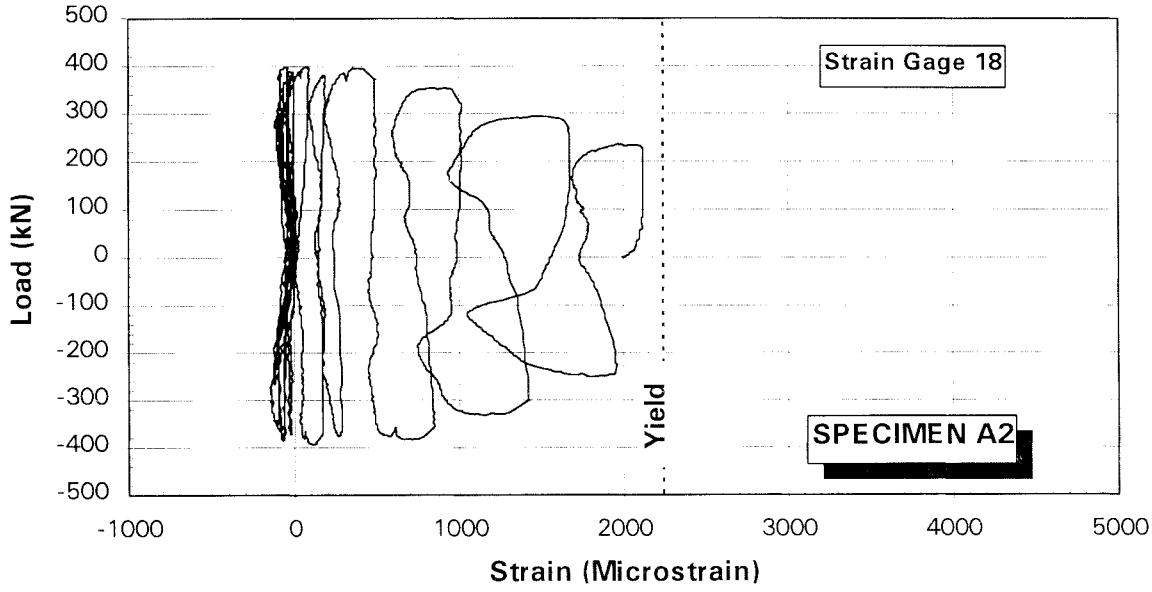

Figure 3-32 Measured Lateral Load-Strain in Specimen A2 Lateral Steel at SG 18

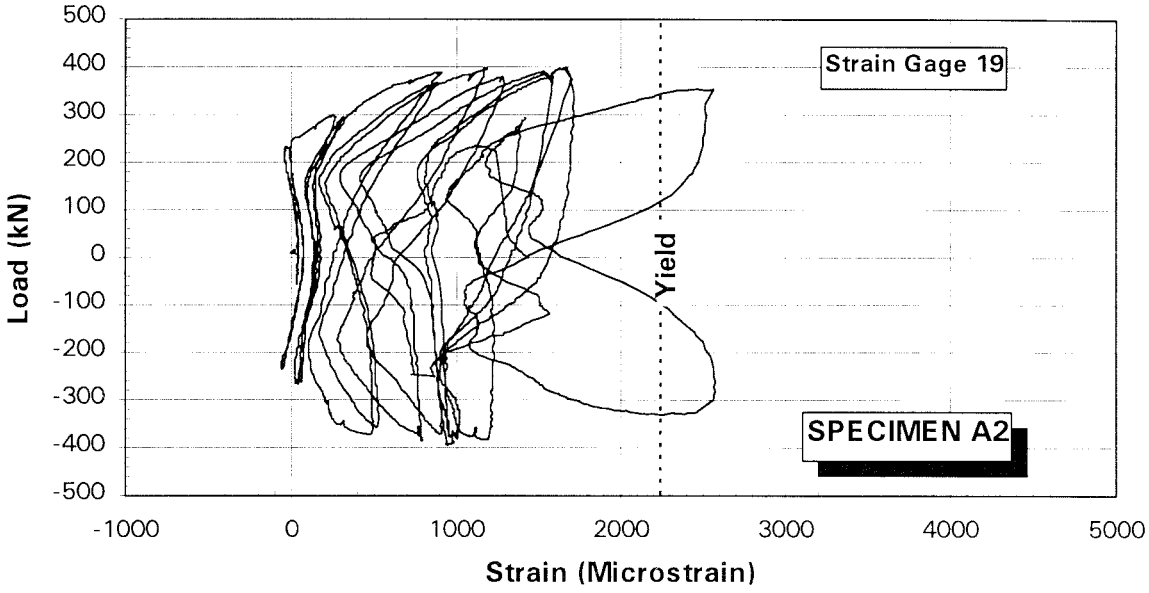

Figure 3-33 Measured Lateral Load-Strain in Specimen A2 Lateral Steel at SG 19

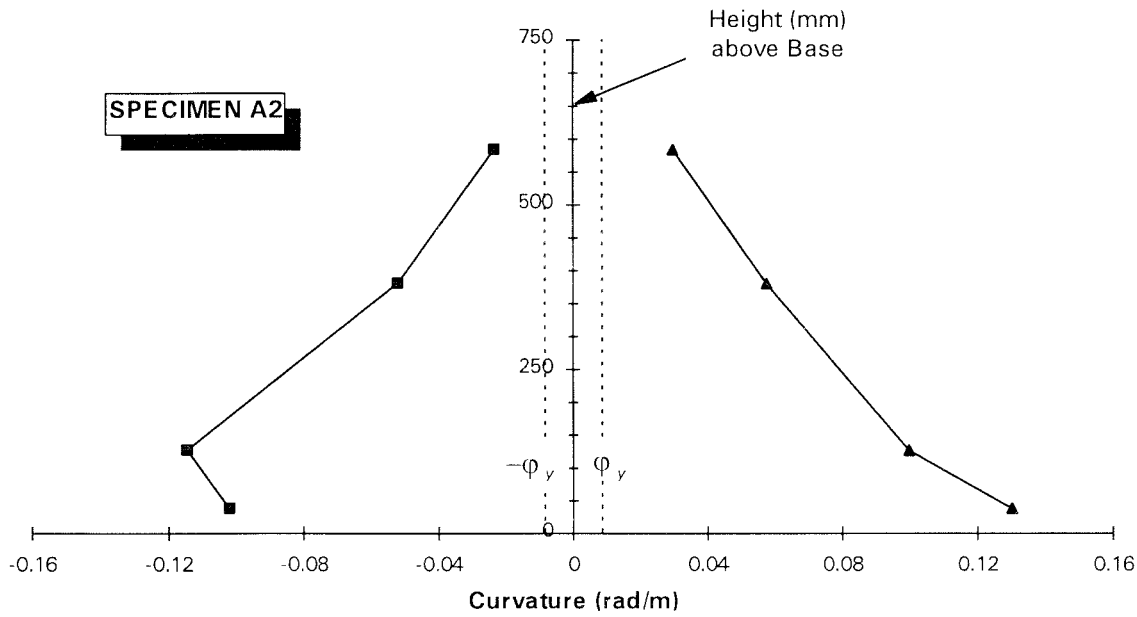

Figure 3-34 Measured Curvature Envelope along the Plastic Hinge of Specimen A2

At displacement ductility $\mu_\Delta = +2$, first loop, the cover concrete at the bottom of the column started to spall. As the test progressed and the column was pushed to higher drifts, the cover concrete spalling spread upward along the potential plastic hinge length. The hysteresis loops were stable up to a displacement ductility of 6 although signs of minor stiffness degradation were showing during second loops. During the second cycle of $\mu_\Delta = +6$, the 90° hook of the second tie set on the compression side started to open. At displacement ductility of 7, the core concrete deteriorated rapidly and the end hooks of the second and the third tie sets opened. This was accompanied by buckling of the longitudinal bars and strength decay. As the specimen was pushed to the target displacement ductility of 8, the second bar of the first steel layer on the compression side fractured due to low-cycle fatigue. The test was terminated when the lateral load dropped to 209 kN (47 Kips) at a ram displacement of 186 mm (7.33 in.). The peak recorded lateral load was 379 kN (85 Kips) and it occurred at $\mu_\Delta = +6$, first loop. The load at failure was 55 percent of the measured peak load and 75 percent of the nominal lateral load. Figures 3-37 through 3-40 show Specimen B1 during different stages of the test.

The longitudinal bar load-strain behavior in Specimen B1 was similar to those of Specimen A1 and Specimen A2. The outer two layers longitudinal bars yielded early in the test as is shown in Figure 3-41 (Gage No. 1 in Figure 3-9). The yielding in the transverse steel occurred on the onset of specimen failure. Figures 3-42 and 3-43 present the lateral load versus tie strain at two locations in the specimen (Gages No. 20 and 22, respectively, in Figure 3-10).

The measured curvature envelope along the potential plastic hinge length is shown in Figure 3-44. Since the top segment of the right-hand-side envelope was not realistic (Figure 3-44), it was decided that this segment could be more appropriately represented by the extension of the second envelope segment from the top. The corresponding measured plastic hinge length would be 767 mm (30.2 in.).

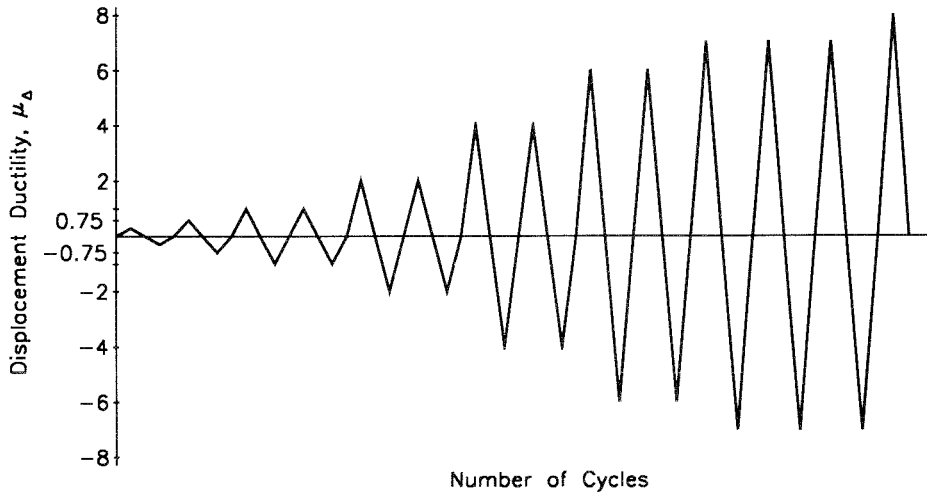

Figure 3-35 Lateral Load History for Specimen B1

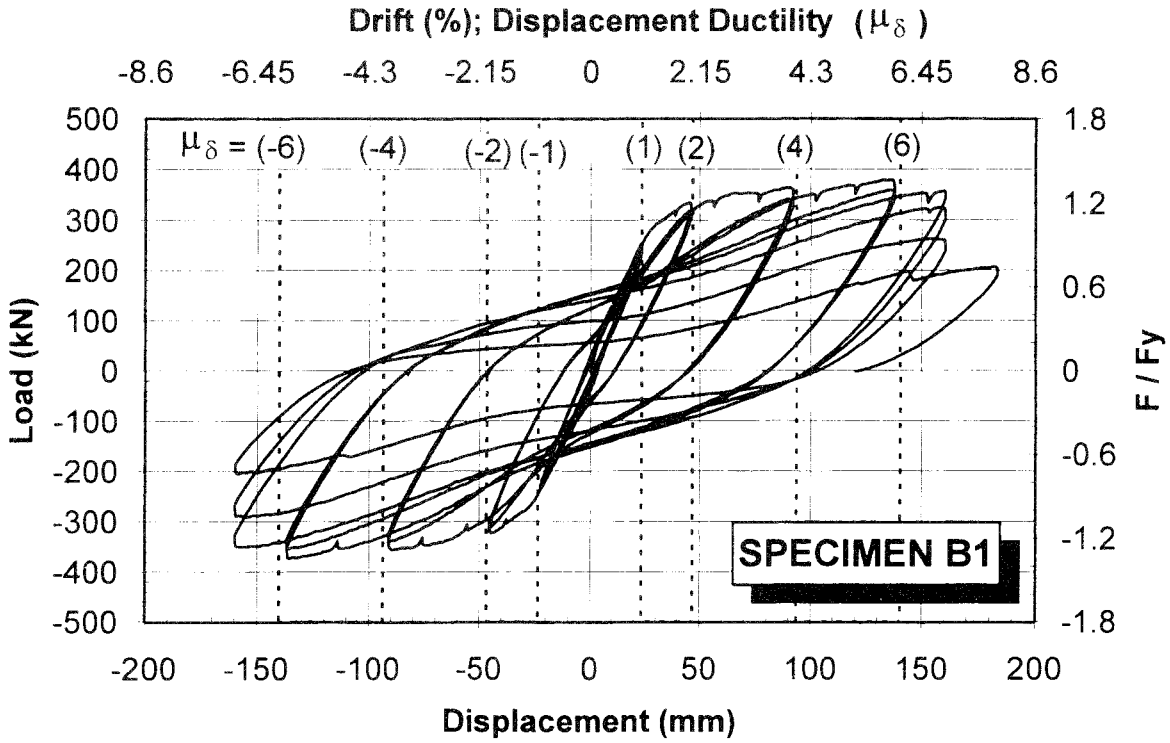

Figure 3-36 Measured Lateral Load-Deflection Hysteresis Loops for Specimen B1

Figure 3-37 Specimen B1 at μ_Δ = -4 (1st Excursion)

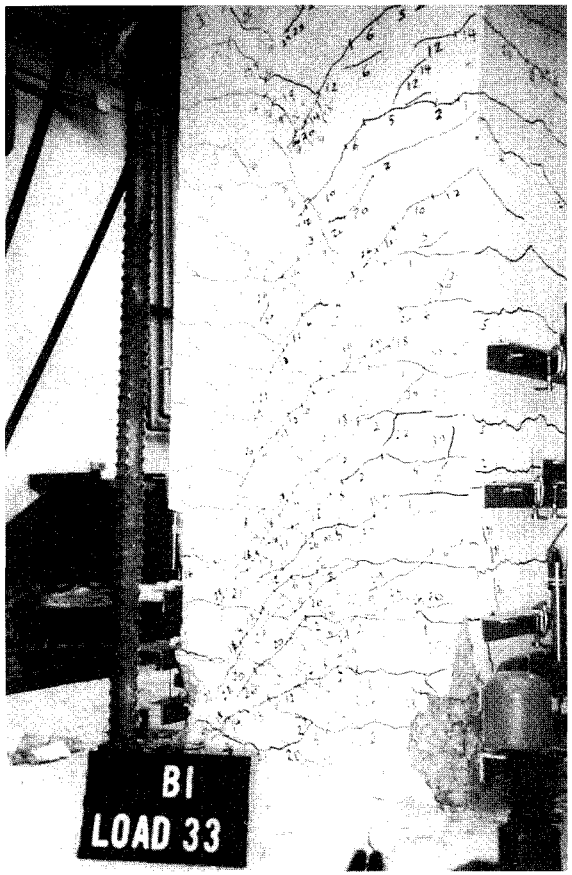

Figure 3-38 Specimen B1 at μ_Δ = -6 (1st Excursion)

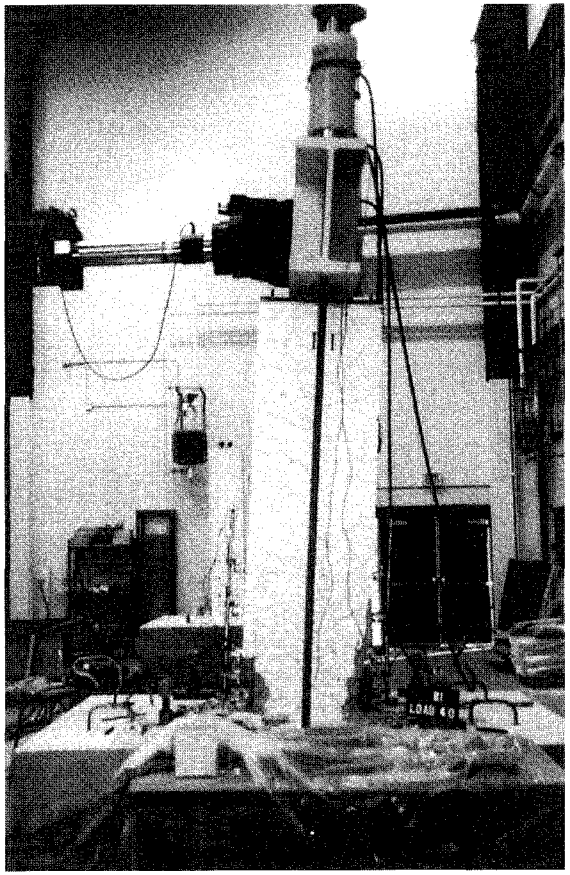

Figure 3-39 Specimen B1 at μ_Δ = +8

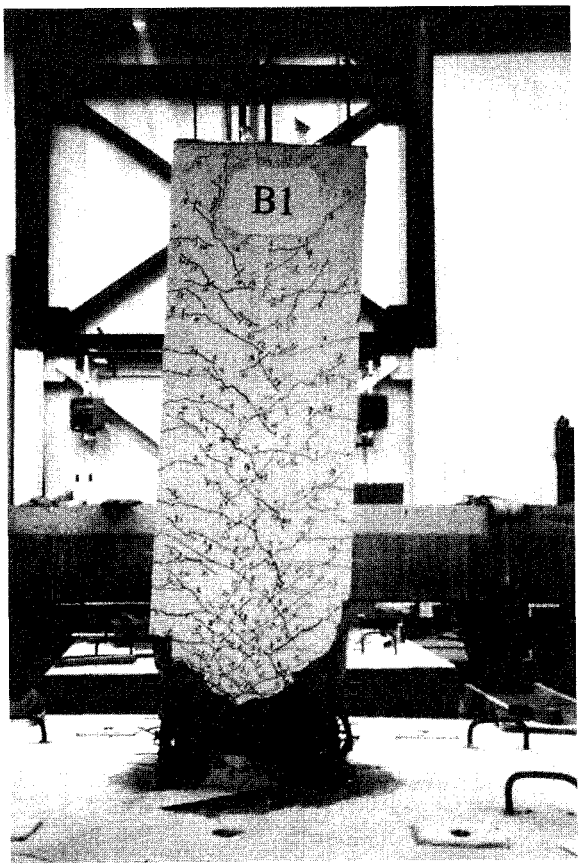

Figure 3-40 Plastic Hinge in Specimen B1 at the End of the Test

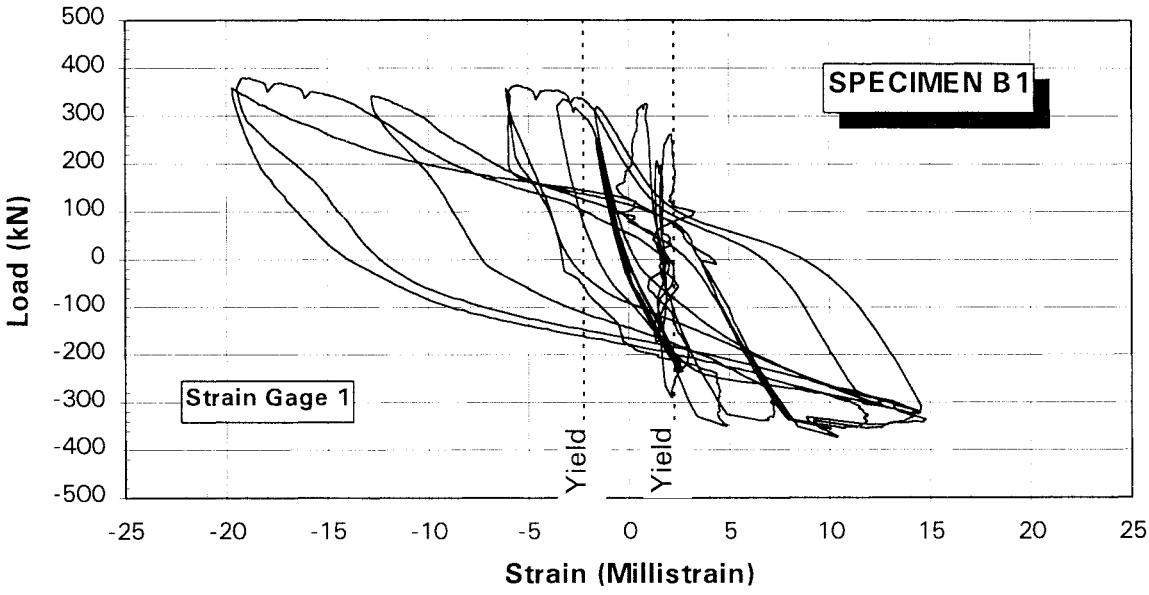

Figure 3-41 Measured Lateral Load-Strain Hysteresis in Specimen B1 Longitudinal Bar

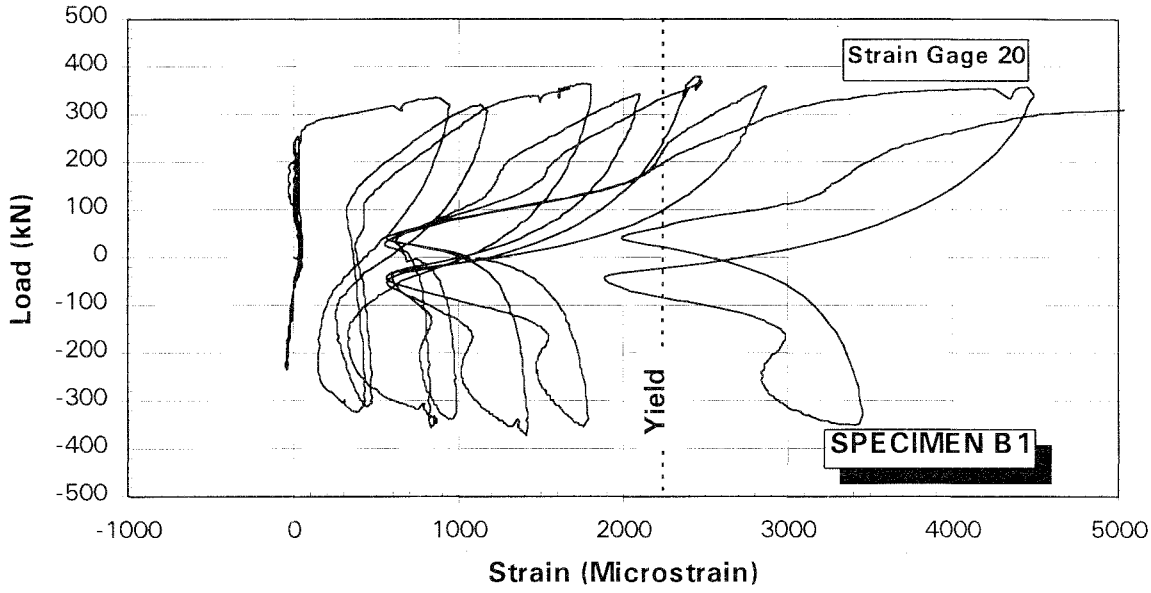

Figure 3-42 Measured Lateral Load-Strain in Specimen B1 Lateral Steel at SG 20

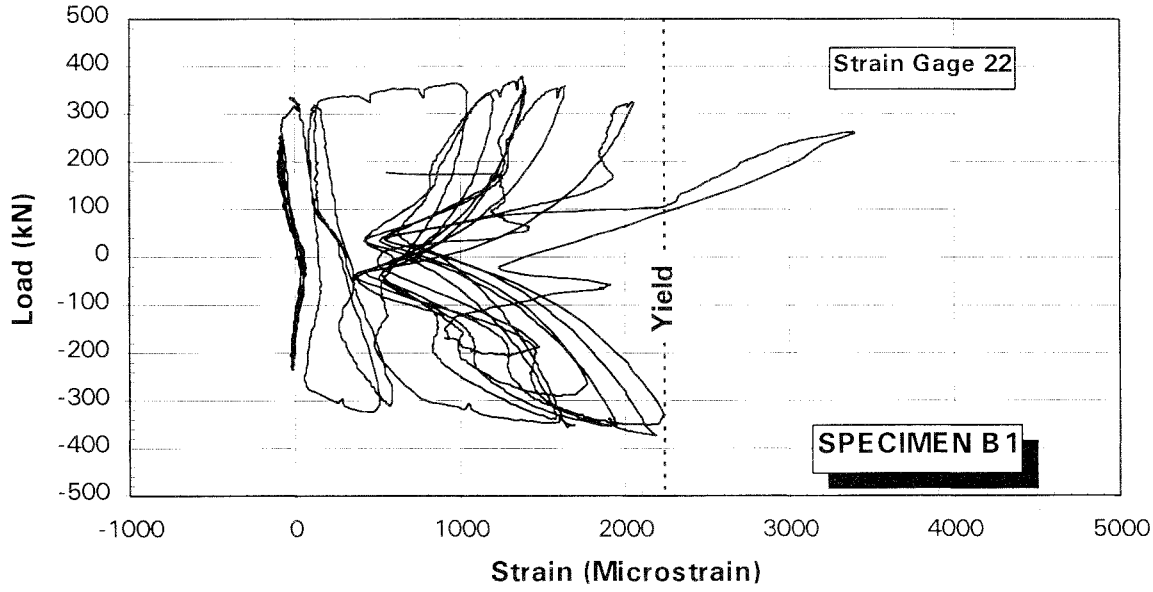

Figure 3-43 Measured Lateral Load-Strain in Specimen B1 Lateral Steel at SG 22

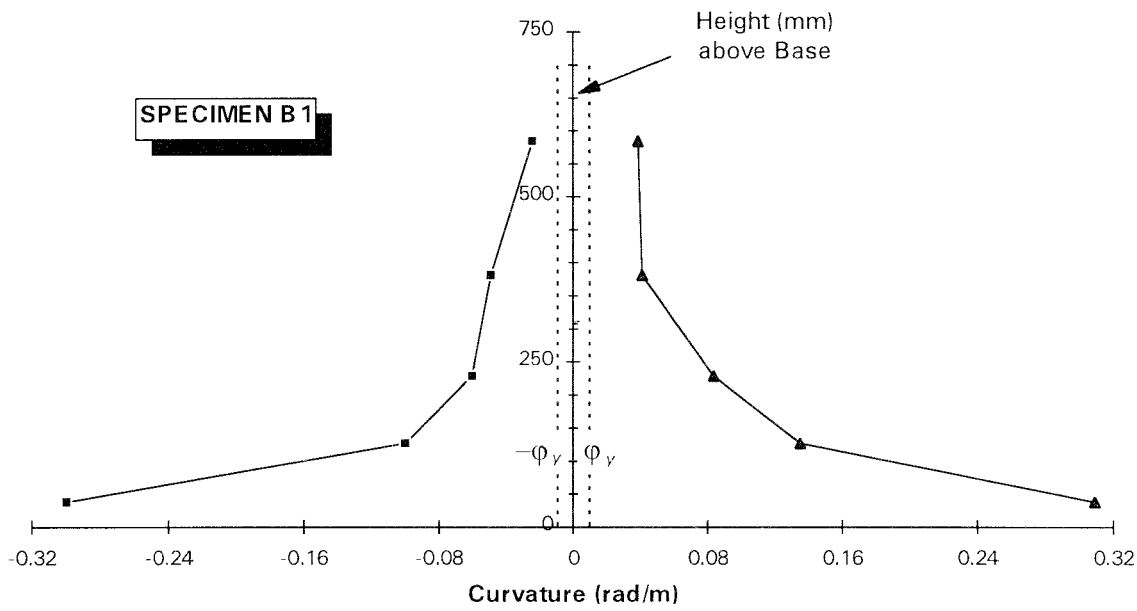

Figure 3-44 Measured Curvature Envelope along the Plastic Hinge of Specimen B1

3.7.5 Specimen B2

Specimen B2 was subjected to an initial axial load of 1514 kN (340 Kips) corresponding to an axial load index of 0.23. At low amplitude displacements, the minimum measured axial load was 1497 kN (336 Kips). A maximum axial load of 1603 kN (360 Kips) was recorded during high amplitude displacements. Based on an axial load of 1532 kN (344 Kips), the calculated effective yield moment and the corresponding lateral load were 742 kN-m (6570 Kip-in) and 318 kN (71.3 Kips), respectively.

The lateral load history for Specimen B2 is shown in Figure 3-45. Similar to the other specimens, flexural cracks along the column height started to develop before the section effective yield was reached. The measured effective yield displacement was 21 mm (0.81 in.). The sudden jump to a high displacement in the fifth loading cycle was due to a malfunction in the hydraulic system which caused the actuator to increase the lateral displacement from 30 mm (1.16 in.) to more than 76 mm (3 in.) in about five seconds. The lateral loads corresponding to those displacements were 356 kN (75.4 Kips) and 408 kN (91.5 Kips), respectively. The induced high lateral load initiated the spall of cover concrete at the compression side. The hysteretic load-displacement response for Specimen B2 is shown in Figure 3-46.

Specimen B2 exhibited very stable hysteresis loops up to a displacement ductility of 6. At this point, the lateral load peaked at 417 kN (93.7 Kips). During the second excursion of $\mu_\Delta = +6$, the 90° hook

of the third tie set started to open on the compression side of the specimen. The core concrete was deteriorating at a faster rate during the third cycle of $\mu_\Delta = 6$ and the longitudinal bars started to buckle. The test was terminated after the specimen was pushed to a lateral displacement of 150 mm (5.95 in.) and the corresponding lateral load dropped to 258 kN (58.0 Kips). The failure load was 62 percent of the measured peak load or 81 percent of the effective lateral yield load. Figures 3-47 through 3-50 show Specimen B2 at different stages of the test.

Figure 3-51 and Figures 3-52 and 3-53 present the measured lateral load-strain relationships at one longitudinal bar and two transverse bars, respectively (Gages No. 1, 19 and 22, respectively, in Figures 3-9 and 3-10). The measured plastic hinge length at the end of the test was 612 mm (24.1 in.). The measured curvature envelope and plastic hinge length at the bottom of the column are reflected in Figure 3-54.

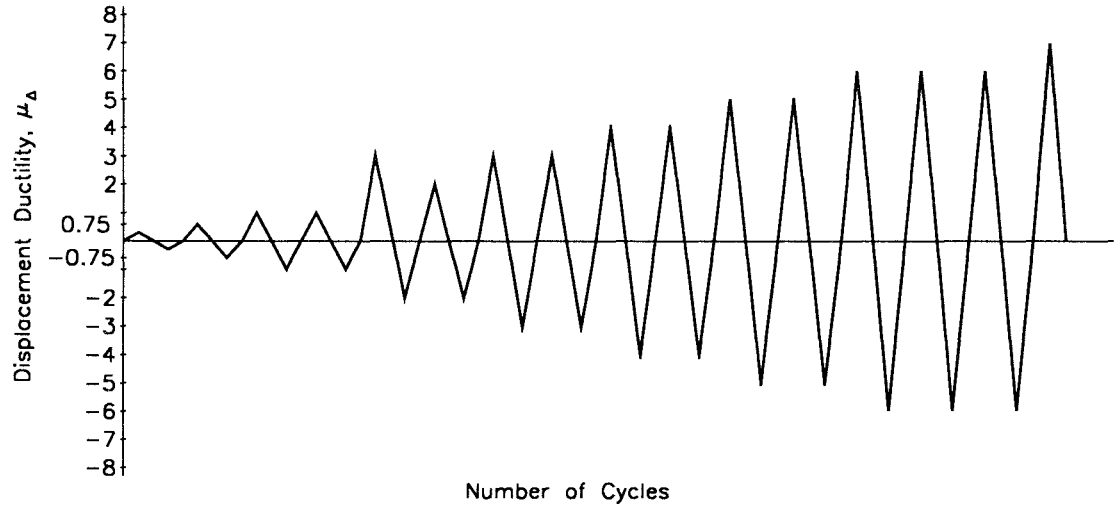

Figure 3-45 Lateral Load History for Specimen B2

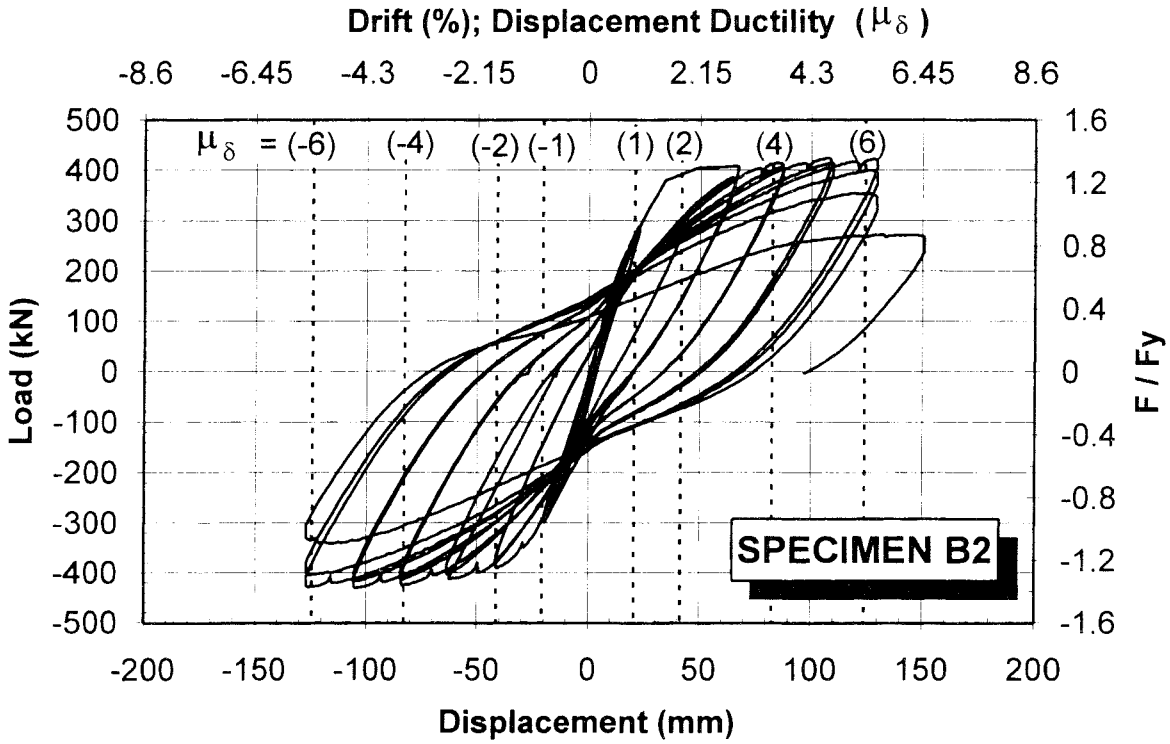

Figure 3-46 Measured Lateral Load-Deflection Hysteresis Loops for Specimen B2

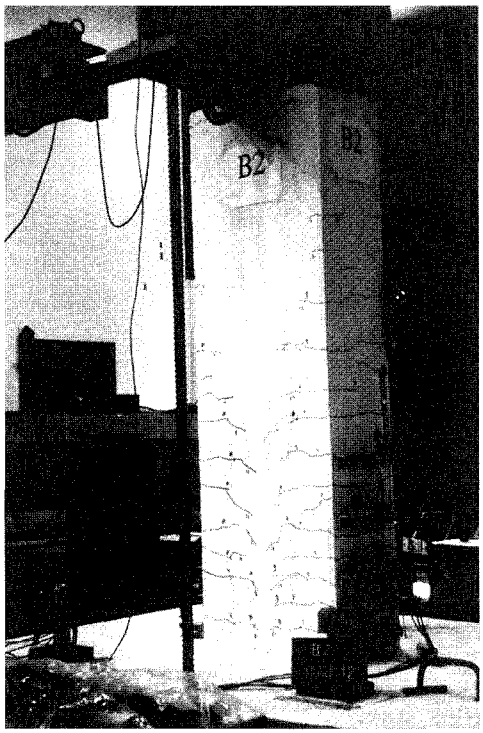

Figure 3-47 Specimen B2 at μ_Δ = -1 (1st Excursion)

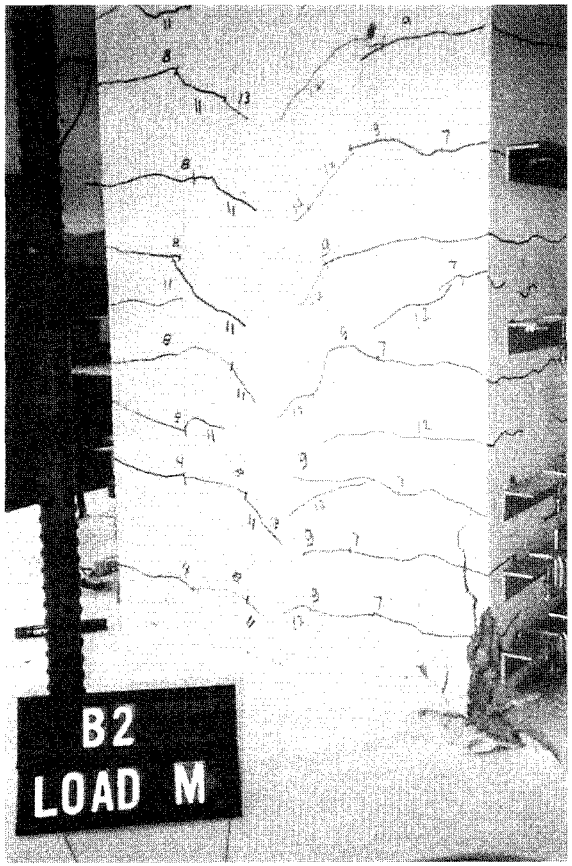

Figure 3-48 Specimen B2 at μ_Δ = +3 (1st Excursion)

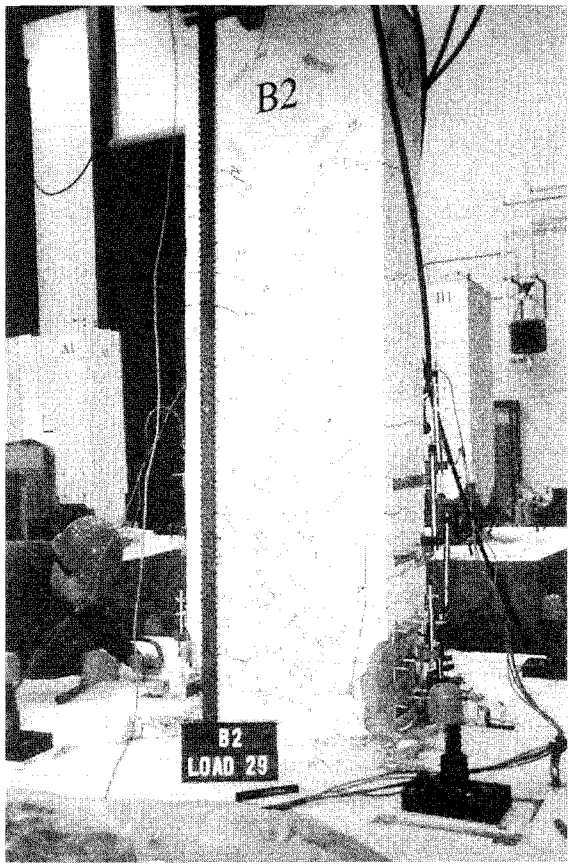

Figure 3-49 Specimen B2 at μ_Δ = +4 (1st Excursion)

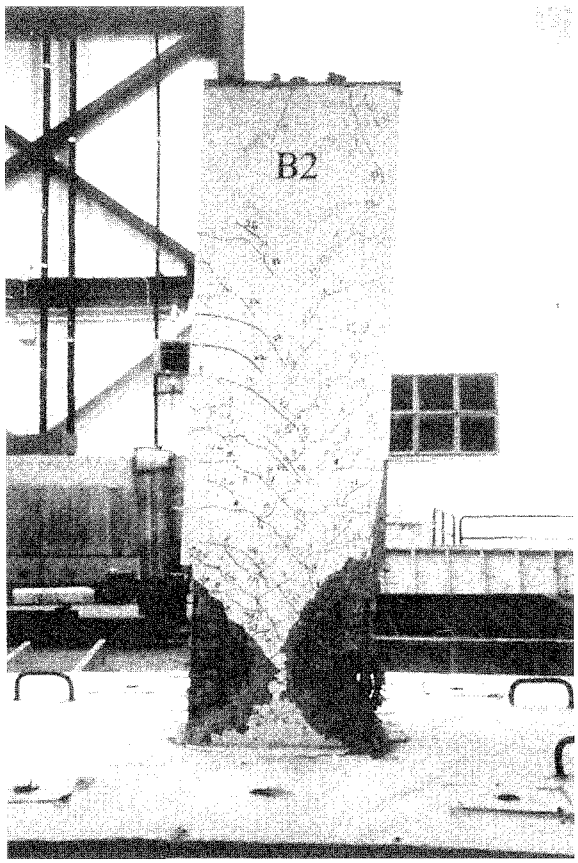

Figure 3-50 Plastic Hinge in Specimen B2 at the End of the Test

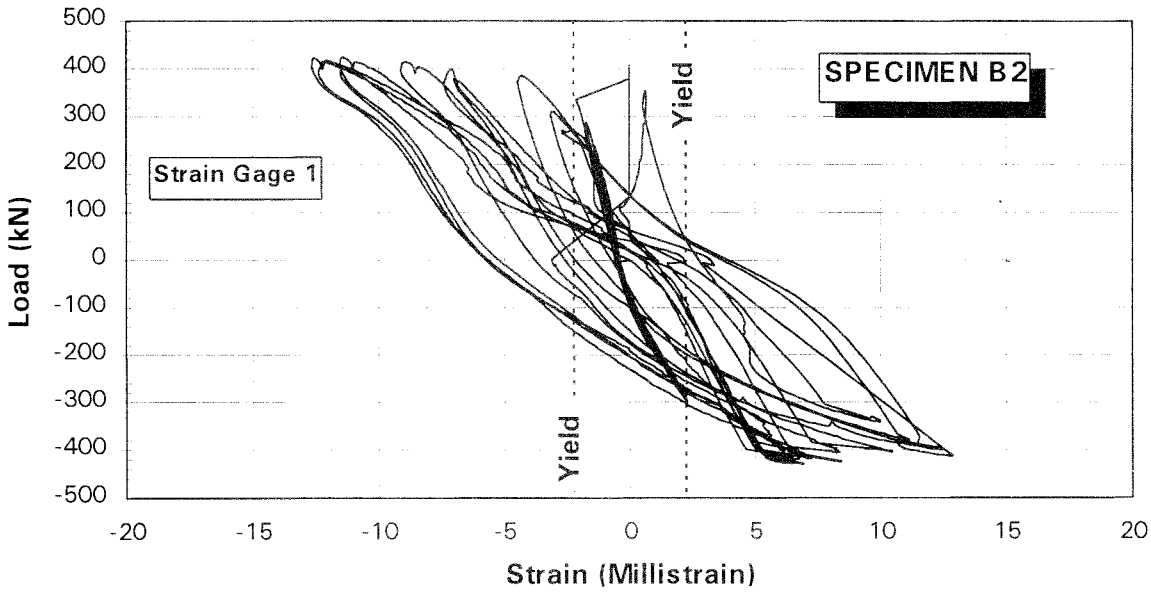

Figure 3-51 Measured Lateral Load-Strain Hysteresis in Specimen B2 Longitudinal Bar

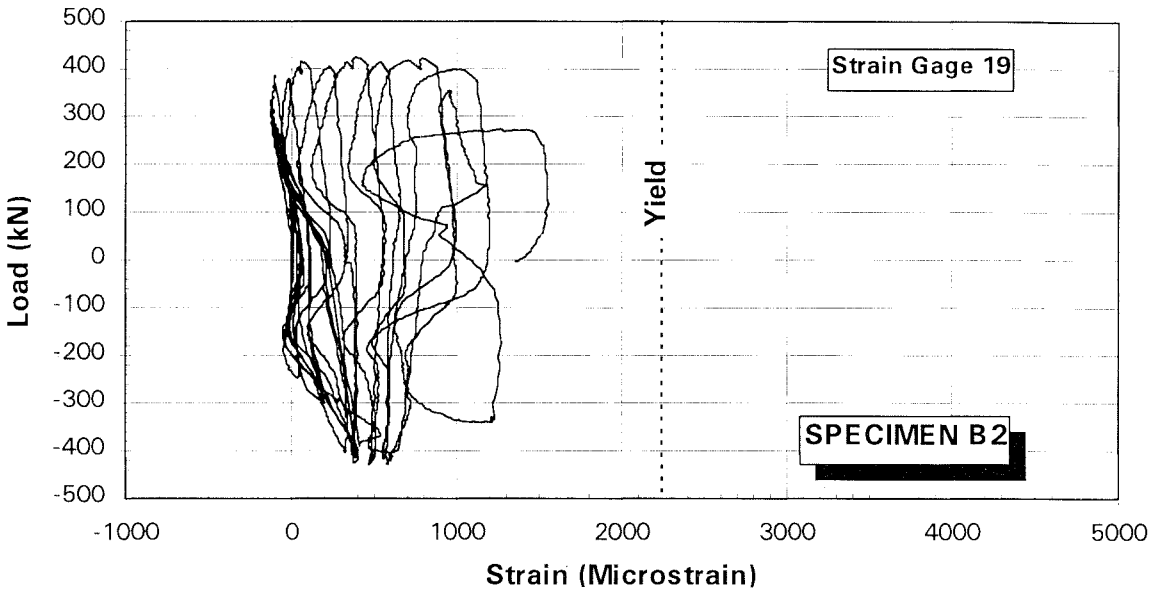

Figure 3-52 Measured Lateral Load-Strain in Specimen B2 Lateral Steel at SG 19

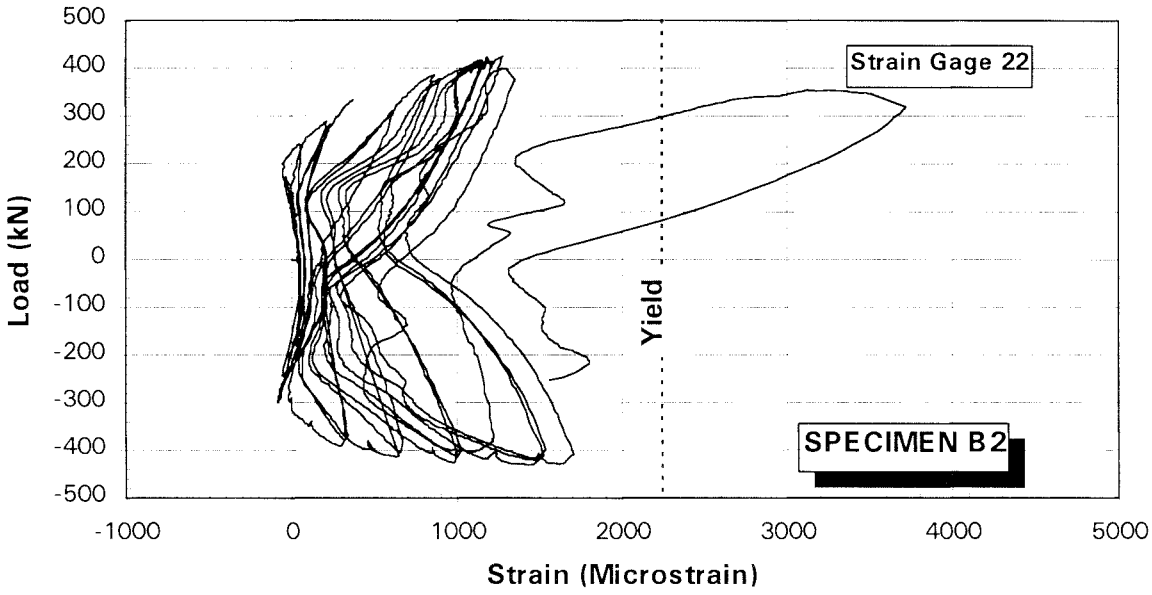

Figure 3-53 Measured Lateral Load-Strain in Specimen B2 lateral Steel at SG 22

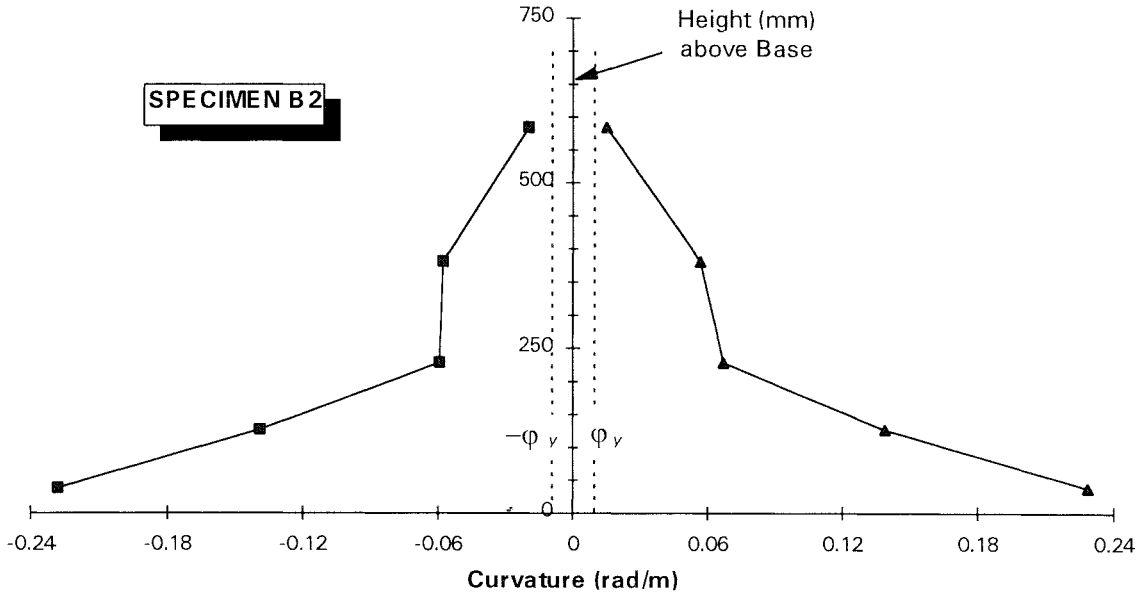

Figure 3-54 Measured Curvature Envelope along the Plastic Hinge of Specimen B2

3.8 Summary and Observations

A summary of the measured lateral loads, curvature at yield, and plastic hinge lengths is presented in Table 3-6.

Table 3-6 Measured Lateral Loads, Yield Curvatures, and Plastic Hinge Lengths

Specimen	Yield Curvature φ_y rad/m (rad/in)	Lateral Force, kN (Kips)		Plastic Hinge Length, mm (in)	
		@ Yield	Peak	Based on Measured Loads	Based on Measured Curvatures
A1	8.19×10^{-3} (0.208×10^{-3})	275 (61.8)	361 (81.0)	554 (21.8)	645 (25.4)
A2	8.46×10^{-3} (0.215×10^{-3})	314 (70.4)	396 (89.0)	488 (19.2)	747 (29.4)
B1	9.45×10^{-3} (0.240×10^{-3})	276 (62.0)	379 (85.0)	632 (24.9)	767 (30.2)
B2	$9.45x 10^{-3}$ (0.240×10^{-3})	318 (71.3)	417 (93.7)	526 (20.7)	612 (24.1)

Review and comparison of the test data allowed for several observations as follows:

1. The lateral deflection response of concrete members such as those tested in this study consists mainly of three components: flexural, shear, and bond slip (Paulay and Priestley, 1992). When deflection is mainly due to flexure, the hysteresis loops are normally wide and "fat" with little pinching effect at the beginning of the reloading stage. On the other hand, when a major portion of the response is due to high shear and/or bond slip deflections, the hysteresis loops are characterized by strong pinching effect. Examination of the measured lateral load-deflection hysteresis loops of the specimens tested in this study indicate that the deflection response was mainly flexural. The prominent pinching at higher ductility levels can be attributed to the closing of flexural cracks prior to which the applied load is met with little resistance until the cracks are closed.

2. The effect of axial load on ductility can be observed by comparing the measured ductilities of specimens with the same transverse steel amount. Specimens A1 and B1 attained slightly higher ductilities than specimens A2 and B2, respectively. Although the specimens with lower axial load (approximately $0.1 f_c'A_g$) reached higher ductilities than their respective counterparts with higher axial loads (approximately $0.25 f_c'A_g$), the difference in ductilities was not substantial. This is probably due to the fact that at relatively low axial load ranges the axial load effect on ductility is minimal.

3. Even though the lateral steel ratio was approximately 40 percent of that required by codes in Specimens A1 and A2, the specimens were able to carry the vertical load up to displacement ductility of 5 and a drift ratio in excess of 4 percent.

4. Even with reduced amounts of lateral steel below those required by the codes for seismic provision, specimens with higher amounts of transverse steel (B1 and B2) attained higher ductilities than their respective counterparts with lower amounts of lateral steel (A1 and A2). This observation holds true provided that shear failure and premature longitudinal bar buckling are prevented by proper design and detailing.

5. The absence of the "P-Δ effect" in the tests was due to the fact that the Dywidag™ bars applying the axial load assumed a curvature similar to the column curvature as the specimen was pushed to higher drift levels. Thus, the axial load remained nearly concentric throughout the test.

6. The number of specimens tested in this study was too limited to draw conclusive remarks relating the plastic hinge length to the lateral steel amount and the axial load level. However, it was observed that there was no specific trend associating the plastic hinge length to either the confining steel amount or the axial load level.

SECTION 4
ANALYTICAL STUDY

4.1 Introduction

In Section 3, it was experimentally shown that rectangular reinforced concrete bridge columns with approximately 50 percent less lateral steel than the minimum required by AASHTO were able to attain moderate displacement ductilities ranging between 4 and 7. In this section, the analytical models used to predict the response of such columns are discussed.

The analysis was based on existing models and procedures that have been widely used to predict the response of reinforced concrete columns to lateral loading. To calculate column deflections, models pertaining to concrete stress-strain relationship, bond slip and shear deformations, and plastic hinge length were first selected. The calculated response beyond the yield point was highly sensitive to the estimated plastic hinge length and, to a lesser extent, to the stress-strain concrete model. This section describes the theoretical derivations and results. The analytical results are also presented and compared to the test results.

4.2 Theoretical Analysis

4.2.1 Lateral Deflection

For a cantilever column subjected to a lateral load at the free end, the total lateral deflection can be attributed to deformations due to flexure, bond slip (yield penetration) between the bar anchored in the footing and the surrounding concrete, and shear. Additional lateral deflection due to rocking of the footing may also occur. The cantilever column may represent a fixed-pinned column and may also represent the segment of a fixed-fixed column between the section of maximum bending moment and the point of contraflexure. When footing rotation is prevented, the total lateral tip deflection of the cantilever column, Δ_t, may be expressed as (Paulay and Priestley, 1992):

$$\Delta_t = \Delta_f + \Delta_s + \Delta_{sh} \tag{4-1}$$

where
Δ_f = deflection due to flexure
Δ_s = deflection due to bond slip
Δ_{sh} = deflection due to shear

When the lateral deformation of the column is mainly due to flexure, it is possible for the column to form a plastic hinge at the critical section. For a column with uniform cross section, the plastic hinge forms at the fixed end. As is shown in Figure 4-1, the flexural deflection can be found as:

$$\Delta_f = \Delta_y + \Delta_p \tag{4-2}$$

where

Δ_y = lateral deflection at effective flexural yield of the critical section
Δ_p = additional deflection due to rigid body rotation at the plastic hinge

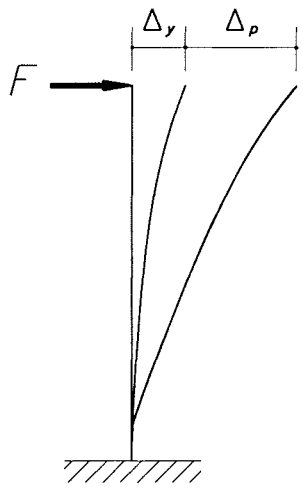

Figure 4-1 Flexural Deflection of a Cantilever Column

Figure 4-2 shows the bending moment diagram and the corresponding curvature of the cantilever column when the fixed end reaches the yield moment, M_y. M_{cr} and φ_{cr} are the cracking moment and the corresponding curvature, respectively. The lateral tip deflection at yield, Δ_y, can then be found by applying the moment area theorem as follows

$$\Delta_y = \int_0^l \varphi x \, dx \tag{4-3}$$

which is the static moment of the area under the curvature diagram about the free end of the column.

When a plastic hinge is formed at the fixed end of the cantilever column, the additional lateral tip deflection, Δ_p, due to rigid body rotation associated with plastic hinging can be found from geometry. Figure 4-3 presents an idealized curvature profile of the cantilever column after the plastic hinge has developed. In this idealization, the actual plastic hinge length is replaced by an equivalent plastic hinge length that would result in the same plastic displacement at the free end. Assuming that the total plastic rotation is concentrated at the middle of the equivalent plastic hinge, Δ_p can be found as (Paulay and Priestley, 1992)

$$\Delta_p = (\varphi_u - \varphi_y) l_p \left(l - \frac{l_p}{2} \right) \tag{4-4}$$

where

φ_u = ultimate curvature of the column cross section
φ_y = yield curvature
l_p = equivalent plastic hinge length
l = total length of the cantilever column

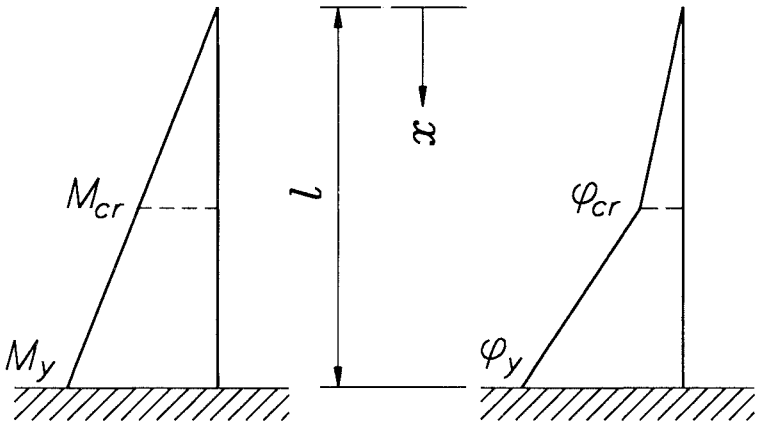

Figure 4-2 Bending Moment and Curvature at Yield of Fixed End

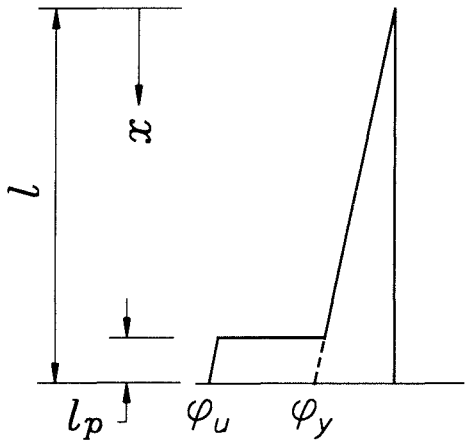

Figure 4-3 Idealized Curvature at the Equivalent Plastic Hinge

To account for the additional deflection due to yield penetration into the footing, the bond slip rotation at the fixed end is first estimated. It has been shown that the bond slip rotation, θ', can be found as (see Appendix A for derivation)

$$\theta' = \frac{1}{8}\frac{d_b}{E_s u}\frac{f_y^2}{d - d'}\left(\frac{M}{M_y}\right)^2 \qquad (4\text{-}5)$$

where

d_b = bar diameter
E_s = modulus of elasticity of steel reinforcement
f_y = yield stress of steel
M_y = yield moment
M = applied moment
d = distance of tension bars to the extreme compression fibers
d' = distance of compression bars to the extreme compression fiber
u = bond strength of main bars

For SI No. 35 (#11) or smaller deformed bars, the basic bond strength of tension bars can be found as (10)

$$u = \frac{20\sqrt{f_c'}}{d_b} \leq 5.5 \quad (MPa) \qquad (4\text{-}6)$$

$$u = \frac{9.5\sqrt{f_c'}}{d_b} \leq 800 \quad (psi) \qquad (4\text{-}7)$$

At yield, the bond slip rotation, θ', can be found from Equation 4-5 where the applied moment is set equal to the effective yield moment of the column. The corresponding lateral tip deflection of the column can then be found by multiplying the bond slip rotation by the cantilever length. Bond slip rotation beyond yield can be implicit in Equation 4-4 by using an appropriate l_p. Thus, the bond slip deflection term, Δ_s, in Equation 4-1 can be reduced to

$$\Delta_s = \theta' . l \qquad (4\text{-}8)$$

Since the column specimens in this study were subjected to relatively low axial loads, the lateral deflection due to shear may be estimated by utilizing shear deflection formulas used for reinforced concrete beams. Although such approach would slightly overestimate the shear deflection, yet the calculated shear deflections would be indicative of the magnitude order of the actual shear deflections. For a beam with 45° diagonal cracks, Park and Paulay (1975) derive the beam shear stiffness , $K_{v,45}$, as

$$K_{v,45} = \frac{\rho_v}{1 + 4n\rho_v} E_s b_w d \qquad (4\text{-}9)$$

where

$K_{v,45}$ = shear deflection in one unit length due to one unit shear load
E_s = elastic modulus of shear reinforcement
b_w = section width perpendicular to applied shear
d = effective section depth parallel to applied shear
n = E_s/E_c (modular ratio)
E_c = elastic modulus of concrete
ρ_v = A_v/sb_w (shear reinforcement ratio)
A_v = area of shear reinforcement
s = spacing of shear reinforcement sets along the member longitudinal axis

Knowing the member shear stiffness, applied shear, and member length, it would be possible to calculate the tip shear deflection of a reinforced concrete cantilever.

4.2.2 Moment-Curvature Analysis

The theoretical moment-curvature relationships of the test specimens were calculated based on plane section analysis which assumes that plane sections before bending remain plane after bending (linear strain gradient). To facilitate the analysis, the constitutive relationships of steel and concrete were first idealized, then the moment-curvature analysis was performed using the computer program IA1.UNR (1989). The program is written in FORTRAN-77 and it calculates the moment-curvature of rectangular reinforced concrete sections. In addition to the axial load and the outermost concrete strain limit for which the analysis is required, the input data include the geometrical dimensions of the section, the areas and locations of the main reinforcement layers, and the constitutive relationships of steel and concrete.

The constitutive relationship for steel was idealized using a tri-linear curve. The first segment represented the stress-strain behavior of steel up to the yield point, followed by a yield plateau up to the beginning of strain hardening, and finally, a strain hardening segment up to the fracture of steel. The longitudinal steel idealized stress-strain curve used in the analysis is shown in Figure 4-4.

Since the computer program IA1.UNR can use only one concrete constitutive relationship, the section of each test specimen was analyzed twice. In the first analysis, the concrete was assumed to be unconfined up to the section effective yield point. Full section properties were used in this analysis. To calculate the curvature and the corresponding moment at ultimate, the section was analyzed again presuming that the cover concrete had spalled and that the core concrete had assumed a confined concrete stress-strain behavior. Thus, two concrete models were needed to represent the constitutive relationships of unconfined and confined concrete sections.

The Kent and Park concrete model (1971) was selected to represent the behavior of unconfined concrete. This model is the basis of the modified Kent and Park model for confined concrete which was presented in Section 2.2.1 of this report. To define the unconfined model, a K factor of unity

is used in Equations 2-1, 2-3 and 2-4. Figure 4-5 shows the theoretical unconfined concrete stress-strain relationships for the specimens in Group I and Group II.

Two different models were used to represent the behavior of confined concrete. The first model was the modified Kent and Park (1971) and the other was the model by Mander et al (1988) as modified by Paulay and Priestley (1992). The two models were presented in Section 2.2 of this report. The theoretical stress-strain relationships of both models are shown in Figure 4-6 and Figure 4-7 for the specimens in Group I and Group II, respectively.

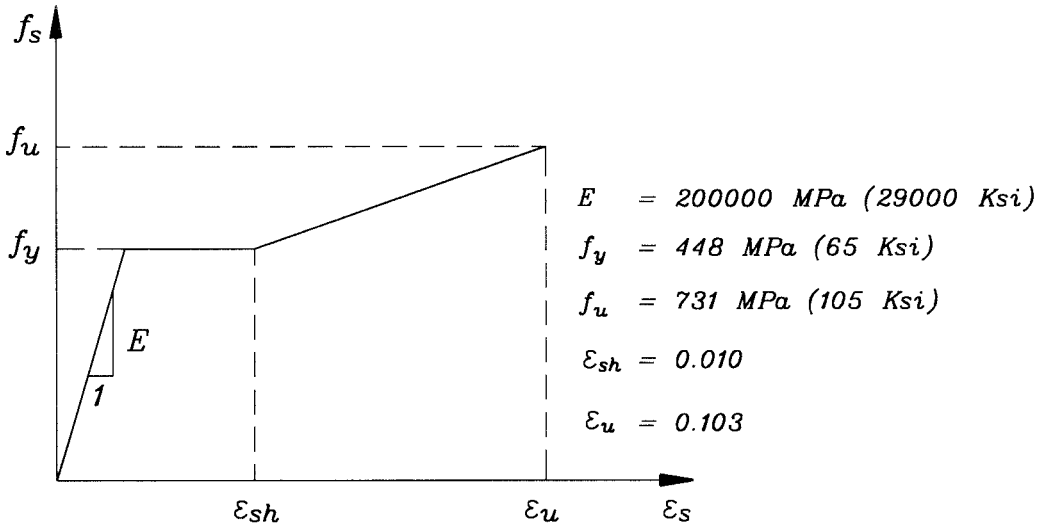

Figure 4-4 Idealized Stress-Strain Curve of Main Steel

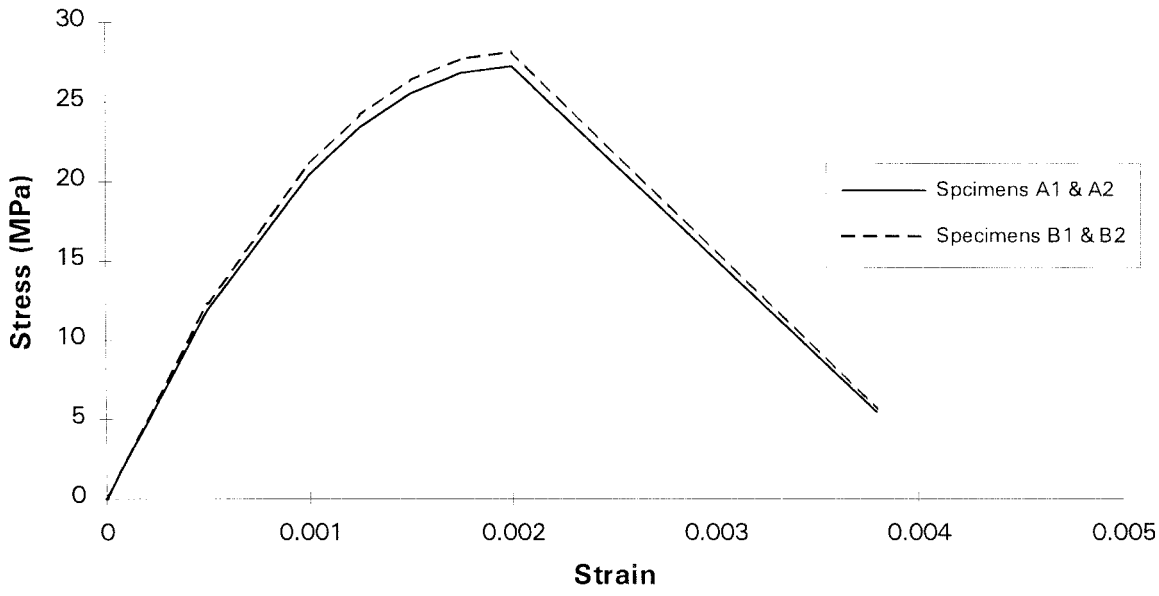

Figure 4-5 Unconfined Concrete Models

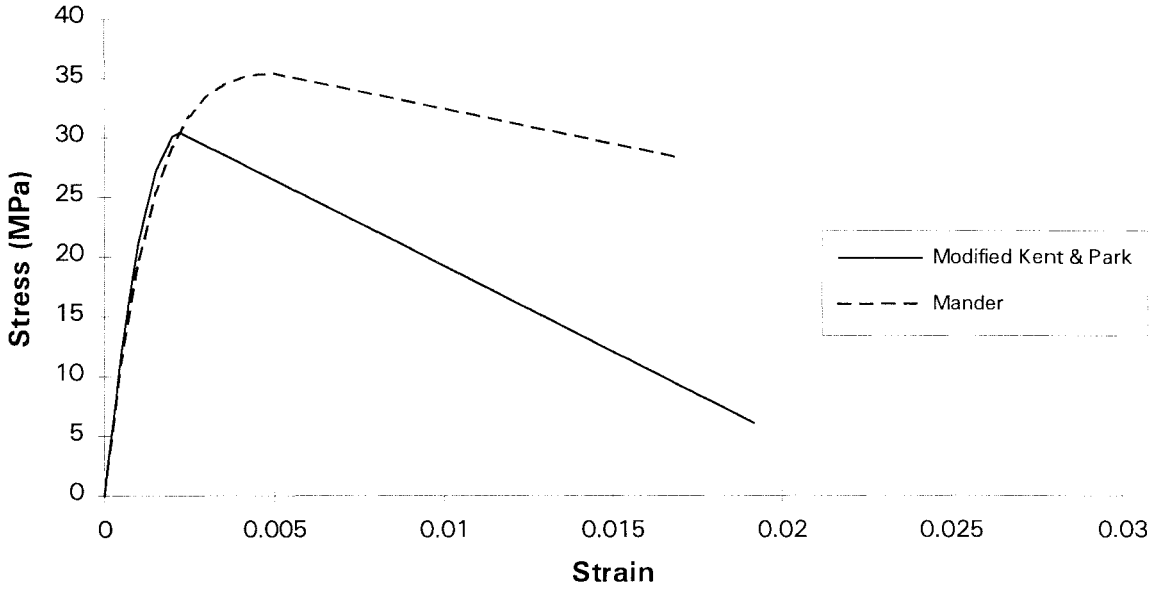

Figure 4-6 Confined Concrete Models for Specimens A1 and A2

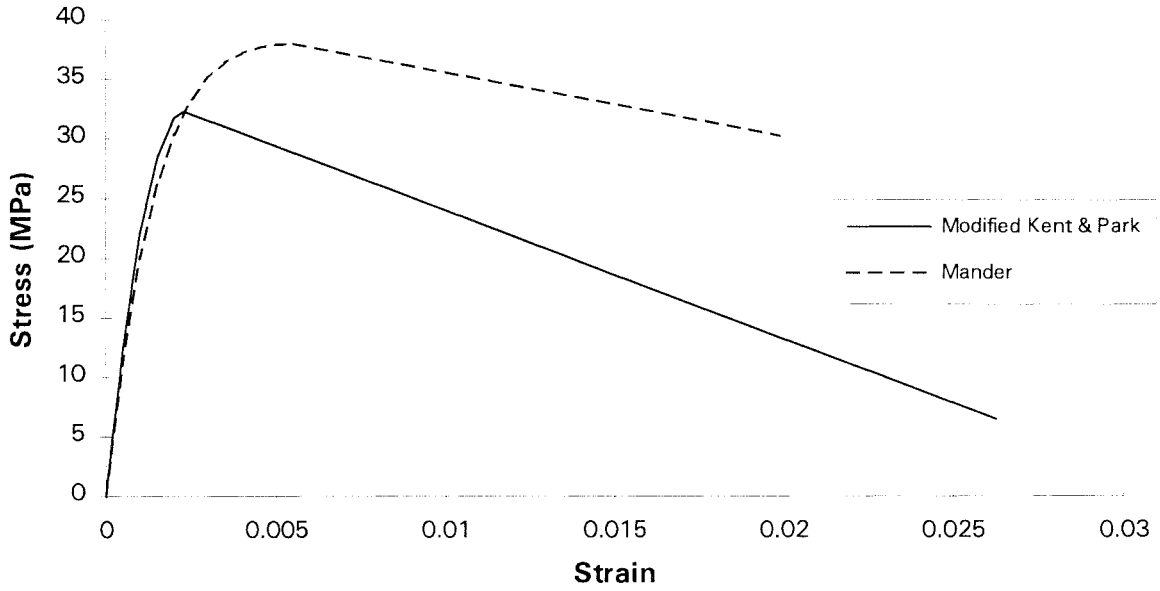

Figure 4-7 Confined Concrete Models for Specimens B1 and B2

Based on the measured material properties and the applied axial loads, the curvatures at section cracking, yield, and ultimate were calculated for the four test specimens. The calculated results are presented in Table 4-1.

Table 4-1 Calculated Curvature

Specimen	Curvature rad/m (rad/in)			
	Kent & Park		Modified Kent & Park	Mander et al.*
	φ_{cr}	φ_y	φ_u	φ_u
A1	0.787×10^{-3} (0.020×10^{-3})	7.91×10^{-3} (0.201×10^{-3})	92.5×10^{-3} (2.35×10^{-3})	97.2×10^{-3} (2.47×10^{-3})
A2	1.300×10^{-3} (0.033×10^{-3})	8.19×10^{-3} (0.208×10^{-3})	66.1×10^{-3} (1.68×10^{-3})	72.8×10^{-3} (1.85×10^{-3})
B1	0.787×10^{-3} (0.020×10^{-3})	7.87×10^{-3} (0.200×10^{-3})	128.4×10^{-3} (3.26×10^{-3})	116.5×10^{-3} (2.96×10^{-3})
B2	1.300×10^{-3} (0.033×10^{-3})	8.11×10^{-3} (0.206×10^{-3})	92.9×10^{-3} (2.36×10^{-3})	89.4×10^{-3} (2.27×10^{-3})

* As modified by Paulay and Priestley

4.2.3 Plastic Hinge Length

To calculate the plastic deflection, Δ_p using Equation 4-4, it is essential to properly evaluate the equivalent plastic hinge length, l_p. Based on previous studies by other researchers, two empirical methods were selected and used in this study to calculate the equivalent plastic hinge length.

Baker (1964) investigated plastic hinging of reinforced concrete members and presented two different expressions for the evaluation of the plastic hinge length of unconfined and confined members. For members with unconfined concrete, the equivalent plastic hinge length is given by

$$l_p = k_1 k_2 k_3 \left(\frac{z}{d} \right)^{1/4} d \qquad (4\text{-}10)$$

where

k_1 = 0.7 for mild steel and 0.9 for cold-worked steel
k_2 = $1 + 0.5 P_u / P_0$
P_u = axial compressive load
P_0 = axial compressive strength of member

k_3 = 0.6 for f_c' = 35.2 MPa (5100 psi)
= 0.9 for f_c' = 11.7 MPa (1700 psi)
z = distance of critical section to point of contraflexure
d = effective depth of member

For members confined with transverse steel, Baker proposed a modified version of Equation 4-10 to calculate the equivalent plastic hinge length as follows

$$l_p = 0.8 k_1 k_3 \left(\frac{z}{d} \right) c \qquad (4\text{-}11)$$

where

c = neutral axis depth under the ultimate moment

It can be seen that Baker's equation for confined concrete implicitly includes the effects of axial load (through c) and confinement on the equivalent plastic hinge length.

Paulay and Priestley (1992), on the other hand, proposed an empirical expression to calculate the equivalent plastic hinge length of reinforced concrete members which is independent of the axial load and the amount of confining steel. This expression is given by

$$l_p = 0.08 l + 0.022 d_b f_y \qquad (MPa) \qquad (4\text{-}12)$$

$$l_p = 0.08 l + 0.15 d_b f_y \qquad (Ksi) \qquad (4\text{-}13)$$

where

l = length of member between critical section and point of contraflexure
d_b = longitudinal bar diameter
f_y = yield stress of longitudinal bars

Based on Equations 4-11 and 4-12, the equivalent plastic hinge length of each test specimen was calculated twice using measured material properties. The calculated equivalent plastic hinge lengths are presented in Table 4-2. Note that the Baker method resulted in equivalent plastc hinge lengths which were 7 to 47 percent higher than those based on Paulay and Priestley.

4.2.4 Calculated Deflections

Based on the analytical procedures presented in section 4.2.1, the lateral deflections were calculated at yield and ultimate points. In this section, the calculated displacements according to different models are presented and compared. Measured material properties were used.

At yield, the calculated lateral deflections due to flexure (Δ_f) and bond slip (Δ_s) were 13.2 mm (0.52 in.) and 2.0 mm (0.08 in.), respectively, for all four specimens. The calculated values were identical in all specimens due to the fact that at low axial loads, the modest change in the applied axial load from $0.1\ f_c'A_g$ to $0.25 f_c'A_g$ resulted in negligible difference in the calculated displacements. Moreover, the small variation in the concrete compressive strengths did not cause any significant difference in the calculated displacements.

Table 4-2 Calculated Equivalent Plastic Hinge Lengths

Specimen	l_p, mm (in)	
	Paulay & Priestley	Baker
A1	375 (14.7)	410 (16.2)
A2	375 (14.7)	550 (21.7)
B1	375 (14.7)	400 (15.8)
B2	375 (14.7)	530 (20.9)

The calculated plastic displacement (Δ_p), in contrast, was strongly sensitive to the models selected for the equivalent plastic hinge length and the stress-strain relationship of confined concrete. For each equivalent plastic hinge length given in Table 4-2, the plastic displacement was calculated twice corresponding to the two confined concrete models considered in this study. The calculated plastic displacements are presented in Table 4-3.

Table 4-3 Calculated Ultimate Plastic Displacement, Δ_p

Specimen	Calculated* Plastic Displacement, Δ_p mm (in.)			
	Modified Kent & Park Concrete Model		Mander et al. Concrete Model**	
	l_p by Priestley	l_p by Baker	l_p by Priestley	l_p by Baker
A1	67.8 (2.67)	74.2 (2.92)	71.6 (2.82)	78.3 (3.08)
A2	46.5 (1.83)	65.8 (2.59)	51.8 (2.04)	73.4 (2.89)
B1	95.5 (3.80)	103.3 (4.07)	87.1 (3.43)	93.2 (3.67)
B2	67.8 (2.67)	93.3 (3.67)	65.0 (2.56)	89.4 (3.52)

* Based on measured material properties and applied axial loads

** As modified by Paulay and Priestley

Beam shear deflections were calculated based on the shear stiffness given by Equation 4-9. Because the steel cross beam depth should not be considered as part of the shear span, a concrete beam length of 2032 mm (80 in.) was considered in the shear deflection analysis. The calculated beam shear deflections are presented in Table 4-4.

The calculated total displacements and displacement ductilities were found by summing the calculated displacement components at yield and at ultimate. This process was repeated for all plastic hinge length and confined concrete model combinations. Table 4-5 presents the calculated results according to the modified Kent and Park concrete model whereas Table 4-6 presents the calculated results corresponding to the Mander et al. concrete model.

Table 4-4 Calculated Beam Shear Deflections

Specimen	Beam Shear Deflection, Δ_{sh} mm (in.)	
	@ Yield	@ Ultimate
A1	4.8 (0.19)	6.4 (0.25)
A2	5.6 (0.22)	6.9 (0.27)
B1	3.8 (0.15)	5.3 (0.21)
B2	4.3 (0.17)	5.6 (0.22)

Table 4-5 Calculated Displacements* and Ductilities-Modified Kent and Park Model

Specimen	$(\Delta_t)_y$ mm (in.)	l_p by Priestley			l_p by Baker		
		$(\Delta_t)_u$ mm (in.)	μ_Δ	Drift Ratio %	$(\Delta_t)_u$ mm (in.)	μ_Δ	Drift Ratio %
A1	20.0 (0.79)	87.8 (3.46)	4.4	3.8	94.2 (3.71)	4.7	4.0
A2	20.8 (0.82)	67.3 (2.65)	3.2	2.9	86.6 (3.41)	4.2	3.7
B1	19.0 (0.75)	114.5 (4.55)	6.1	4.9	122.3 (4.82)	6.4	5.2
B2	19.5 (0.77)	87.3 (3.44)	4.5	3.7	112.8 (4.44)	5.8	4.8

* Including flexural, bond slip, and shear displacements

Table 4-6 Calculated Displacements* and Ductilities-Mander et al. Model**

Specimen	$(\Delta_t)_y$ mm (in.)	l_p by Priestley			l_p by Baker		
		$(\Delta_t)_u$ mm (in.)	μ_Δ	Drift Ratio %	$(\Delta_t)_u$ mm (in.)	μ_Δ	Drift Ratio %
A1	20.0 (0.79)	91.6 (3.61)	4.6	3.9	98.3 (3.87)	4.9	4.2
A2	20.8 (0.82)	72.6 (2.86)	3.5	3.1	94.2 (3.71)	4.5	4.0
B1	19.0 (0.75)	106.1 (4.18)	5.6	4.5	112.2 (4.42)	5.9	4.8
B2	19.5 (0.77)	84.5 (3.33)	4.3	3.6	108.9 (4.29)	5.6	4.7

* Including flexural, bond slip, and shear displacements

** As modified by Paulay and Priestley

4.3 Remarks and Observations

The use of different mathematical models in the analytical study allowed for the evaluation of those models and their applicability to predict the response of rectangular bridge columns to lateral loading.

The calculated ultimate displacements revealed that the flexural component of the lateral displacement is highly sensitive to the equivalent plastic hinge length. The expression given by Baker (Equation 4-11) to calculate the equivalent plastic hinge length yielded closer results to the measured values than the expression given by Paulay and Priestley (Equation 4-12).

The predicted displacements and ductilities were not very sensitive to the selected confined concrete model. When the calculated plastic hinge length as given by Baker's equation was considered, the predicted response was very close to the measured response as can be seen in Tables 4-5, 4-6 and 3-5. The concrete model by Mander et al. (as modified by Paulay and Priestley) resulted in better response predictions for Specimens A1 and A2 than the Modified Kent and Park model. For Specimens B1 and B2, the calculated response according to the Modified Kent and Park model was in better agreement with the measured response than that according to the modified Mander's model.

The theoretical analysis appears to slightly underestimate the actual response. Comparisons between the calculated and measured displacements at yield and ultimate are presented in Tables 4-7 and 4-8, respectively. The calculated ultimate displacements were always less than their respective measured displacements. This could be partly because the theoretical models applied in this study are inherently conservative (lower bound) especially in predicting the ultimate confined concrete strain. The measured displacements could also be artificially higher due to some additional displacements

induced by the loading mechanism. Under lateral loads, the top cross steel beam might have slightly rotated or slid until it became tightly snug against the anchor bolts at the top of the column. These effects, of course, are only significant in the yield displacements.

Table 4-7 Measured and Calculated Displacements at Yield

Specimen	Measured $(\Delta_y)_m$ mm (in.)	Calculated $(\Delta_y)_c$ mm (in.)	$(\Delta_y)_c / (\Delta_y)_m$
A1	23 (0.92)	20 (0.79)	0.86
A2	20 (0.79)	20.8 (0.82)	1.04
B1	23 (0.92)	19.0 (0.75)	0.82
B2	21 (0.82)	19.5 (0.77)	0.94

Table 4-8 Comparison of Measured and Calculated Displacements at Ultimate

Specimen	Measured $(\Delta_u)_m$ mm (in.)	Calculated/Measured Displacement at Ultimate			
		l_p by Baker		l_p by Priestley	
		Modified Kent & Park Concrete Model	Mander at al. Concrete Model	Modified Kent & Park Concrete Model	Mander at al. Concrete Model
		$(\Delta_u)_c / (\Delta_u)_m$	$(\Delta_u)_c / (\Delta_u)_m$	$(\Delta_u)_c / (\Delta_u)_m$	$(\Delta_u)_c / (\Delta_u)_m$
A1	122 (4.82)	0.77	0.80	0.72	0.75
A2	102 (4.02)	0.85	0.92	0.66	0.71
B1	161 (6.33)	0.76	0.70	0.72	0.66
B2	130 (5.10)	0.87	0.84	0.67	0.65

In general, the existing analytical tools for monotonic loading analysis appear to result in reasonably accurate prediction of ductilities of rectangular bridge columns with moderate confinement. Moreover, the design equation given by Paulay and Priestley (Equation 1-4) to calculate the required amount of confining steel agrees well with the test results of the specimens that were subjected to an axial load index of 0.25 (Specimens A2 and B2). For an axial load index of 0.25, Equation 1-4 results in confinement steel ratios ($A_s/s \cdot h_c$) of 0.0042 and 0.0048 for required displacement ductilities of 5 and 6, respectively (see Figure 1-2). The confinement steel ratios in Specimens A2 and B2 were 0.0033 and 0.0043, respectively, and the corresponding measured displacement ductilities were 5.1 and 6.2. At the lower axial load index of 0.1 (Specimens A1 and B1), Equation 1-4 would result in

confinement steel ratios less than those required by the codes for non-seismic design. However, other considerstions, such as shear capacity and longitudinal bar buckling, would rather govern the required minimum amount of lateral steel.

SECTION 5
SUMMARY AND CONCLUSIONS

5.1 Summary

The study presented in this report examined the ductility and behavior of rectangular reinforced concrete bridge columns with moderate confinement. The research comprised experimental and analytical investigation of the response of such columns when subjected to lateral loading.

5.1.1 Experimental Study

For the experimental part of the study, four half-scaled rectangular bridge columns were built and tested. The geometrical dimensions and the amount of longitudinal reinforcement were kept the same for all specimens. The cross section of each column was 380 mm (15 in.) by 610 mm (24 in.) with longitudinal reinforcement volumetric ratio, ρ_l, of 2.2 percent. The columns were built as cantilever columns with a total height between the horizontal loading point and the top of the footing of 2335 mm (92 in.). Each specimen was tested under constant axial load while subjected to lateral load reversals with increasing drift levels. The loading was quasi-static and it was uniaxial in the column strong direction.

Two parameters were varied: the transverse steel reinforcement amount and the axial load level. Based on the amount of lateral steel, the specimens were divided into two groups. The transverse reinforcement ratios, $A_s/(s \cdot h)$, in the long direction for Group I (Specimens A1 and A2) and Group II (Specimens B1 and B2) were 0.0033 and 0.0043, respectively. These ratios corresponded to 42 percent and 54 percent of the minimum lateral reinforcement required by AASHTO for seismic detailing. The tie sets vertical spacing was kept less than six longitudinal bar diameters. Other confinement details pertaining to hook extension and longitudinal bar engagement were maintained according to AASHTO requirements. The nominal shear capacity of the specimens was calculated and was found to exceed the shear demand under the test conditions. The applied axial loads were approximately $0.1 f_c' A_g$ for Specimens A1 and B1 and $0.25 f_c' A_g$ for Specimens A2 and B2.

The specimens were tested to failure. Failure was considered to have occurred when the lateral load carrying capacity was reduced by at least 15 percent of the maximum measured lateral load. Although flexural-shear cracks developed along the column height, all specimens were able to attain moderate ductilities without failing in shear. The measured displacement ductilities of Specimens A1, A2, B1 and B2 were 5.2, 5.1 6.9 and 6.2, respectively. The corresponding drift ratios were 5.2 percent, 4.4 percent, 6.9 percent and 5.5 percent. Plastic hinges were developed in all four specimens at the bottom of the columns. The measured plastic hinge lengths were 645 mm (25.4 in.), 747 mm (29.4 in.), 767 mm (30.2 in.) and 612 mm (24.1 in.) for Specimens A1, A2, B1 and B2, respectively.

5.1.2 Analytical Study

The calculated response of the test specimens to lateral loading was based on plane section analysis. To calculate column deflections, models pertaining to concrete stress-strain relationship, bond slip and shear deformations, and plastic hinge length were selected.

The Kent and Park model (1971) was employed to represent the constitutive relationship of unconfined concrete. For confined concrete, two widely used models were selected for this study. One model was the modified Kent and Park (1971), and the other was based on a model developed by Mander, et al. (1988).

The plastic hinge length was calculated according to two different empirical expressions. The first expression, given by Baker (1964), implicitly included the effects of axial load level and the amount of confining steel on the plastic hinge length. The other model was presented by Paulay and Priestley (1992) and was independent of the degree of confinement and the applied axial load.

Bond slip rotation was calculated using an expression that was derived from basic relationships relating to geometry, compatibility, and bond strength between the main bars and the concrete in the footing.

Since the test specimens were subjected to relatively low axial loads, shear deformations were approximated by utilizing a method used for calculating the shear deflection of reinforced concrete beams. The method, described in Park and Paulay (1975), required that a unit shear stiffness term be calculated first. Based on the unit shear stiffness, column length, and applied shear force, the shear deflection at the top of the column specimen was calculated.

The moment-curvature analysis was performed using the computer program IA1.UNR. The program was written in FORTRAN-77 and it calculates the moment-curvature of rectangular reinforced concrete sections.

The calculated equivalent plastic hinge length varied widely between the two equivalent plastic hinge length expressions employed in this study. According to the expression by Paulay and Priestley (1992), the calculated equivalent plastic hinge length was 375 mm (14.7 in.) for all four column specimens. On the other hand, Baker's equation (1964) resulted in equivalent plastic hinge lengths of 410 mm (16.2 in.), 550 mm (21.7 in.), 400 mm (15.8 in.), and 530 mm (20.9 in.) for Specimens A1, A2, B1, and B2, respectively.

The analysis result revealed that the yield displacements were only slightly dependent on the concrete model used in the analysis. However, the calculated ultimate displacements were very sensitive to the calculated ultimate concrete strain and the equivalent plastic hinge length. The displacements at the top of the columns were calculated for all combinations of concrete models and plastic hinge lengths. The results were summarized in Tables 4-5 and 4-6.

5.2 Conclusions

Based on the experimental observations, test data analysis, and theoretical study performed in this research, the following conclusions can be drawn.

1. At relatively low axial loads ($0.1 f_c' A_g$ to $0.25 f_c' A_g$) such as those encountered in bridges, rectangular reinforced concrete columns with confinement steel at approximately 50 per cent the minimum amount required by the AASHTO seismic provisions may exhibit moderate displacement ductilities ranging between 4 and 7. This would be true provided that shear failure and premature bar buckling are prevented by proper detailing of transverse steel.

2. For rectangular bridge columns with relatively low axial loads and moderate confinement such as those employed in this study, it is possible to predict with reasonable accuracy the response of the columns to lateral cyclic loading. However, proper evaluation of the plastic hinge length would greatly enhance the accuracy of the predicted ultimate displacements.

3. Within the range of parameters included in this study, the calculated ultimate displacements based on Baker's equation (1964) for the equivalent plastic hinge length were closer to the measured ultimate displacements than those calculated using the equivalent plastic hinge length expression given by Paulay and Priestley.

4. The inclusion of shear deformations in this study resulted in more accurate prediction of displacements and ductilities. The calculated shear displacements constituted approximately 20 percent of the yield displacements.

5. Even at low axial loads and moderate confinement, some observations made in this study conform with the results of previous studies done by other researchers on columns with significantly higher axial loads and confinement levels. For the same degree of confinement, the ductility capacity of reinforced concrete columns decreases as the applied axial load increases. On the other hand, for the same axial load, the ductility capacity of reinforced concrete columns is enhanced with higher level of confinement. Moreover, failure in ductile columns is normally initiated by opening of the hoop bends in the plastic hinge region, followed by buckling of main bars.

6. The equation given by Paulay and Priestley (Equation 1-4) relating the amount of confinement steel to the ductility capacity and the applied axial load was in good agreement with the test results of the specimens that were subjected to an axial load index of 0.25. However, at an axial load index of 0.1, the equation underestimates the required amount of confinement steel.

5.3 Recommendations

Current design philosophy in earthquake engineering is based on the "Demand-Capacity" concept. Recent developments in earthquake ground motion estimation (1994) has made it possible to

produce Uniform Hazard Spectra (UHS) maps for all regions of the United States. In the UHS maps, the spectral values for different structural periods are based on the same probability of being exceeded for a specified time window. These maps can be used to estimate the seismic "demand" on bridge structures in different parts of the country.

In locations where the demand is moderate, it would be practical to design bridge columns to attain moderate ductility levels. In this study, it was shown that for rectangular columns with moderate amount of confinement steel, it was possible to achieve moderate ductilities without compromising the axial load carrying capacity of the columns. Thus good seismic performance of rectangular columns with moderate amount of transverse reinforcement may be expected in areas of low to moderate seismicity. However, post-earthquake serviceability can not be guaranteed since the strength of such columns is limited by lateral steel hook opening or hoop fracture which is difficult to repair.

SECTION 6
REFERENCES

1. American Association of State Highway and Transportation Officials, *"Standard Specifications for Highway Bridges,"* Fifteenth Edition, Washington, D.C., 1992.

2. American Concrete Institute Committee 318, *"Building Code Requirements for Reinforced Concrete and Commentary,"* American Concrete Institute, Detroit, Michigan, 1992.

3. Azizinamini, A., W. Corley, and L. Johal, *"Effects of Transverse Reinforcement on Seismic Performance of Columns,"* ACI Structural Journal, July-August, 1992, pp. 442-450.

4. Baker, A.L.L. and A.M.N. Amarakone, *"Inelastic Hyperstatic Frames Analysis,"* Proceedings of the International Symposium on the Flexural Mechanics of Reinforced Concrete, ASCE-ACI, Miami, November, 1964, pp. 85-142.

5. California Department of Transportation, *"Bridge Design Specifications, 1983 AASHTO with Interims and Revisions by Caltrans,"* Sacramento, California.

6. Commission of the European Communities, *"Eurocode 8 -- Structures in Seismic Regions - Design, Part 2 - Bridges,"* Draft Report, March, 1994.

7. Federal Highway Administration, *"Seismic Retrofitting Manual for Highway Bridges,"* Publication No. FHWA-RD-94-052, May 1995, 6300 Georgetown Pike, McLean, Virginia 22101-2296.

8. Frankel, A., P. Thenhaus, D. Perkins, E.V. Leyendecker, *"Ground Motion Mapping--Past, Present and Future,"* Proceedings of Seminar on New Developments in Earthquake Motion Estimation and Implications for Engineering Design Practice, ATC 35-1, 1994.

9. Kent, D.C. and R. Park, *"Flexural Members with Confined Concrete,"* ASCE Journal of the Structural Division, Vol. 97, No. ST7, July, 1971, pp. 1969-1990.

10. Leet, K., *"Reinforced Concrete Design,"* Second Edition, McGraw Hill, Inc., New York, 1991.

11. Mander, J.B., M.J.N. Priestley, and R. Park, *"Theoretical Stress-Strain Model for Confined Concrete Columns,"* ASCE Journal of Structural Engineering, Vol. 114, No. 8, August, 1988, pp. 1804-1826.

12. Ozcebe, G. and M. Saatcioglu, *"Confinement of Concrete Columns for Seismic Loading,"* ACI Structural Journal, July-August, 1987, pp. 308-315.

13. Park, R., M.J.N. Priestley, and W. Gill, *"Ductility of Square Confined Concrete Columns,"* ASCE Journal of Structural Division, Vol. 108, April, 1982, pp. 929-980.

14. Park, R. and T. Paulay, *"Reinforced Concrete Structures,"* John Wiley & Sons, New York, 1975.

15. Paulay, T. and M.J.N. Priestley, *"Seismic Design of Reinforced Concrete and Masonry Buildings,"* John Wiley & Sons, Inc., New York, 1992.

16. Priestley, M. J. N. and R. Park, *"Strength and Ductility of Concrete Bridge Columns under Seismic Loading,"* ACI Structural Journal, January-February, 1987, pp. 61-76.

17. Priestley, M. J. N., Verma, R., and Xiao, Y., "*Seismic Shear Strength of Reinforced Concrete Columns,*" ASCE Journal of Structural Engineering, Vol. 120, No. 8 August, 1994, pp. 2310-2329.

18. Saatcioglu, M. and R. Razvi, *"Strength and Ductility of Confined Concrete,"* ASCE Journal of Structural Engineering, Vol. 118, No. 6, June, 1992, pp. 1590-1607.

19. Sheikh, S. and S. Khoury, *"Confined Concrete Columns with Stubs,"* ACI Structural Journal, July-August, 1993, pp. 414-431.

20. Sheikh, S.A. and S.M. Uzumeri, *"Analytical Model for Concrete Confinement in Tied Columns,"* ASCE Journal of the Structural Division, Vol. 108, No. ST12, December, 1982, pp. 2703-2722.

21. Soesianawati, M., R. Park, and N. Priestley, *"Flexural Ductility of Reinforced Concrete Columns with Low Axial Load and Limited Transverse Reinforcement,"* Proceedings of the Pacific Conference on Earthquake Engineering, New Zealand, 5-7 August, 1987, Vol. 1, pp. 201-212.

22. Standard Association of New Zealand, *"Code of Practice for Design of Concrete Structures, NSZ 3101 Part 1: 1982,"* Wellington, New Zealand, 1982.

23. Watson, S., Zahn, F. A., and Park, R., "*Confining Reinforcement for Concrete Columns,*" ASCE Journal of Structural Engineering, Vol. 120, No. 6, June, 1994, pp. 1798-1823.

24. Zahn, F., A., Park, R., Priestley, M. J. N., and Chapman, H., E., "*Development of Design Procedures for the Flexural Strength and Ductility of Reinforced Concrete Bridge Columns,*" Bulletin of the New Zealand National Society for Earthquake Engineering, Vol. 19, No. 3, September, 1986, pp. 200-212.

25. *"Bridge Memo to Designers Manual, Memo 20-4,"* State of California, Department of Transportation, Office of the Structure Division, Sacramento, California.

26. *"IA1.UNR, User's Manual, Computer Program for Moment-Curvature Analysis of R/C Sections,"* 1989.

APPENDIX A
BOND SLIP ROTATION

Consider the reinforced concrete member shown in Figure A-1. The tensile steel bar has a development length l_d and bar diameter d_b. When the member is subjected to a bending moment M, the bond slip of the embedded tensile bar in the adjacent member causes a rotation θ'.

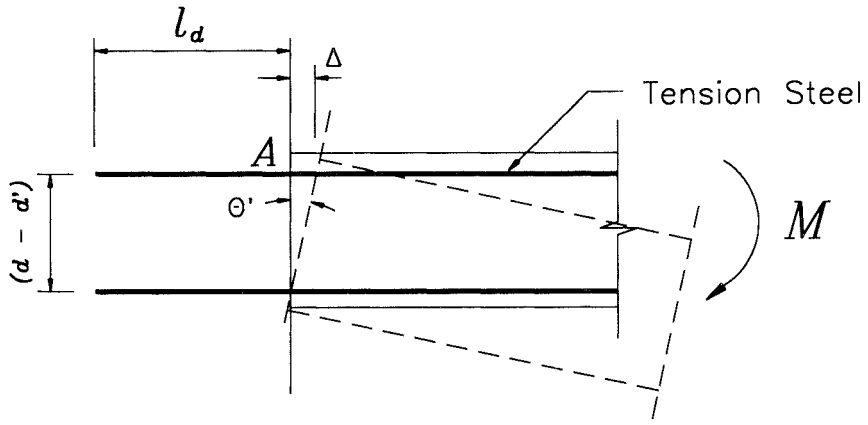

Figure A-1 Bond Slip Rotation

Assume that the bond stress, u, along the embedded bar development length is uniform and that the stress in the tension bar at point A is f_s. From equlibrium it follows that the tensile stress of the tension bar along l_d varies linearly from zero at the free end of the bar to f_s at the interface. Hence, the average stress in the embedded portion of the tension bar is $f_s/2$.

Consider the free body of the embedded length l_d of the tensile bar. From equilibrium of forces the following equality can be written

$$l_d(\pi d_b)u = A_s f_s \tag{A-1}$$

Then, the development length, l_d, can be expressed as

$$l_d = \frac{A_s f_s}{\pi u d_b} \tag{A-2}$$

The average strain along the development length may be written as

$$\epsilon_s = \frac{(f_s/2)}{E_s} \tag{A-3}$$

where E_s is the modulus of elasticity of the steel bar.

The total bar extension, Δ, at the interface can be found from $\Delta = \epsilon_s l_d$. Substituting from Equations A-2 and A-3, the bar extension would be

$$\Delta = \frac{d_b f_s^2}{8 E_s u} \tag{A-4}$$

Assuming that the beam will rotate about the centroid of the compression bar, the corresponding concrete element rotation, θ', is related to the bar extension as follows

$$\theta' = \frac{\Delta}{d - d'} \tag{A-5}$$

where $(d - d')$ is the distance between tension and compression bars.

Knowing that $f_s/f_y \simeq M/M_y$, the tensile stress in the tension bar may be expressed as

$$f_s \simeq f_y \frac{M}{M_y} \tag{A-6}$$

Substituting Equations A-4 and A-6 into Equation A-5 the bond slip rotation is obtained as

$$\theta' = \frac{1}{8} \frac{d_b}{E_s u} \frac{f_y^2}{d - d'} \left(\frac{M}{M_y} \right)^2 \tag{A-7}$$

NATIONAL CENTER FOR EARTHQUAKE ENGINEERING RESEARCH
LIST OF TECHNICAL REPORTS

The National Center for Earthquake Engineering Research (NCEER) publishes technical reports on a variety of subjects related to earthquake engineering written by authors funded through NCEER. These reports are available from both NCEER Publications and the National Technical Information Service (NTIS). Requests for reports should be directed to NCEER Publications, National Center for Earthquake Engineering Research, State University of New York at Buffalo, Red Jacket Quadrangle, Buffalo, New York 14261. Reports can also be requested through NTIS, 5285 Port Royal Road, Springfield, Virginia 22161. NTIS accession numbers are shown in parenthesis, if available.

NCEER-87-0001 "First-Year Program in Research, Education and Technology Transfer," 3/5/87, (PB88-134275, A04, MF-A01).

NCEER-87-0002 "Experimental Evaluation of Instantaneous Optimal Algorithms for Structural Control," by R.C. Lin, T.T. Soong and A.M. Reinhorn, 4/20/87, (PB88-134341, A04, MF-A01).

NCEER-87-0003 "Experimentation Using the Earthquake Simulation Facilities at University at Buffalo," by A.M. Reinhorn and R.L. Ketter, to be published.

NCEER-87-0004 "The System Characteristics and Performance of a Shaking Table," by J.S. Hwang, K.C. Chang and G.C. Lee, 6/1/87, (PB88-134259, A03, MF-A01). This report is available only through NTIS (see address given above).

NCEER-87-0005 "A Finite Element Formulation for Nonlinear Viscoplastic Material Using a Q Model," by O. Gyebi and G. Dasgupta, 11/2/87, (PB88-213764, A08, MF-A01).

NCEER-87-0006 "Symbolic Manipulation Program (SMP) - Algebraic Codes for Two and Three Dimensional Finite Element Formulations," by X. Lee and G. Dasgupta, 11/9/87, (PB88-218522, A05, MF-A01).

NCEER-87-0007 "Instantaneous Optimal Control Laws for Tall Buildings Under Seismic Excitations," by J.N. Yang, A. Akbarpour and P. Ghaemmaghami, 6/10/87, (PB88-134333, A06, MF-A01). This report is only available through NTIS (see address given above).

NCEER-87-0008 "IDARC: Inelastic Damage Analysis of Reinforced Concrete Frame - Shear-Wall Structures," by Y.J. Park, A.M. Reinhorn and S.K. Kunnath, 7/20/87, (PB88-134325, A09, MF-A01). This report is only available through NTIS (see address given above).

NCEER-87-0009 "Liquefaction Potential for New York State: A Preliminary Report on Sites in Manhattan and Buffalo," by M. Budhu, V. Vijayakumar, R.F. Giese and L. Baumgras, 8/31/87, (PB88-163704, A03, MF-A01). This report is available only through NTIS (see address given above).

NCEER-87-0010 "Vertical and Torsional Vibration of Foundations in Inhomogeneous Media," by A.S. Veletsos and K.W. Dotson, 6/1/87, (PB88-134291, A03, MF-A01). This report is only available through NTIS (see address given above).

NCEER-87-0011 "Seismic Probabilistic Risk Assessment and Seismic Margins Studies for Nuclear Power Plants," by Howard H.M. Hwang, 6/15/87, (PB88-134267, A03, MF-A01). This report is only available through NTIS (see address given above).

NCEER-87-0012 "Parametric Studies of Frequency Response of Secondary Systems Under Ground-Acceleration Excitations," by Y. Yong and Y.K. Lin, 6/10/87, (PB88-134309, A03, MF-A01). This report is only available through NTIS (see address given above).

NCEER-87-0013 "Frequency Response of Secondary Systems Under Seismic Excitation," by J.A. HoLung, J. Cai and Y.K. Lin, 7/31/87, (PB88-134317, A05, MF-A01). This report is only available through NTIS (see address given above).

NCEER-87-0014 "Modelling Earthquake Ground Motions in Seismically Active Regions Using Parametric Time Series Methods," by G.W. Ellis and A.S. Cakmak, 8/25/87, (PB88-134283, A08, MF-A01). This report is only available through NTIS (see address given above).

NCEER-87-0015 "Detection and Assessment of Seismic Structural Damage," by E. DiPasquale and A.S. Cakmak, 8/25/87, (PB88-163712, A05, MF-A01). This report is only available through NTIS (see address given above).

NCEER-87-0016 "Pipeline Experiment at Parkfield, California," by J. Isenberg and E. Richardson, 9/15/87, (PB88-163720, A03, MF-A01). This report is available only through NTIS (see address given above).

NCEER-87-0017 "Digital Simulation of Seismic Ground Motion," by M. Shinozuka, G. Deodatis and T. Harada, 8/31/87, (PB88-155197, A04, MF-A01). This report is available only through NTIS (see address given above).

NCEER-87-0018 "Practical Considerations for Structural Control: System Uncertainty, System Time Delay and Truncation of Small Control Forces," J.N. Yang and A. Akbarpour, 8/10/87, (PB88-163738, A08, MF-A01). This report is only available through NTIS (see address given above).

NCEER-87-0019 "Modal Analysis of Nonclassically Damped Structural Systems Using Canonical Transformation," by J.N. Yang, S. Sarkani and F.X. Long, 9/27/87, (PB88-187851, A04, MF-A01).

NCEER-87-0020 "A Nonstationary Solution in Random Vibration Theory," by J.R. Red-Horse and P.D. Spanos, 11/3/87, (PB88-163746, A03, MF-A01).

NCEER-87-0021 "Horizontal Impedances for Radially Inhomogeneous Viscoelastic Soil Layers," by A.S. Veletsos and K.W. Dotson, 10/15/87, (PB88-150859, A04, MF-A01).

NCEER-87-0022 "Seismic Damage Assessment of Reinforced Concrete Members," by Y.S. Chung, C. Meyer and M. Shinozuka, 10/9/87, (PB88-150867, A05, MF-A01). This report is available only through NTIS (see address given above).

NCEER-87-0023 "Active Structural Control in Civil Engineering," by T.T. Soong, 11/11/87, (PB88-187778, A03, MF-A01).

NCEER-87-0024 "Vertical and Torsional Impedances for Radially Inhomogeneous Viscoelastic Soil Layers," by K.W. Dotson and A.S. Veletsos, 12/87, (PB88-187786, A03, MF-A01).

NCEER-87-0025 "Proceedings from the Symposium on Seismic Hazards, Ground Motions, Soil-Liquefaction and Engineering Practice in Eastern North America," October 20-22, 1987, edited by K.H. Jacob, 12/87, (PB88-188115, A23, MF-A01).

NCEER-87-0026 "Report on the Whittier-Narrows, California, Earthquake of October 1, 1987," by J. Pantelic and A. Reinhorn, 11/87, (PB88-187752, A03, MF-A01). This report is available only through NTIS (see address given above).

NCEER-87-0027 "Design of a Modular Program for Transient Nonlinear Analysis of Large 3-D Building Structures," by S. Srivastav and J.F. Abel, 12/30/87, (PB88-187950, A05, MF-A01). This report is only available through NTIS (see address given above).

NCEER-87-0028 "Second-Year Program in Research, Education and Technology Transfer," 3/8/88, (PB88-219480, A04, MF-A01).

NCEER-88-0001 "Workshop on Seismic Computer Analysis and Design of Buildings With Interactive Graphics," by W. McGuire, J.F. Abel and C.H. Conley, 1/18/88, (PB88-187760, A03, MF-A01). This report is only available through NTIS (see address given above).

NCEER-88-0002 "Optimal Control of Nonlinear Flexible Structures," by J.N. Yang, F.X. Long and D. Wong, 1/22/88, (PB88-213772, A06, MF-A01).

NCEER-88-0003 "Substructuring Techniques in the Time Domain for Primary-Secondary Structural Systems," by G.D. Manolis and G. Juhn, 2/10/88, (PB88-213780, A04, MF-A01).

NCEER-88-0004 "Iterative Seismic Analysis of Primary-Secondary Systems," by A. Singhal, L.D. Lutes and P.D. Spanos, 2/23/88, (PB88-213798, A04, MF-A01).

NCEER-88-0005 "Stochastic Finite Element Expansion for Random Media," by P.D. Spanos and R. Ghanem, 3/14/88, (PB88-213806, A03, MF-A01).

NCEER-88-0006 "Combining Structural Optimization and Structural Control," by F.Y. Cheng and C.P. Pantelides, 1/10/88, (PB88-213814, A05, MF-A01).

NCEER-88-0007 "Seismic Performance Assessment of Code-Designed Structures," by H.H-M. Hwang, J-W. Jaw and H-J. Shau, 3/20/88, (PB88-219423, A04, MF-A01). This report is only available through NTIS (see address given above).

NCEER-88-0008 "Reliability Analysis of Code-Designed Structures Under Natural Hazards," by H.H-M. Hwang, H. Ushiba and M. Shinozuka, 2/29/88, (PB88-229471, A07, MF-A01). This report is only available through NTIS (see address given above).

NCEER-88-0009 "Seismic Fragility Analysis of Shear Wall Structures," by J-W Jaw and H.H-M. Hwang, 4/30/88, (PB89-102867, A04, MF-A01).

NCEER-88-0010 "Base Isolation of a Multi-Story Building Under a Harmonic Ground Motion - A Comparison of Performances of Various Systems," by F-G Fan, G. Ahmadi and I.G. Tadjbakhsh, 5/18/88, (PB89-122238, A06, MF-A01). This report is only available through NTIS (see address given above).

NCEER-88-0011 "Seismic Floor Response Spectra for a Combined System by Green's Functions," by F.M. Lavelle, L.A. Bergman and P.D. Spanos, 5/1/88, (PB89-102875, A03, MF-A01).

NCEER-88-0012 "A New Solution Technique for Randomly Excited Hysteretic Structures," by G.Q. Cai and Y.K. Lin, 5/16/88, (PB89-102883, A03, MF-A01).

NCEER-88-0013 "A Study of Radiation Damping and Soil-Structure Interaction Effects in the Centrifuge," by K. Weissman, supervised by J.H. Prevost, 5/24/88, (PB89-144703, A06, MF-A01).

NCEER-88-0014 "Parameter Identification and Implementation of a Kinematic Plasticity Model for Frictional Soils," by J.H. Prevost and D.V. Griffiths, to be published.

NCEER-88-0015 "Two- and Three- Dimensional Dynamic Finite Element Analyses of the Long Valley Dam," by D.V. Griffiths and J.H. Prevost, 6/17/88, (PB89-144711, A04, MF-A01).

NCEER-88-0016 "Damage Assessment of Reinforced Concrete Structures in Eastern United States," by A.M. Reinhorn, M.J. Seidel, S.K. Kunnath and Y.J. Park, 6/15/88, (PB89-122220, A04, MF-A01). This report is only available through NTIS (see address given above).

NCEER-88-0017 "Dynamic Compliance of Vertically Loaded Strip Foundations in Multilayered Viscoelastic Soils," by S. Ahmad and A.S.M. Israil, 6/17/88, (PB89-102891, A04, MF-A01).

NCEER-88-0018 "An Experimental Study of Seismic Structural Response With Added Viscoelastic Dampers," by R.C. Lin, Z. Liang, T.T. Soong and R.H. Zhang, 6/30/88, (PB89-122212, A05, MF-A01). This report is available only through NTIS (see address given above).

NCEER-88-0019 "Experimental Investigation of Primary - Secondary System Interaction," by G.D. Manolis, G. Juhn and A.M. Reinhorn, 5/27/88, (PB89-122204, A04, MF-A01).

NCEER-88-0020 "A Response Spectrum Approach For Analysis of Nonclassically Damped Structures," by J.N. Yang, S. Sarkani and F.X. Long, 4/22/88, (PB89-102909, A04, MF-A01).

NCEER-88-0021 "Seismic Interaction of Structures and Soils: Stochastic Approach," by A.S. Veletsos and A.M. Prasad, 7/21/88, (PB89-122196, A04, MF-A01). This report is only available through NTIS (see address given above).

NCEER-88-0022 "Identification of the Serviceability Limit State and Detection of Seismic Structural Damage," by E. DiPasquale and A.S. Cakmak, 6/15/88, (PB89-122188, A05, MF-A01). This report is available only through NTIS (see address given above).

NCEER-88-0023 "Multi-Hazard Risk Analysis: Case of a Simple Offshore Structure," by B.K. Bhartia and E.H. Vanmarcke, 7/21/88, (PB89-145213, A05, MF-A01).

NCEER-88-0024 "Automated Seismic Design of Reinforced Concrete Buildings," by Y.S. Chung, C. Meyer and M. Shinozuka, 7/5/88, (PB89-122170, A06, MF-A01). This report is available only through NTIS (see address given above).

NCEER-88-0025 "Experimental Study of Active Control of MDOF Structures Under Seismic Excitations," by L.L. Chung, R.C. Lin, T.T. Soong and A.M. Reinhorn, 7/10/88, (PB89-122600, A04, MF-A01).

NCEER-88-0026 "Earthquake Simulation Tests of a Low-Rise Metal Structure," by J.S. Hwang, K.C. Chang, G.C. Lee and R.L. Ketter, 8/1/88, (PB89-102917, A04, MF-A01).

NCEER-88-0027 "Systems Study of Urban Response and Reconstruction Due to Catastrophic Earthquakes," by F. Kozin and H.K. Zhou, 9/22/88, (PB90-162348, A04, MF-A01).

NCEER-88-0028 "Seismic Fragility Analysis of Plane Frame Structures," by H.H-M. Hwang and Y.K. Low, 7/31/88, (PB89-131445, A06, MF-A01).

NCEER-88-0029 "Response Analysis of Stochastic Structures," by A. Kardara, C. Bucher and M. Shinozuka, 9/22/88, (PB89-174429, A04, MF-A01).

NCEER-88-0030 "Nonnormal Accelerations Due to Yielding in a Primary Structure," by D.C.K. Chen and L.D. Lutes, 9/19/88, (PB89-131437, A04, MF-A01).

NCEER-88-0031 "Design Approaches for Soil-Structure Interaction," by A.S. Veletsos, A.M. Prasad and Y. Tang, 12/30/88, (PB89-174437, A03, MF-A01). This report is available only through NTIS (see address given above).

NCEER-88-0032 "A Re-evaluation of Design Spectra for Seismic Damage Control," by C.J. Turkstra and A.G. Tallin, 11/7/88, (PB89-145221, A05, MF-A01).

NCEER-88-0033 "The Behavior and Design of Noncontact Lap Splices Subjected to Repeated Inelastic Tensile Loading," by V.E. Sagan, P. Gergely and R.N. White, 12/8/88, (PB89-163737, A08, MF-A01).

NCEER-88-0034 "Seismic Response of Pile Foundations," by S.M. Mamoon, P.K. Banerjee and S. Ahmad, 11/1/88, (PB89-145239, A04, MF-A01).

NCEER-88-0035 "Modeling of R/C Building Structures With Flexible Floor Diaphragms (IDARC2)," by A.M. Reinhorn, S.K. Kunnath and N. Panahshahi, 9/7/88, (PB89-207153, A07, MF-A01).

NCEER-88-0036 "Solution of the Dam-Reservoir Interaction Problem Using a Combination of FEM, BEM with Particular Integrals, Modal Analysis, and Substructuring," by C-S. Tsai, G.C. Lee and R.L. Ketter, 12/31/88, (PB89-207146, A04, MF-A01).

NCEER-88-0037 "Optimal Placement of Actuators for Structural Control," by F.Y. Cheng and C.P. Pantelides, 8/15/88, (PB89-162846, A05, MF-A01).

NCEER-88-0038 "Teflon Bearings in Aseismic Base Isolation: Experimental Studies and Mathematical Modeling," by A. Mokha, M.C. Constantinou and A.M. Reinhorn, 12/5/88, (PB89-218457, A10, MF-A01). This report is available only through NTIS (see address given above).

NCEER-88-0039 "Seismic Behavior of Flat Slab High-Rise Buildings in the New York City Area," by P. Weidlinger and M. Ettouney, 10/15/88, (PB90-145681, A04, MF-A01).

NCEER-88-0040 "Evaluation of the Earthquake Resistance of Existing Buildings in New York City," by P. Weidlinger and M. Ettouney, 10/15/88, to be published.

NCEER-88-0041 "Small-Scale Modeling Techniques for Reinforced Concrete Structures Subjected to Seismic Loads," by W. Kim, A. El-Attar and R.N. White, 11/22/88, (PB89-189625, A05, MF-A01).

NCEER-88-0042 "Modeling Strong Ground Motion from Multiple Event Earthquakes," by G.W. Ellis and A.S. Cakmak, 10/15/88, (PB89-174445, A03, MF-A01).

NCEER-88-0043 "Nonstationary Models of Seismic Ground Acceleration," by M. Grigoriu, S.E. Ruiz and E. Rosenblueth, 7/15/88, (PB89-189617, A04, MF-A01).

NCEER-88-0044 "SARCF User's Guide: Seismic Analysis of Reinforced Concrete Frames," by Y.S. Chung, C. Meyer and M. Shinozuka, 11/9/88, (PB89-174452, A08, MF-A01).

NCEER-88-0045 "First Expert Panel Meeting on Disaster Research and Planning," edited by J. Pantelic and J. Stoyle, 9/15/88, (PB89-174460, A05, MF-A01). This report is only available through NTIS (see address given above).

NCEER-88-0046 "Preliminary Studies of the Effect of Degrading Infill Walls on the Nonlinear Seismic Response of Steel Frames," by C.Z. Chrysostomou, P. Gergely and J.F. Abel, 12/19/88, (PB89-208383, A05, MF-A01).

NCEER-88-0047 "Reinforced Concrete Frame Component Testing Facility - Design, Construction, Instrumentation and Operation," by S.P. Pessiki, C. Conley, T. Bond, P. Gergely and R.N. White, 12/16/88, (PB89-174478, A04, MF-A01).

NCEER-89-0001 "Effects of Protective Cushion and Soil Compliancy on the Response of Equipment Within a Seismically Excited Building," by J.A. HoLung, 2/16/89, (PB89-207179, A04, MF-A01).

NCEER-89-0002 "Statistical Evaluation of Response Modification Factors for Reinforced Concrete Structures," by H.H-M. Hwang and J-W. Jaw, 2/17/89, (PB89-207187, A05, MF-A01).

NCEER-89-0003 "Hysteretic Columns Under Random Excitation," by G-Q. Cai and Y.K. Lin, 1/9/89, (PB89-196513, A03, MF-A01).

NCEER-89-0004 "Experimental Study of `Elephant Foot Bulge' Instability of Thin-Walled Metal Tanks," by Z-H. Jia and R.L. Ketter, 2/22/89, (PB89-207195, A03, MF-A01).

NCEER-89-0005 "Experiment on Performance of Buried Pipelines Across San Andreas Fault," by J. Isenberg, E. Richardson and T.D. O'Rourke, 3/10/89, (PB89-218440, A04, MF-A01). This report is available only through NTIS (see address given above).

NCEER-89-0006 "A Knowledge-Based Approach to Structural Design of Earthquake-Resistant Buildings," by M. Subramani, P. Gergely, C.H. Conley, J.F. Abel and A.H. Zaghw, 1/15/89, (PB89-218465, A06, MF-A01).

NCEER-89-0007 "Liquefaction Hazards and Their Effects on Buried Pipelines," by T.D. O'Rourke and P.A. Lane, 2/1/89, (PB89-218481, A09, MF-A01).

NCEER-89-0008 "Fundamentals of System Identification in Structural Dynamics," by H. Imai, C-B. Yun, O. Maruyama and M. Shinozuka, 1/26/89, (PB89-207211, A04, MF-A01).

NCEER-89-0009 "Effects of the 1985 Michoacan Earthquake on Water Systems and Other Buried Lifelines in Mexico," by A.G. Ayala and M.J. O'Rourke, 3/8/89, (PB89-207229, A06, MF-A01).

NCEER-89-R010 "NCEER Bibliography of Earthquake Education Materials," by K.E.K. Ross, Second Revision, 9/1/89, (PB90-125352, A05, MF-A01). This report is replaced by NCEER-92-0018.

NCEER-89-0011 "Inelastic Three-Dimensional Response Analysis of Reinforced Concrete Building Structures (IDARC-3D), Part I - Modeling," by S.K. Kunnath and A.M. Reinhorn, 4/17/89, (PB90-114612, A07, MF-A01).

NCEER-89-0012 "Recommended Modifications to ATC-14," by C.D. Poland and J.O. Malley, 4/12/89, (PB90-108648, A15, MF-A01).

NCEER-89-0013 "Repair and Strengthening of Beam-to-Column Connections Subjected to Earthquake Loading," by M. Corazao and A.J. Durrani, 2/28/89, (PB90-109885, A06, MF-A01).

NCEER-89-0014 "Program EXKAL2 for Identification of Structural Dynamic Systems," by O. Maruyama, C-B. Yun, M. Hoshiya and M. Shinozuka, 5/19/89, (PB90-109877, A09, MF-A01).

NCEER-89-0015 "Response of Frames With Bolted Semi-Rigid Connections, Part I - Experimental Study and Analytical Predictions," by P.J. DiCorso, A.M. Reinhorn, J.R. Dickerson, J.B. Radziminski and W.L. Harper, 6/1/89, to be published.

NCEER-89-0016 "ARMA Monte Carlo Simulation in Probabilistic Structural Analysis," by P.D. Spanos and M.P. Mignolet, 7/10/89, (PB90-109893, A03, MF-A01).

NCEER-89-P017 "Preliminary Proceedings from the Conference on Disaster Preparedness - The Place of Earthquake Education in Our Schools," Edited by K.E.K. Ross, 6/23/89, (PB90-108606, A03, MF-A01).

NCEER-89-0017 "Proceedings from the Conference on Disaster Preparedness - The Place of Earthquake Education in Our Schools," Edited by K.E.K. Ross, 12/31/89, (PB90-207895, A012, MF-A02). This report is available only through NTIS (see address given above).

NCEER-89-0018 "Multidimensional Models of Hysteretic Material Behavior for Vibration Analysis of Shape Memory Energy Absorbing Devices, by E.J. Graesser and F.A. Cozzarelli, 6/7/89, (PB90-164146, A04, MF-A01).

NCEER-89-0019 "Nonlinear Dynamic Analysis of Three-Dimensional Base Isolated Structures (3D-BASIS)," by S. Nagarajaiah, A.M. Reinhorn and M.C. Constantinou, 8/3/89, (PB90-161936, A06, MF-A01). This report has been replaced by NCEER-93-0011.

NCEER-89-0020 "Structural Control Considering Time-Rate of Control Forces and Control Rate Constraints," by F.Y. Cheng and C.P. Pantelides, 8/3/89, (PB90-120445, A04, MF-A01).

NCEER-89-0021 "Subsurface Conditions of Memphis and Shelby County," by K.W. Ng, T-S. Chang and H-H.M. Hwang, 7/26/89, (PB90-120437, A03, MF-A01).

NCEER-89-0022 "Seismic Wave Propagation Effects on Straight Jointed Buried Pipelines," by K. Elhmadi and M.J. O'Rourke, 8/24/89, (PB90-162322, A10, MF-A02).

NCEER-89-0023 "Workshop on Serviceability Analysis of Water Delivery Systems," edited by M. Grigoriu, 3/6/89, (PB90-127424, A03, MF-A01).

NCEER-89-0024 "Shaking Table Study of a 1/5 Scale Steel Frame Composed of Tapered Members," by K.C. Chang, J.S. Hwang and G.C. Lee, 9/18/89, (PB90-160169, A04, MF-A01).

NCEER-89-0025 "DYNA1D: A Computer Program for Nonlinear Seismic Site Response Analysis - Technical Documentation," by Jean H. Prevost, 9/14/89, (PB90-161944, A07, MF-A01). This report is available only through NTIS (see address given above).

NCEER-89-0026 "1:4 Scale Model Studies of Active Tendon Systems and Active Mass Dampers for Aseismic Protection," by A.M. Reinhorn, T.T. Soong, R.C. Lin, Y.P. Yang, Y. Fukao, H. Abe and M. Nakai, 9/15/89, (PB90-173246, A10, MF-A02).

NCEER-89-0027 "Scattering of Waves by Inclusions in a Nonhomogeneous Elastic Half Space Solved by Boundary Element Methods," by P.K. Hadley, A. Askar and A.S. Cakmak, 6/15/89, (PB90-145699, A07, MF-A01).

NCEER-89-0028 "Statistical Evaluation of Deflection Amplification Factors for Reinforced Concrete Structures," by H.H.M. Hwang, J-W. Jaw and A.L. Ch'ng, 8/31/89, (PB90-164633, A05, MF-A01).

NCEER-89-0029 "Bedrock Accelerations in Memphis Area Due to Large New Madrid Earthquakes," by H.H.M. Hwang, C.H.S. Chen and G. Yu, 11/7/89, (PB90-162330, A04, MF-A01).

NCEER-89-0030 "Seismic Behavior and Response Sensitivity of Secondary Structural Systems," by Y.Q. Chen and T.T. Soong, 10/23/89, (PB90-164658, A08, MF-A01).

NCEER-89-0031 "Random Vibration and Reliability Analysis of Primary-Secondary Structural Systems," by Y. Ibrahim, M. Grigoriu and T.T. Soong, 11/10/89, (PB90-161951, A04, MF-A01).

NCEER-89-0032 "Proceedings from the Second U.S. - Japan Workshop on Liquefaction, Large Ground Deformation and Their Effects on Lifelines, September 26-29, 1989," Edited by T.D. O'Rourke and M. Hamada, 12/1/89, (PB90-209388, A22, MF-A03).

NCEER-89-0033 "Deterministic Model for Seismic Damage Evaluation of Reinforced Concrete Structures," by J.M. Bracci, A.M. Reinhorn, J.B. Mander and S.K. Kunnath, 9/27/89, (PB91-108803, A06, MF-A01).

NCEER-89-0034 "On the Relation Between Local and Global Damage Indices," by E. DiPasquale and A.S. Cakmak, 8/15/89, (PB90-173865, A05, MF-A01).

NCEER-89-0035 "Cyclic Undrained Behavior of Nonplastic and Low Plasticity Silts," by A.J. Walker and H.E. Stewart, 7/26/89, (PB90-183518, A10, MF-A01).

NCEER-89-0036 "Liquefaction Potential of Surficial Deposits in the City of Buffalo, New York," by M. Budhu, R. Giese and L. Baumgrass, 1/17/89, (PB90-208455, A04, MF-A01).

NCEER-89-0037 "A Deterministic Assessment of Effects of Ground Motion Incoherence," by A.S. Veletsos and Y. Tang, 7/15/89, (PB90-164294, A03, MF-A01).

NCEER-89-0038 "Workshop on Ground Motion Parameters for Seismic Hazard Mapping," July 17-18, 1989, edited by R.V. Whitman, 12/1/89, (PB90-173923, A04, MF-A01).

NCEER-89-0039 "Seismic Effects on Elevated Transit Lines of the New York City Transit Authority," by C.J. Costantino, C.A. Miller and E. Heymsfield, 12/26/89, (PB90-207887, A06, MF-A01).

NCEER-89-0040 "Centrifugal Modeling of Dynamic Soil-Structure Interaction," by K. Weissman, Supervised by J.H. Prevost, 5/10/89, (PB90-207879, A07, MF-A01).

NCEER-89-0041 "Linearized Identification of Buildings With Cores for Seismic Vulnerability Assessment," by I-K. Ho and A.E. Aktan, 11/1/89, (PB90-251943, A07, MF-A01).

NCEER-90-0001 "Geotechnical and Lifeline Aspects of the October 17, 1989 Loma Prieta Earthquake in San Francisco," by T.D. O'Rourke, H.E. Stewart, F.T. Blackburn and T.S. Dickerman, 1/90, (PB90-208596, A05, MF-A01).

NCEER-90-0002 "Nonnormal Secondary Response Due to Yielding in a Primary Structure," by D.C.K. Chen and L.D. Lutes, 2/28/90, (PB90-251976, A07, MF-A01).

NCEER-90-0003 "Earthquake Education Materials for Grades K-12," by K.E.K. Ross, 4/16/90, (PB91-251984, A05, MF-A05). This report has been replaced by NCEER-92-0018.

NCEER-90-0004 "Catalog of Strong Motion Stations in Eastern North America," by R.W. Busby, 4/3/90, (PB90-251984, A05, MF-A01).

NCEER-90-0005 "NCEER Strong-Motion Data Base: A User Manual for the GeoBase Release (Version 1.0 for the Sun3)," by P. Friberg and K. Jacob, 3/31/90 (PB90-258062, A04, MF-A01).

NCEER-90-0006 "Seismic Hazard Along a Crude Oil Pipeline in the Event of an 1811-1812 Type New Madrid Earthquake," by H.H.M. Hwang and C-H.S. Chen, 4/16/90, (PB90-258054, A04, MF-A01).

NCEER-90-0007 "Site-Specific Response Spectra for Memphis Sheahan Pumping Station," by H.H.M. Hwang and C.S. Lee, 5/15/90, (PB91-108811, A05, MF-A01).

NCEER-90-0008 "Pilot Study on Seismic Vulnerability of Crude Oil Transmission Systems," by T. Ariman, R. Dobry, M. Grigoriu, F. Kozin, M. O'Rourke, T. O'Rourke and M. Shinozuka, 5/25/90, (PB91-108837, A06, MF-A01).

NCEER-90-0009 "A Program to Generate Site Dependent Time Histories: EQGEN," by G.W. Ellis, M. Srinivasan and A.S. Cakmak, 1/30/90, (PB91-108829, A04, MF-A01).

NCEER-90-0010 "Active Isolation for Seismic Protection of Operating Rooms," by M.E. Talbott, Supervised by M. Shinozuka, 6/8/9, (PB91-110205, A05, MF-A01).

NCEER-90-0011 "Program LINEARID for Identification of Linear Structural Dynamic Systems," by C-B. Yun and M. Shinozuka, 6/25/90, (PB91-110312, A08, MF-A01).

NCEER-90-0012 "Two-Dimensional Two-Phase Elasto-Plastic Seismic Response of Earth Dams," by A.N. Yiagos, Supervised by J.H. Prevost, 6/20/90, (PB91-110197, A13, MF-A02).

NCEER-90-0013 "Secondary Systems in Base-Isolated Structures: Experimental Investigation, Stochastic Response and Stochastic Sensitivity," by G.D. Manolis, G. Juhn, M.C. Constantinou and A.M. Reinhorn, 7/1/90, (PB91-110320, A08, MF-A01).

NCEER-90-0014 "Seismic Behavior of Lightly-Reinforced Concrete Column and Beam-Column Joint Details," by S.P. Pessiki, C.H. Conley, P. Gergely and R.N. White, 8/22/90, (PB91-108795, A11, MF-A02).

NCEER-90-0015 "Two Hybrid Control Systems for Building Structures Under Strong Earthquakes," by J.N. Yang and A. Danielians, 6/29/90, (PB91-125393, A04, MF-A01).

NCEER-90-0016 "Instantaneous Optimal Control with Acceleration and Velocity Feedback," by J.N. Yang and Z. Li, 6/29/90, (PB91-125401, A03, MF-A01).

NCEER-90-0017 "Reconnaissance Report on the Northern Iran Earthquake of June 21, 1990," by M. Mehrain, 10/4/90, (PB91-125377, A03, MF-A01).

NCEER-90-0018 "Evaluation of Liquefaction Potential in Memphis and Shelby County," by T.S. Chang, P.S. Tang, C.S. Lee and H. Hwang, 8/10/90, (PB91-125427, A09, MF-A01).

NCEER-90-0019 "Experimental and Analytical Study of a Combined Sliding Disc Bearing and Helical Steel Spring Isolation System," by M.C. Constantinou, A.S. Mokha and A.M. Reinhorn, 10/4/90, (PB91-125385, A06, MF-A01). This report is available only through NTIS (see address given above).

NCEER-90-0020 "Experimental Study and Analytical Prediction of Earthquake Response of a Sliding Isolation System with a Spherical Surface," by A.S. Mokha, M.C. Constantinou and A.M. Reinhorn, 10/11/90, (PB91-125419, A05, MF-A01).

NCEER-90-0021 "Dynamic Interaction Factors for Floating Pile Groups," by G. Gazetas, K. Fan, A. Kaynia and E. Kausel, 9/10/90, (PB91-170381, A05, MF-A01).

NCEER-90-0022 "Evaluation of Seismic Damage Indices for Reinforced Concrete Structures," by S. Rodriguez-Gomez and A.S. Cakmak, 9/30/90, PB91-171322, A06, MF-A01).

NCEER-90-0023 "Study of Site Response at a Selected Memphis Site," by H. Desai, S. Ahmad, E.S. Gazetas and M.R. Oh, 10/11/90, (PB91-196857, A03, MF-A01).

NCEER-90-0024 "A User's Guide to Strongmo: Version 1.0 of NCEER's Strong-Motion Data Access Tool for PCs and Terminals," by P.A. Friberg and C.A.T. Susch, 11/15/90, (PB91-171272, A03, MF-A01).

NCEER-90-0025 "A Three-Dimensional Analytical Study of Spatial Variability of Seismic Ground Motions," by L-L. Hong and A.H.-S. Ang, 10/30/90, (PB91-170399, A09, MF-A01).

NCEER-90-0026 "MUMOID User's Guide - A Program for the Identification of Modal Parameters," by S. Rodriguez-Gomez and E. DiPasquale, 9/30/90, (PB91-171298, A04, MF-A01).

NCEER-90-0027 "SARCF-II User's Guide - Seismic Analysis of Reinforced Concrete Frames," by S. Rodriguez-Gomez, Y.S. Chung and C. Meyer, 9/30/90, (PB91-171280, A05, MF-A01).

NCEER-90-0028 "Viscous Dampers: Testing, Modeling and Application in Vibration and Seismic Isolation," by N. Makris and M.C. Constantinou, 12/20/90 (PB91-190561, A06, MF-A01).

NCEER-90-0029 "Soil Effects on Earthquake Ground Motions in the Memphis Area," by H. Hwang, C.S. Lee, K.W. Ng and T.S. Chang, 8/2/90, (PB91-190751, A05, MF-A01).

NCEER-91-0001 "Proceedings from the Third Japan-U.S. Workshop on Earthquake Resistant Design of Lifeline Facilities and Countermeasures for Soil Liquefaction, December 17-19, 1990," edited by T.D. O'Rourke and M. Hamada, 2/1/91, (PB91-179259, A99, MF-A04).

NCEER-91-0002 "Physical Space Solutions of Non-Proportionally Damped Systems," by M. Tong, Z. Liang and G.C. Lee, 1/15/91, (PB91-179242, A04, MF-A01).

NCEER-91-0003 "Seismic Response of Single Piles and Pile Groups," by K. Fan and G. Gazetas, 1/10/91, (PB92-174994, A04, MF-A01).

NCEER-91-0004 "Damping of Structures: Part 1 - Theory of Complex Damping," by Z. Liang and G. Lee, 10/10/91, (PB92-197235, A12, MF-A03).

NCEER-91-0005 "3D-BASIS - Nonlinear Dynamic Analysis of Three Dimensional Base Isolated Structures: Part II," by S. Nagarajaiah, A.M. Reinhorn and M.C. Constantinou, 2/28/91, (PB91-190553, A07, MF-A01). This report has been replaced by NCEER-93-0011.

NCEER-91-0006 "A Multidimensional Hysteretic Model for Plasticity Deforming Metals in Energy Absorbing Devices," by E.J. Graesser and F.A. Cozzarelli, 4/9/91, (PB92-108364, A04, MF-A01).

NCEER-91-0007 "A Framework for Customizable Knowledge-Based Expert Systems with an Application to a KBES for Evaluating the Seismic Resistance of Existing Buildings," by E.G. Ibarra-Anaya and S.J. Fenves, 4/9/91, (PB91-210930, A08, MF-A01).

NCEER-91-0008 "Nonlinear Analysis of Steel Frames with Semi-Rigid Connections Using the Capacity Spectrum Method," by G.G. Deierlein, S-H. Hsieh, Y-J. Shen and J.F. Abel, 7/2/91, (PB92-113828, A05, MF-A01).

NCEER-91-0009 "Earthquake Education Materials for Grades K-12," by K.E.K. Ross, 4/30/91, (PB91-212142, A06, MF-A01). This report has been replaced by NCEER-92-0018.

NCEER-91-0010 "Phase Wave Velocities and Displacement Phase Differences in a Harmonically Oscillating Pile," by N. Makris and G. Gazetas, 7/8/91, (PB92-108356, A04, MF-A01).

NCEER-91-0011 "Dynamic Characteristics of a Full-Size Five-Story Steel Structure and a 2/5 Scale Model," by K.C. Chang, G.C. Yao, G.C. Lee, D.S. Hao and Y.C. Yeh," 7/2/91, (PB93-116648, A06, MF-A02).

NCEER-91-0012 "Seismic Response of a 2/5 Scale Steel Structure with Added Viscoelastic Dampers," by K.C. Chang, T.T. Soong, S-T. Oh and M.L. Lai, 5/17/91, (PB92-110816, A05, MF-A01).

NCEER-91-0013 "Earthquake Response of Retaining Walls; Full-Scale Testing and Computational Modeling," by S. Alampalli and A-W.M. Elgamal, 6/20/91, to be published.

NCEER-91-0014 "3D-BASIS-M: Nonlinear Dynamic Analysis of Multiple Building Base Isolated Structures," by P.C. Tsopelas, S. Nagarajaiah, M.C. Constantinou and A.M. Reinhorn, 5/28/91, (PB92-113885, A09, MF-A02).

NCEER-91-0015 "Evaluation of SEAOC Design Requirements for Sliding Isolated Structures," by D. Theodossiou and M.C. Constantinou, 6/10/91, (PB92-114602, A11, MF-A03).

NCEER-91-0016 "Closed-Loop Modal Testing of a 27-Story Reinforced Concrete Flat Plate-Core Building," by H.R. Somaprasad, T. Toksoy, H. Yoshiyuki and A.E. Aktan, 7/15/91, (PB92-129980, A07, MF-A02).

NCEER-91-0017 "Shake Table Test of a 1/6 Scale Two-Story Lightly Reinforced Concrete Building," by A.G. El-Attar, R.N. White and P. Gergely, 2/28/91, (PB92-222447, A06, MF-A02).

NCEER-91-0018 "Shake Table Test of a 1/8 Scale Three-Story Lightly Reinforced Concrete Building," by A.G. El-Attar, R.N. White and P. Gergely, 2/28/91, (PB93-116630, A08, MF-A02).

NCEER-91-0019 "Transfer Functions for Rigid Rectangular Foundations," by A.S. Veletsos, A.M. Prasad and W.H. Wu, 7/31/91, to be published.

NCEER-91-0020 "Hybrid Control of Seismic-Excited Nonlinear and Inelastic Structural Systems," by J.N. Yang, Z. Li and A. Danielians, 8/1/91, (PB92-143171, A06, MF-A02).

NCEER-91-0021 "The NCEER-91 Earthquake Catalog: Improved Intensity-Based Magnitudes and Recurrence Relations for U.S. Earthquakes East of New Madrid," by L. Seeber and J.G. Armbruster, 8/28/91, (PB92-176742, A06, MF-A02).

NCEER-91-0022 "Proceedings from the Implementation of Earthquake Planning and Education in Schools: The Need for Change - The Roles of the Changemakers," by K.E.K. Ross and F. Winslow, 7/23/91, (PB92-129998, A12, MF-A03).

NCEER-91-0023 "A Study of Reliability-Based Criteria for Seismic Design of Reinforced Concrete Frame Buildings," by H.H.M. Hwang and H-M. Hsu, 8/10/91, (PB92-140235, A09, MF-A02).

NCEER-91-0024 "Experimental Verification of a Number of Structural System Identification Algorithms," by R.G. Ghanem, H. Gavin and M. Shinozuka, 9/18/91, (PB92-176577, A18, MF-A04).

NCEER-91-0025 "Probabilistic Evaluation of Liquefaction Potential," by H.H.M. Hwang and C.S. Lee," 11/25/91, (PB92-143429, A05, MF-A01).

NCEER-91-0026 "Instantaneous Optimal Control for Linear, Nonlinear and Hysteretic Structures - Stable Controllers," by J.N. Yang and Z. Li, 11/15/91, (PB92-163807, A04, MF-A01).

NCEER-91-0027 "Experimental and Theoretical Study of a Sliding Isolation System for Bridges," by M.C. Constantinou, A. Kartoum, A.M. Reinhorn and P. Bradford, 11/15/91, (PB92-176973, A10, MF-A03).

NCEER-92-0001 "Case Studies of Liquefaction and Lifeline Performance During Past Earthquakes, Volume 1: Japanese Case Studies," Edited by M. Hamada and T. O'Rourke, 2/17/92, (PB92-197243, A18, MF-A04).

NCEER-92-0002 "Case Studies of Liquefaction and Lifeline Performance During Past Earthquakes, Volume 2: United States Case Studies," Edited by T. O'Rourke and M. Hamada, 2/17/92, (PB92-197250, A20, MF-A04).

NCEER-92-0003 "Issues in Earthquake Education," Edited by K. Ross, 2/3/92, (PB92-222389, A07, MF-A02).

NCEER-92-0004 "Proceedings from the First U.S. - Japan Workshop on Earthquake Protective Systems for Bridges," Edited by I.G. Buckle, 2/4/92, (PB94-142239, A99, MF-A06).

NCEER-92-0005 "Seismic Ground Motion from a Haskell-Type Source in a Multiple-Layered Half-Space," A.P. Theoharis, G. Deodatis and M. Shinozuka, 1/2/92, to be published.

NCEER-92-0006 "Proceedings from the Site Effects Workshop," Edited by R. Whitman, 2/29/92, (PB92-197201, A04, MF-A01).

NCEER-92-0007 "Engineering Evaluation of Permanent Ground Deformations Due to Seismically-Induced Liquefaction," by M.H. Baziar, R. Dobry and A-W.M. Elgamal, 3/24/92, (PB92-222421, A13, MF-A03).

NCEER-92-0008 "A Procedure for the Seismic Evaluation of Buildings in the Central and Eastern United States," by C.D. Poland and J.O. Malley, 4/2/92, (PB92-222439, A20, MF-A04).

NCEER-92-0009 "Experimental and Analytical Study of a Hybrid Isolation System Using Friction Controllable Sliding Bearings," by M.Q. Feng, S. Fujii and M. Shinozuka, 5/15/92, (PB93-150282, A06, MF-A02).

NCEER-92-0010 "Seismic Resistance of Slab-Column Connections in Existing Non-Ductile Flat-Plate Buildings," by A.J. Durrani and Y. Du, 5/18/92, (PB93-116812, A06, MF-A02).

NCEER-92-0011 "The Hysteretic and Dynamic Behavior of Brick Masonry Walls Upgraded by Ferrocement Coatings Under Cyclic Loading and Strong Simulated Ground Motion," by H. Lee and S.P. Prawel, 5/11/92, to be published.

NCEER-92-0012 "Study of Wire Rope Systems for Seismic Protection of Equipment in Buildings," by G.F. Demetriades, M.C. Constantinou and A.M. Reinhorn, 5/20/92, (PB93-116655, A08, MF-A02).

NCEER-92-0013 "Shape Memory Structural Dampers: Material Properties, Design and Seismic Testing," by P.R. Witting and F.A. Cozzarelli, 5/26/92, (PB93-116663, A05, MF-A01).

NCEER-92-0014 "Longitudinal Permanent Ground Deformation Effects on Buried Continuous Pipelines," by M.J. O'Rourke, and C. Nordberg, 6/15/92, (PB93-116671, A08, MF-A02).

NCEER-92-0015 "A Simulation Method for Stationary Gaussian Random Functions Based on the Sampling Theorem," by M. Grigoriu and S. Balopoulou, 6/11/92, (PB93-127496, A05, MF-A01).

NCEER-92-0016 "Gravity-Load-Designed Reinforced Concrete Buildings: Seismic Evaluation of Existing Construction and Detailing Strategies for Improved Seismic Resistance," by G.W. Hoffmann, S.K. Kunnath, A.M. Reinhorn and J.B. Mander, 7/15/92, (PB94-142007, A08, MF-A02).

NCEER-92-0017 "Observations on Water System and Pipeline Performance in the Limón Area of Costa Rica Due to the April 22, 1991 Earthquake," by M. O'Rourke and D. Ballantyne, 6/30/92, (PB93-126811, A06, MF-A02).

NCEER-92-0018 "Fourth Edition of Earthquake Education Materials for Grades K-12," Edited by K.E.K. Ross, 8/10/92, (PB93-114023, A07, MF-A02).

NCEER-92-0019 "Proceedings from the Fourth Japan-U.S. Workshop on Earthquake Resistant Design of Lifeline Facilities and Countermeasures for Soil Liquefaction," Edited by M. Hamada and T.D. O'Rourke, 8/12/92, (PB93-163939, A99, MF-E11).

NCEER-92-0020 "Active Bracing System: A Full Scale Implementation of Active Control," by A.M. Reinhorn, T.T. Soong, R.C. Lin, M.A. Riley, Y.P. Wang, S. Aizawa and M. Higashino, 8/14/92, (PB93-127512, A06, MF-A02).

NCEER-92-0021 "Empirical Analysis of Horizontal Ground Displacement Generated by Liquefaction-Induced Lateral Spreads," by S.F. Bartlett and T.L. Youd, 8/17/92, (PB93-188241, A06, MF-A02).

NCEER-92-0022 "IDARC Version 3.0: Inelastic Damage Analysis of Reinforced Concrete Structures," by S.K. Kunnath, A.M. Reinhorn and R.F. Lobo, 8/31/92, (PB93-227502, A07, MF-A02).

NCEER-92-0023 "A Semi-Empirical Analysis of Strong-Motion Peaks in Terms of Seismic Source, Propagation Path and Local Site Conditions, by M. Kamiyama, M.J. O'Rourke and R. Flores-Berrones, 9/9/92, (PB93-150266, A08, MF-A02).

NCEER-92-0024 "Seismic Behavior of Reinforced Concrete Frame Structures with Nonductile Details, Part I: Summary of Experimental Findings of Full Scale Beam-Column Joint Tests," by A. Beres, R.N. White and P. Gergely, 9/30/92, (PB93-227783, A05, MF-A01).

NCEER-92-0025 "Experimental Results of Repaired and Retrofitted Beam-Column Joint Tests in Lightly Reinforced Concrete Frame Buildings," by A. Beres, S. El-Borgi, R.N. White and P. Gergely, 10/29/92, (PB93-227791, A05, MF-A01).

NCEER-92-0026 "A Generalization of Optimal Control Theory: Linear and Nonlinear Structures," by J.N. Yang, Z. Li and S. Vongchavalitkul, 11/2/92, (PB93-188621, A05, MF-A01).

NCEER-92-0027 "Seismic Resistance of Reinforced Concrete Frame Structures Designed Only for Gravity Loads: Part I - Design and Properties of a One-Third Scale Model Structure," by J.M. Bracci, A.M. Reinhorn and J.B. Mander, 12/1/92, (PB94-104502, A08, MF-A02).

NCEER-92-0028 "Seismic Resistance of Reinforced Concrete Frame Structures Designed Only for Gravity Loads: Part II - Experimental Performance of Subassemblages," by L.E. Aycardi, J.B. Mander and A.M. Reinhorn, 12/1/92, (PB94-104510, A08, MF-A02).

NCEER-92-0029 "Seismic Resistance of Reinforced Concrete Frame Structures Designed Only for Gravity Loads: Part III - Experimental Performance and Analytical Study of a Structural Model," by J.M. Bracci, A.M. Reinhorn and J.B. Mander, 12/1/92, (PB93-227528, A09, MF-A01).

NCEER-92-0030 "Evaluation of Seismic Retrofit of Reinforced Concrete Frame Structures: Part I - Experimental Performance of Retrofitted Subassemblages," by D. Choudhuri, J.B. Mander and A.M. Reinhorn, 12/8/92, (PB93-198307, A07, MF-A02).

NCEER-92-0031 "Evaluation of Seismic Retrofit of Reinforced Concrete Frame Structures: Part II - Experimental Performance and Analytical Study of a Retrofitted Structural Model," by J.M. Bracci, A.M. Reinhorn and J.B. Mander, 12/8/92, (PB93-198315, A09, MF-A03).

NCEER-92-0032 "Experimental and Analytical Investigation of Seismic Response of Structures with Supplemental Fluid Viscous Dampers," by M.C. Constantinou and M.D. Symans, 12/21/92, (PB93-191435, A10, MF-A03).

NCEER-92-0033 "Reconnaissance Report on the Cairo, Egypt Earthquake of October 12, 1992," by M. Khater, 12/23/92, (PB93-188621, A03, MF-A01).

NCEER-92-0034 "Low-Level Dynamic Characteristics of Four Tall Flat-Plate Buildings in New York City," by H. Gavin, S. Yuan, J. Grossman, E. Pekelis and K. Jacob, 12/28/92, (PB93-188217, A07, MF-A02).

NCEER-93-0001 "An Experimental Study on the Seismic Performance of Brick-Infilled Steel Frames With and Without Retrofit," by J.B. Mander, B. Nair, K. Wojtkowski and J. Ma, 1/29/93, (PB93-227510, A07, MF-A02).

NCEER-93-0002 "Social Accounting for Disaster Preparedness and Recovery Planning," by S. Cole, E. Pantoja and V. Razak, 2/22/93, (PB94-142114, A12, MF-A03).

NCEER-93-0003 "Assessment of 1991 NEHRP Provisions for Nonstructural Components and Recommended Revisions," by T.T. Soong, G. Chen, Z. Wu, R-H. Zhang and M. Grigoriu, 3/1/93, (PB93-188639, A06, MF-A02).

NCEER-93-0004 "Evaluation of Static and Response Spectrum Analysis Procedures of SEAOC/UBC for Seismic Isolated Structures," by C.W. Winters and M.C. Constantinou, 3/23/93, (PB93-198299, A10, MF-A03).

NCEER-93-0005 "Earthquakes in the Northeast - Are We Ignoring the Hazard? A Workshop on Earthquake Science and Safety for Educators," edited by K.E.K. Ross, 4/2/93, (PB94-103066, A09, MF-A02).

NCEER-93-0006 "Inelastic Response of Reinforced Concrete Structures with Viscoelastic Braces," by R.F. Lobo, J.M. Bracci, K.L. Shen, A.M. Reinhorn and T.T. Soong, 4/5/93, (PB93-227486, A05, MF-A02).

NCEER-93-0007 "Seismic Testing of Installation Methods for Computers and Data Processing Equipment," by K. Kosar, T.T. Soong, K.L. Shen, J.A. HoLung and Y.K. Lin, 4/12/93, (PB93-198299, A07, MF-A02).

NCEER-93-0008 "Retrofit of Reinforced Concrete Frames Using Added Dampers," by A. Reinhorn, M. Constantinou and C. Li, to be published.

NCEER-93-0009 "Seismic Behavior and Design Guidelines for Steel Frame Structures with Added Viscoelastic Dampers," by K.C. Chang, M.L. Lai, T.T. Soong, D.S. Hao and Y.C. Yeh, 5/1/93, (PB94-141959, A07, MF-A02).

NCEER-93-0010 "Seismic Performance of Shear-Critical Reinforced Concrete Bridge Piers," by J.B. Mander, S.M. Waheed, M.T.A. Chaudhary and S.S. Chen, 5/12/93, (PB93-227494, A08, MF-A02).

NCEER-93-0011 "3D-BASIS-TABS: Computer Program for Nonlinear Dynamic Analysis of Three Dimensional Base Isolated Structures," by S. Nagarajaiah, C. Li, A.M. Reinhorn and M.C. Constantinou, 8/2/93, (PB94-141819, A09, MF-A02).

NCEER-93-0012 "Effects of Hydrocarbon Spills from an Oil Pipeline Break on Ground Water," by O.J. Helweg and H.H.M. Hwang, 8/3/93, (PB94-141942, A06, MF-A02).

NCEER-93-0013 "Simplified Procedures for Seismic Design of Nonstructural Components and Assessment of Current Code Provisions," by M.P. Singh, L.E. Suarez, E.E. Matheu and G.O. Maldonado, 8/4/93, (PB94-141827, A09, MF-A02).

NCEER-93-0014 "An Energy Approach to Seismic Analysis and Design of Secondary Systems," by G. Chen and T.T. Soong, 8/6/93, (PB94-142767, A11, MF-A03).

NCEER-93-0015 "Proceedings from School Sites: Becoming Prepared for Earthquakes - Commemorating the Third Anniversary of the Loma Prieta Earthquake," Edited by F.E. Winslow and K.E.K. Ross, 8/16/93, (PB94-154275, A16, MF-A02).

NCEER-93-0016 "Reconnaissance Report of Damage to Historic Monuments in Cairo, Egypt Following the October 12, 1992 Dahshur Earthquake," by D. Sykora, D. Look, G. Croci, E. Karaesmen and E. Karaesmen, 8/19/93, (PB94-142221, A08, MF-A02).

NCEER-93-0017 "The Island of Guam Earthquake of August 8, 1993," by S.W. Swan and S.K. Harris, 9/30/93, (PB94-141843, A04, MF-A01).

NCEER-93-0018 "Engineering Aspects of the October 12, 1992 Egyptian Earthquake," by A.W. Elgamal, M. Amer, K. Adalier and A. Abul-Fadl, 10/7/93, (PB94-141983, A05, MF-A01).

NCEER-93-0019 "Development of an Earthquake Motion Simulator and its Application in Dynamic Centrifuge Testing," by I. Krstelj, Supervised by J.H. Prevost, 10/23/93, (PB94-181773, A-10, MF-A03).

NCEER-93-0020 "NCEER-Taisei Corporation Research Program on Sliding Seismic Isolation Systems for Bridges: Experimental and Analytical Study of a Friction Pendulum System (FPS)," by M.C. Constantinou, P. Tsopelas, Y-S. Kim and S. Okamoto, 11/1/93, (PB94-142775, A08, MF-A02).

NCEER-93-0021 "Finite Element Modeling of Elastomeric Seismic Isolation Bearings," by L.J. Billings, Supervised by R. Shepherd, 11/8/93, to be published.

NCEER-93-0022 "Seismic Vulnerability of Equipment in Critical Facilities: Life-Safety and Operational Consequences," by K. Porter, G.S. Johnson, M.M. Zadeh, C. Scawthorn and S. Eder, 11/24/93, (PB94-181765, A16, MF-A03).

NCEER-93-0023 "Hokkaido Nansei-oki, Japan Earthquake of July 12, 1993, by P.I. Yanev and C.R. Scawthorn, 12/23/93, (PB94-181500, A07, MF-A01).

NCEER-94-0001 "An Evaluation of Seismic Serviceability of Water Supply Networks with Application to the San Francisco Auxiliary Water Supply System," by I. Markov, Supervised by M. Grigoriu and T. O'Rourke, 1/21/94, (PB94-204013, A07, MF-A02).

NCEER-94-0002 "NCEER-Taisei Corporation Research Program on Sliding Seismic Isolation Systems for Bridges: Experimental and Analytical Study of Systems Consisting of Sliding Bearings, Rubber Restoring Force Devices and Fluid Dampers," Volumes I and II, by P. Tsopelas, S. Okamoto, M.C. Constantinou, D. Ozaki and S. Fujii, 2/4/94, (PB94-181740, A09, MF-A02 and PB94-181757, A12, MF-A03).

NCEER-94-0003 "A Markov Model for Local and Global Damage Indices in Seismic Analysis," by S. Rahman and M. Grigoriu, 2/18/94, (PB94-206000, A12, MF-A03).

NCEER-94-0004 "Proceedings from the NCEER Workshop on Seismic Response of Masonry Infills," edited by D.P. Abrams, 3/1/94, (PB94-180783, A07, MF-A02).

NCEER-94-0005 "The Northridge, California Earthquake of January 17, 1994: General Reconnaissance Report," edited by J.D. Goltz, 3/11/94, (PB193943, A10, MF-A03).

NCEER-94-0006 "Seismic Energy Based Fatigue Damage Analysis of Bridge Columns: Part I - Evaluation of Seismic Capacity," by G.A. Chang and J.B. Mander, 3/14/94, (PB94-219185, A11, MF-A03).

NCEER-94-0007 "Seismic Isolation of Multi-Story Frame Structures Using Spherical Sliding Isolation Systems," by T.M. Al-Hussaini, V.A. Zayas and M.C. Constantinou, 3/17/94, (PB193745, A09, MF-A02).

NCEER-94-0008 "The Northridge, California Earthquake of January 17, 1994: Performance of Highway Bridges," edited by I.G. Buckle, 3/24/94, (PB94-193851, A06, MF-A02).

NCEER-94-0009 "Proceedings of the Third U.S.-Japan Workshop on Earthquake Protective Systems for Bridges," edited by I.G. Buckle and I. Friedland, 3/31/94, (PB94-195815, A99, MF-A06).

NCEER-94-0010 "3D-BASIS-ME: Computer Program for Nonlinear Dynamic Analysis of Seismically Isolated Single and Multiple Structures and Liquid Storage Tanks," by P.C. Tsopelas, M.C. Constantinou and A.M. Reinhorn, 4/12/94, (PB94-204922, A09, MF-A02).

NCEER-94-0011 "The Northridge, California Earthquake of January 17, 1994: Performance of Gas Transmission Pipelines," by T.D. O'Rourke and M.C. Palmer, 5/16/94, (PB94-204989, A05, MF-A01).

NCEER-94-0012 "Feasibility Study of Replacement Procedures and Earthquake Performance Related to Gas Transmission Pipelines," by T.D. O'Rourke and M.C. Palmer, 5/25/94, (PB94-206638, A09, MF-A02).

NCEER-94-0013 "Seismic Energy Based Fatigue Damage Analysis of Bridge Columns: Part II - Evaluation of Seismic Demand," by G.A. Chang and J.B. Mander, 6/1/94, (PB95-18106, A08, MF-A02).

NCEER-94-0014 "NCEER-Taisei Corporation Research Program on Sliding Seismic Isolation Systems for Bridges: Experimental and Analytical Study of a System Consisting of Sliding Bearings and Fluid Restoring Force/Damping Devices," by P. Tsopelas and M.C. Constantinou, 6/13/94, (PB94-219144, A10, MF-A03).

NCEER-94-0015 "Generation of Hazard-Consistent Fragility Curves for Seismic Loss Estimation Studies," by H. Hwang and J-R. Huo, 6/14/94, (PB95-181996, A09, MF-A02).

NCEER-94-0016 "Seismic Study of Building Frames with Added Energy-Absorbing Devices," by W.S. Pong, C.S. Tsai and G.C. Lee, 6/20/94, (PB94-219136, A10, A03).

NCEER-94-0017 "Sliding Mode Control for Seismic-Excited Linear and Nonlinear Civil Engineering Structures," by J. Yang, J. Wu, A. Agrawal and Z. Li, 6/21/94, (PB95-138483, A06, MF-A02).

NCEER-94-0018 "3D-BASIS-TABS Version 2.0: Computer Program for Nonlinear Dynamic Analysis of Three Dimensional Base Isolated Structures," by A.M. Reinhorn, S. Nagarajaiah, M.C. Constantinou, P. Tsopelas and R. Li, 6/22/94, (PB95-182176, A08, MF-A02).

NCEER-94-0019 "Proceedings of the International Workshop on Civil Infrastructure Systems: Application of Intelligent Systems and Advanced Materials on Bridge Systems," Edited by G.C. Lee and K.C. Chang, 7/18/94, (PB95-252474, A20, MF-A04).

NCEER-94-0020 "Study of Seismic Isolation Systems for Computer Floors," by V. Lambrou and M.C. Constantinou, 7/19/94, (PB95-138533, A10, MF-A03).

NCEER-94-0021 "Proceedings of the U.S.-Italian Workshop on Guidelines for Seismic Evaluation and Rehabilitation of Unreinforced Masonry Buildings," Edited by D.P. Abrams and G.M. Calvi, 7/20/94, (PB95-138749, A13, MF-A03).

NCEER-94-0022 "NCEER-Taisei Corporation Research Program on Sliding Seismic Isolation Systems for Bridges: Experimental and Analytical Study of a System Consisting of Lubricated PTFE Sliding Bearings and Mild Steel Dampers," by P. Tsopelas and M.C. Constantinou, 7/22/94, (PB95-182184, A08, MF-A02).

NCEER-94-0023 "Development of Reliability-Based Design Criteria for Buildings Under Seismic Load," by Y.K. Wen, H. Hwang and M. Shinozuka, 8/1/94, (PB95-211934, A08, MF-A02).

NCEER-94-0024 "Experimental Verification of Acceleration Feedback Control Strategies for an Active Tendon System," by S.J. Dyke, B.F. Spencer, Jr., P. Quast, M.K. Sain, D.C. Kaspari, Jr. and T.T. Soong, 8/29/94, (PB95-212320, A05, MF-A01).

NCEER-94-0025 "Seismic Retrofitting Manual for Highway Bridges," Edited by I.G. Buckle and I.F. Friedland, to be published.

NCEER-94-0026 "Proceedings from the Fifth U.S.-Japan Workshop on Earthquake Resistant Design of Lifeline Facilities and Countermeasures Against Soil Liquefaction," Edited by T.D. O'Rourke and M. Hamada, 11/7/94, (PB95-220802, A99, MF-E08).

NCEER-95-0001 "Experimental and Analytical Investigation of Seismic Retrofit of Structures with Supplemental Damping: Part 1 - Fluid Viscous Damping Devices," by A.M. Reinhorn, C. Li and M.C. Constantinou, 1/3/95, (PB95-266599, A09, MF-A02).

NCEER-95-0002 "Experimental and Analytical Study of Low-Cycle Fatigue Behavior of Semi-Rigid Top-And-Seat Angle Connections," by G. Pekcan, J.B. Mander and S.S. Chen, 1/5/95, (PB95-220042, A07, MF-A02).

NCEER-95-0003 "NCEER-ATC Joint Study on Fragility of Buildings," by T. Anagnos, C. Rojahn and A.S. Kiremidjian, 1/20/95, (PB95-220026, A06, MF-A02).

NCEER-95-0004 "Nonlinear Control Algorithms for Peak Response Reduction," by Z. Wu, T.T. Soong, V. Gattulli and R.C. Lin, 2/16/95, (PB95-220349, A05, MF-A01).

NCEER-95-0005 "Pipeline Replacement Feasibility Study: A Methodology for Minimizing Seismic and Corrosion Risks to Underground Natural Gas Pipelines," by R.T. Eguchi, H.A. Seligson and D.G. Honegger, 3/2/95, (PB95-252326, A06, MF-A02).

NCEER-95-0006 "Evaluation of Seismic Performance of an 11-Story Frame Building During the 1994 Northridge Earthquake," by F. Naeim, R. DiSulio, K. Benuska, A. Reinhorn and C. Li, to be published.

NCEER-95-0007 "Prioritization of Bridges for Seismic Retrofitting," by N. Basöz and A.S. Kiremidjian, 4/24/95, (PB95-252300, A08, MF-A02).

NCEER-95-0008 "Method for Developing Motion Damage Relationships for Reinforced Concrete Frames," by A. Singhal and A.S. Kiremidjian, 5/11/95, (PB95-266607, A06, MF-A02).

NCEER-95-0009 "Experimental and Analytical Investigation of Seismic Retrofit of Structures with Supplemental Damping: Part II - Friction Devices," by C. Li and A.M. Reinhorn, 7/6/95, (PB96-128087, A11, MF-A03).

NCEER-95-0010 "Experimental Performance and Analytical Study of a Non-Ductile Reinforced Concrete Frame Structure Retrofitted with Elastomeric Spring Dampers," by G. Pekcan, J.B. Mander and S.S. Chen, 7/14/95, (PB96-137161, A08, MF-A02).

NCEER-95-0011 "Development and Experimental Study of Semi-Active Fluid Damping Devices for Seismic Protection of Structures," by M.D. Symans and M.C. Constantinou, 8/3/95, (PB96-136940, A23, MF-A04).

NCEER-95-0012 "Real-Time Structural Parameter Modification (RSPM): Development of Innervated Structures," by Z. Liang, M. Tong and G.C. Lee, 4/11/95, (PB96-137153, A06, MF-A01).

NCEER-95-0013 "Experimental and Analytical Investigation of Seismic Retrofit of Structures with Supplemental Damping: Part III - Viscous Damping Walls," by A.M. Reinhorn and C. Li, 10/1/95.

NCEER-95-0014 "Seismic Fragility Analysis of Equipment and Structures in a Memphis Electric Substation," by J-R. Huo and H.H.M. Hwang, 8/10/95.

NCEER-95-0015 "The Hanshin-Awaji Earthquake of January 17, 1995: Performance of Lifelines," Edited by M. Shinozuka, 11/3/95, (PB96-176383, A15, MF-A03).

NCEER-95-0016 "Highway Culvert Performance During Earthquakes," by T.L. Youd and C.J. Beckman, 11/6/95, to be published.

NCEER-95-0017 "The Hanshin-Awaji Earthquake of January 17, 1995: Performance of Highway Bridges," Edited by I.G. Buckle, 12/1/95, to be published.

NCEER-95-0018 "Modeling of Masonry Infill Panels for Structural Analysis," by A.M. Reinhorn, A. Madan, R.E. Valles, Y. Reichmann and J.B. Mander, 12/8/95.

NCEER-95-0019 "Optimal Polynomial Control for Linear and Nonlinear Structures," by A.K. Agrawal and J.N. Yang, 12/11/95, (PB96-168737, A07, MF-A02).

NCEER-95-0020 "Retrofit of Non-Ductile Reinforced Concrete Frames Using Friction Dampers," by R.S. Rao, P. Gergely and R.N. White, 12/22/95.

NCEER-95-0021 "Parametric Results for Seismic Response of Pile-Supported Bridge Bents," by G. Mylonakis, A. Nikolaou and G. Gazetas, 12/22/95, (PB97-100242, A12, MF-A03).

NCEER-95-0022 "Kinematic Bending Moments in Seismically Stressed Piles," by A. Nikolaou, G. Mylonakis and G. Gazetas, 12/23/95.

NCEER-96-0001 "Dynamic Response of Unreinforced Masonry Buildings with Flexible Diaphragms," by A.C. Costley and D.P. Abrams," 10/10/96.

NCEER-96-0002 "State of the Art Review: Foundations and Retaining Structures," by I. Po Lam, to be published.

NCEER-96-0003 "Ductility of Rectangular Reinforced Concrete Bridge Columns with Moderate Confinement," by N. Wehbe, M. Saiidi, D. Sanders and B. Douglas, 11/7/96.

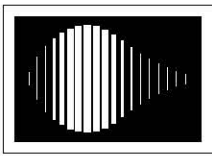

NATIONAL CENTER FOR EARTHQUAKE ENGINEERING RESEARCH

Headquartered at the State University of New York at Buffalo

State University of New York at Buffalo
Red Jacket Quadrangle
Buffalo, New York 14261
Telephone: 716/645-3391
FAX: 716/645-3399

ISSN 1088-3800